STRUCTURAL PERFORMANCE OF OUT-OF-PLANE MOMENT CONNECTIONS IN THE MINOR STRENGTH AXIS OF CROSS-LAMINATED TIMBER PANELS

by

Seyed Armin Hosseini

B.Sc in Civil Engineering, Azad University, Iran, 2014
M.Sc. in Structural Engineering, Semnan University, Iran, 2018

THESIS SUBMITTED IN PARTIAL FULFILLMENT OF
THE REQUIREMENTS FOR THE DEGREE OF
MASTER OF APPLIED SCIENCE
IN
ENGINEERING

UNIVERSITY OF NORTHERN BRITISH COLUMBIA

June 2024

Abstract

The structural performance of panel-to-panel connections in the minor strength axis of cross-laminated timber (CLT) panels was investigated using experimental and numerical methods. These connections are crucial for achieving two-way span action in point-supported floors of a large structural grid. Five different connections were studied: plywood splines attached with inclined self-tapping screws (STS), glued plywood splines, T-joints, wood X-fix shear keys, and steel rebars.

Based on 4-point and 3-point bending tests, the glued splines had the highest rotational stiffness, followed by the STS spline and T-joints. Steel rebar and X-fix connections had the lowest rotational stiffness. In terms of ductility, the glued spline exhibited brittle behavior, whereas others displayed a moderate level of ductility, while the steel rebars provided high ductility. The STS spline and glued spline had similar bending moment capacities, with the glued spline's capacity being affected by plywood quality. Steel rebars, T-joint, and X-fix connections had 70%, 50%, and 23% of this capacity, respectively.

Subsequently, a numerical model, validated by the experimental results, was used to evaluate the connection demands for point-supported CLT floors in the minor direction for different dimensions and applied loads. Increasing the rotational stiffness from 500 to 5000 $kNmrad^{-1}m^{-1}$ significantly improved floor structural performance, reducing the deflection by about 50%. Further increasing rotational stiffness only yielded an additional decrease in deflection of 15%. With the tested configurations, both glued and screwed splines can provide 5000 $kNmrad^{-1}m^{-1}$, T-joints could potentially achieve this value, while an unreasonably high number of connectors would be necessitated for X-fix.

Table of contents

List of figures

List of tables

Acknowledgements

I am deeply grateful to my supervisor, Dr. Thomas Tannert for his support, valuable feedback, and insightful guidance throughout this journey. His supervision has been instrumental in the completion of this thesis.

I also extend my thanks to Dr. Jianhui Zhou and Dr. Md Shahnewaz for their invaluable feedback and expert insights, which significantly enhanced the quality and depth of my research.

Furthermore, I acknowledge with gratitude the support received during the experimental phase of this study from Brandon Sullivan, Manager of the Fast + Epp Concept Lab, and Bernhard Zarnitz, Concept Lab Technician. Their assistance is greatly appreciated.

Finally, I would like to express my profound appreciation to my parents and sister for their unwavering love, encouragement, and belief in me. Their support has been my anchor throughout this endeavor.

1 Introduction

1.1 Background

Cross-laminated timber (CLT) is an engineered wood product, produced by laminating boards in orthogonal cross-layers. This lay-up creates major and minor strength directions (Figure 1-1). A wide range of investigations addressed connections in CLT panels with focus on their in-plane shear performance, with a limited number of studies on the out-of-plane performance of edge-connected CLT floors in the major strength direction using half-lap and single-spline joints [1-9].

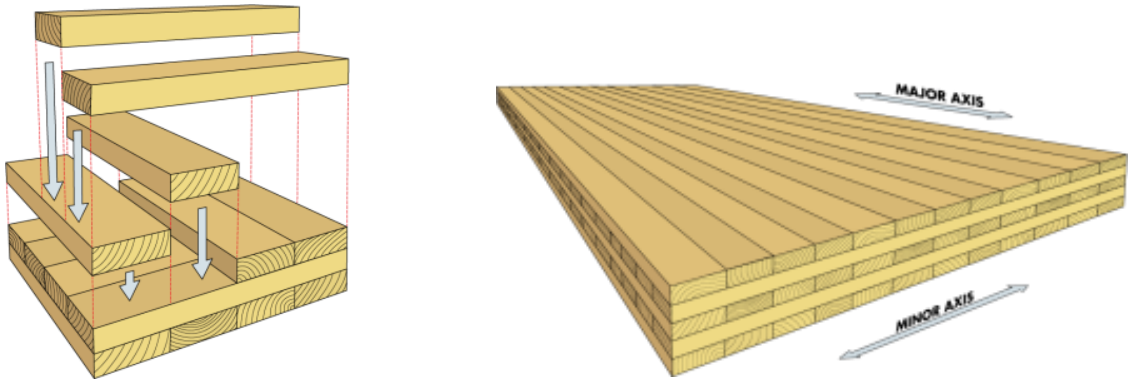

Figure 1-1: CLT: (a) arrangement of lamellas, (b) major and minor direction [9]

In contrast, the out-of-plane behavior of CLT panels connected in the minor axis has only been investigated sparsely [10-13]. This behavior is especially important for point-supported CLT floors because these depend on two-way performance with both major and minor directions providing rotational stiffness and bending moment capacity. Point-supported CLT floors have significant potential due to their ability to create spacious floor areas, resulting in a more flexible layout of columns without beams compared to the one-way-span floors (Figure 1-2). However, it is important to note that CLT exhibits lower strength and stiffness in its minor strength direction compared to the major direction. Additionally, CLT panels are typically available in widths ranging

from 2.4 to 3.5 meters. Therefore, edge-to-edge connections along the minor direction play a crucial role in enabling larger open floor spaces [4], [14].

A variety of solutions are available for establishing edge connections between CLT panels. These technologies encompass wood shear keys, like the X-fix system [15], [16], and half-lapped and single-spline joints connected with self-tapping screws (STS) [5-8, 17, 18], which are widely favored as mechanical fasteners due to their efficiency and cost-effectiveness.

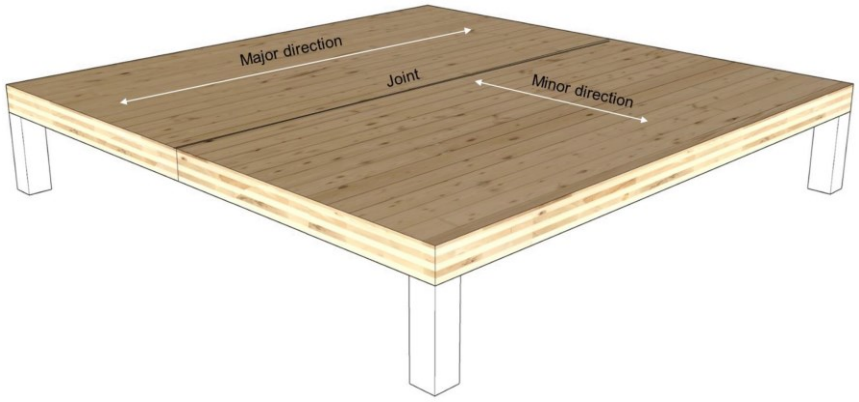

Figure 1-2: Point-supported CLT floor [19]

1.2 **Objectives**

The primary objective of this study is to investigate the out-of-plane performance of connections in the minor direction of edge-connected CLT. For this purpose, the structural performance of five different connection options is assessed: screwed plywood splines, glued plywood splines, wooden X-fix, T-joint, and steel rebar connection. The secondary objective is to numerically determine the moment and shear force demand that should be met by these connections.

1.3 **Organization of thesis**

In Chapter 2, the state-of-the-art on the out-of-plane performance of common connection systems for edge-connected CLT panels is reviewed. Chapter 3 presents the experimental investigations of

edge-to-edge connections in the minor direction of CLT panels, with results that provide fundamental information for subsequent numerical studies. In Chapter 4, the connection demands in different possible scenarios for point-supported CLT floors are evaluated using finite element analyses (FEA). Chapter 5 offers design recommendations based on findings from Chapters 3 and 4, assessing the behavior of connections in critical scenarios of point-supported CLT floors. Finally, Chapter 6 summarizes the main findings and suggests areas for further research.

1.4 **Scope and limitations**

This study focuses on the structural performance of edge-connected CLT panels along the minor direction subjected to quasi-static short-term out-of-plane loads. Tests involving combined, reversed cyclic, long-term, and in-plane shear loading are beyond the scope of this work. Furthermore, the impact of the connections on the vibration, acoustic, and fire performance of CLT floors is not addressed in this study. The numerical modeling is limited to analyzing the linear range of CLT floor and the connection behavior. Additionally, the boundary conditions of the models are confined to point-supported CLT floors.

2 Literature review

2.1 Wood and mass timber as structural material

Timber has been used for millennia due to its accessibility and workability. The use of wood also influenced the culture and architecture of indigenous peoples in North America [20]. As a result of the industrial revolution and the subsequent development of steel and concrete, timber was mostly used for small-scale and residential buildings, while population growth, particularly in rural areas, increased demand for high-rise buildings [21]. However, environmental concerns are driving the use of sustainable building materials, such as wood and engineered wood products.

Wood is an orthotropic material; its mechanical properties are distinct along three mutually perpendicular axes: longitudinal, radial, and tangential. The mechanical properties of wood are influenced by natural tree growth characteristics, such as specific gravity and slope of grain, as well as natural defects such as knots. However, thanks to stress grading, lumber can be suitable for a wide range of applications [22]. As a hygroscopic material, wood properties are sensitive to moisture content; it is recommended that the moisture content of wood during construction is close to the equilibrium moisture content that it will reach during use [22], [23].

Wood is widely utilized in construction, with one of its key attractions being its smaller carbon footprint compared to other building materials. The National Building Code of Canada (NBCC) permits encapsulated mass timber construction up to 12 stories in height [24], and due to the enhanced fire resistance, along with their stiffness and strength, mass timber construction with more than six stories has become increasingly common in practice [25].

2.2 **Cross-laminated timber floors**

As an engineered wood product, CLT is constructed from lumber lamellas that are glued together in an orthogonal pattern to create the composite material. Because of this configuration, CLT panels are a viable alternative to concrete as a structural floor and wall system [5]. In comparison to concrete and steel, the installation of prefabricated CLT panels speeds up construction.

CLT elements can be used as plate and shell elements loaded out-of-plane and in-plane, with floors currently being the main application. The most efficient use of CLT is taking advantage of its two-way resistance, when both major and minor directions contribute to the transfer of the loads to the supports. A two-way spanning CLT panel is around 50% stiffer than a one-way CLT panel [26].

The assessment of rolling shear strength in CLT for point-supported flat slab systems holds significant importance in structural design, especially considering the variations in wood species, stress grading, and panel configurations [27]. Notably, the primary mode of failure, characterized by crack propagation along growth rings, highlights the relationship between material properties and structural behavior. Moreover, a nuanced correlation between lamella aspect ratio and rolling shear strength was identified, emphasizing the necessity for refined design standards to accurately predict shear performance [27]. Popovski et al. [28] research on point-supported CLT floors reveals prevalent failure modes, such as: (i) compression perpendicular to grain failure at specific support points; (ii) a combination of rolling shear and tension perpendicular to grain failure above central support(s), particularly where bending moments were highest; and (iii) instances of partial penetration of middle columns into the CLT floor. Importantly, critical failures tended to occur at central support(s), coinciding with peak bending moments.

Several studies have examined various aspects of CLT panels. Yang et al. [10] and Mestek and Dietsch [29] studied out-of-plane shear strength of short-span panels showing different failure modes (rolling shear and tensile failure) as a function of loading and span. Bogensperger and Jobstl [30] employed nonlinear finite element analyses (FEA) to describe the punching shear behavior of unreinforced CLT point-supported panels.

2.3 **Connections between CLT floor panels**

In a structure, while columns, beams, and floors play crucial roles in transferring loads, their effectiveness greatly depends on the integrity provided by the connections between members [31]. In the following sub-sections, common connection technologies for CLT panels are introduced.

*2.3.1 **Wooden shear keys***

CLT panels can be joined using wood shear keys, such as the X-fix [16]. This dovetail-shaped connection has a wedge form that engages and self-tightens the components during installation without the addition of metal components [28]. X-fix components are made of Beech or Birch plywood, according to EN 13986 [31]. Based on application, this type of connector is divided into two groups: type C and type L. The C type is used as a shear connector for butt joints but can also resist tension loads (Figure 2-1); the L type is used to join CLT wall components. Ayansola and Tannert [32] observed high in-plane load-carrying capacity and stiffness of X-fix connectors, though their low ductility challenges their use in seismic applications. The connector's brittle shear failure was shown to be the most common failure when sufficient spacing is provided.

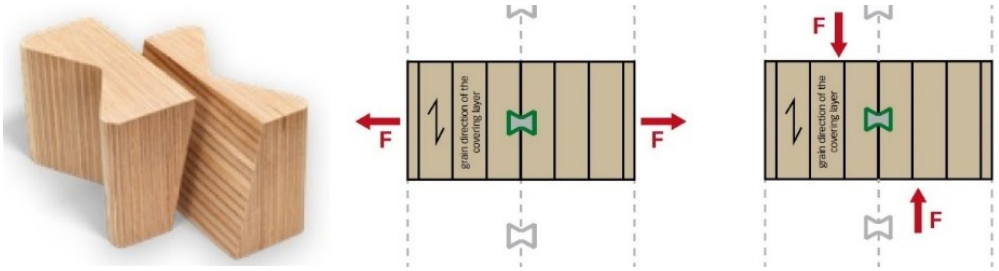

Figure 2-1: X-fix connector: (a) type C, (b) tensile loaded, (b) in-plane shear loaded [15]

2.3.2 ***Self-tapping screws***

Metal dowel-type fasteners, such as nails, screws, and bolts are popular because they efficiently distribute forces and are relatively easy to install [33]. STS, in contrast to other dowel-type fasteners, can be installed faster because predrilling is not required [34], [35]. High strength capacity, sharp cutting blade threads, fully threads length and surface coating eliminated extra works on predrilling. Hossain et al. [2] studied the in-plane shear behavior of double-angled STS assemblies in CLT and found that butt joints provide high and moderate-ductility in static and reversed cyclic loading, respectively (Figure 2-2) [4]. Experimental tests have suggested a group effect reduction for the performance of STS [1].

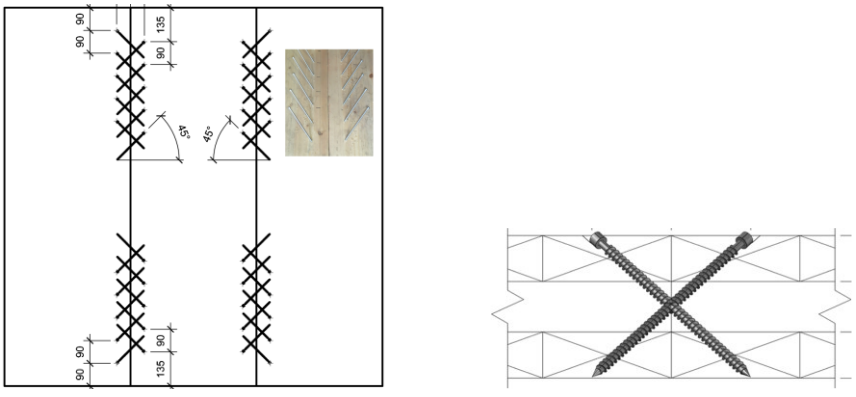

Figure 2-2: Edge connected shear wall: (a) arrangement of screw; (b) cross-sectional view [2]

*2.3.3 **Out-of-plane screw connections***

Spline (single, double and internal) and half-lapped joints present practical solutions for connecting panels, transferring both in-plane and out-of-plane loads. However, achieving a precise fit during installation can be challenging, particularly for internal splines (Figure 2-3) [8].

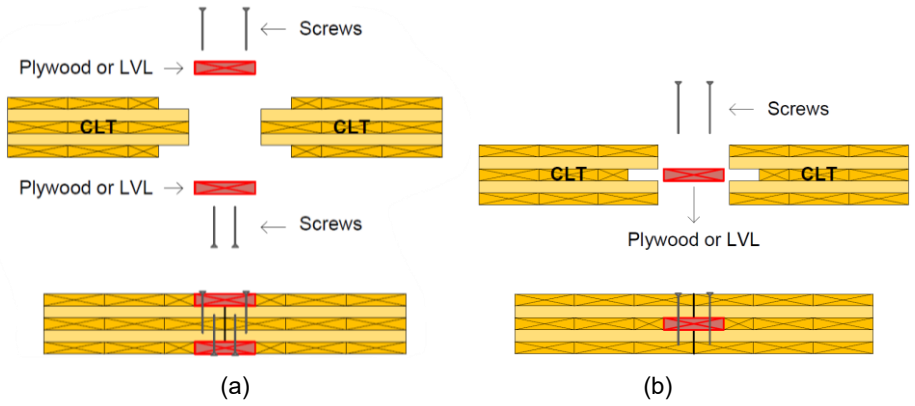

Figure 2-3: Spline connections, (a) double spline joints and (b) internal spline joints [8]

Subhani et al. [3] studied the flexural performance of half-lapped and single-splined CLT joints subjected to 4-point loading (Figure 2-4). Their findings underscored the positive correlation between lap length and moment capacity, rotational rigidity, and ductility. Specifically, extending the lap length from 75 mm to 100 mm yielded substantial enhancements in moment capacities for both bolted and screwed lap connections. Notably, the 100 mm lap length resulted in a 39% increase in moment capacity for bolted connections and a 33% increase for screwed connections. Moreover, an evident improvement in rotational rigidity and ductility accompanied the increase in lap length. Additionally, their study highlighted the superior performance of samples featuring single-splined connections over half-lapped joints, particularly with steel spline connections. While increasing the thickness of spline steel plates had minimal effect on moment capacity, enlarging bolt diameters contributed to its enhancement. Thinner steel plates exhibited better performance,

as the rigidity of thicker plates led to localized bearing failure. Regarding plywood spline connections, the presence of glue had little influence on bending moment, support rotation, and rigidity, with unglued connections demonstrating better performance. However, the incorporation of glue alongside bolts notably enhanced the ductility of plywood spline connections by 26%.

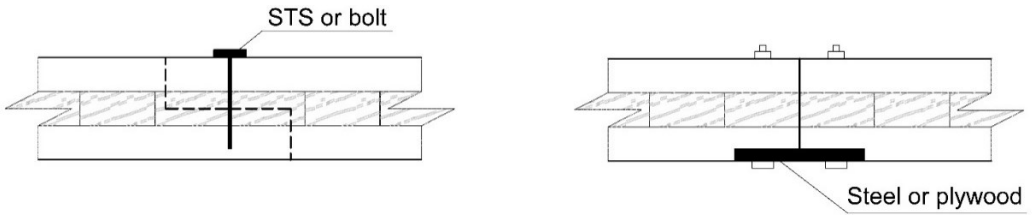

Figure 2-4: Edge-connected CLT panel (a) half-lapped joint (b) single-splined connections

Zhang et al. [5] conducted an assessment on the two-way performance of CLT panels under out-of-plane loads. As depicted in Figure 2-5, the joint in the minor direction was composed of steel plates, STS, and 45° screw washers. Their study revealed that the specimens failed at the tension side of the connection area, specifically at the interface of the outer bottom layers, while no evident damage was observed on other joint components. Furthermore, there was a notable and sudden decrease in loading capacity after reaching peak load. In subsequent testing, LVL was utilized as a replacement for steel plates. Despite experiencing an 87% decrease in stiffness compared to steel plates in H-block tests, LVL emerged as a practical choice considering factors such as manufacturing cost, assembly time, and fire protection. The steel plate connection exhibited a rotational stiffness of 782 kN m/rad, accounting for 98% of the intact panel's stiffness. In contrast, the LVL plate connection, though slightly lower, retained a commendable 92% of the full panel's stiffness [19].

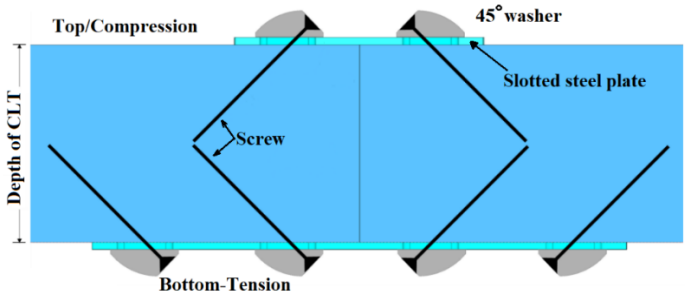

Figure 2-5: Spline connection with steel plate, washer, and inclined STS [19]

Macpherson et al. [6] developed a model for half-lap joints using four springs arranged as illustrated in Figure 2-6. The method was assessed using experimental testing and 3D FEA by considering the orthotropic properties of CLT and the interaction between the screw and wood. The model accurately predicted connection stiffness for a variety of common configurations.

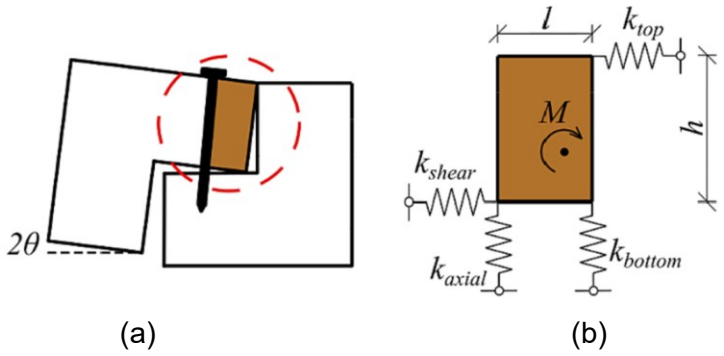

Figure 2-6: Deformed half-lapped joint (a), and simplified model with four springs (b) [9]

The structural integrity and performance of CLT floors are significantly influenced by edge connections, as revealed in recent studies [36]. These connections, such as single surface spline and half-lapped joint, play a pivotal role in determining modal properties and dynamic responses of CLT floors. Research highlights the sensitivity of modal properties to rotational stiffness and emphasizes the need for accurate modeling of connections in numerical simulations. Moreover, experimental estimation of connection stiffnesses is deemed essential for precise vibration analysis.

Sadeghi et al. [18] investigated the out-of-plane performance of edge-to-edge connections in CLT panels by employing STS in half-lapped and single-spline joints, with and without cup washers (Figure 2-7). The out-of-plane behavior of a single spline connection depended on the direction of applied moment, while half-lapped joints had the same performance in both positive and negative moments. Employing washers beneath the screw heads in half-lapped joints with 6 mm screws elevated maximum bending moment capacity and stiffness by 14% to 18% and 21% to 43%, respectively. For half-lapped joints utilizing 8 mm screws, these metrics saw a more moderate increase, ranging from 3% to 10% and 5% to 28%, respectively.

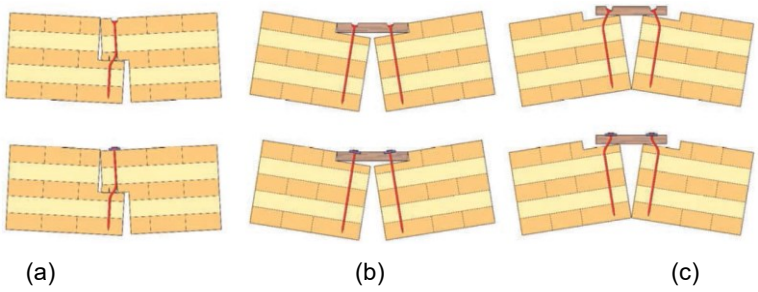

Figure 2-7: Deformation in: (a) half-laps; (b) spline top loading; (c) spline bottom loading [18]

In an experimental and numerical study, Asselstine et al. [4] concentrated on edge-connected CLT panels along minor directions. Different configurations of screwed LVL splines were investigated under out-of-plane bending using a 4-point loading test with the connections positioned at the middle span with no shear. The connections achieved stiffness values close to that of the full panel. For the connection with eight Ø8×220 mm screws at 30˚ and Ø12×260 mm screws at 45˚ on each side, bending moments of 72 kNm/m and 52 kNm/m were transferred, respectively. Different failure modes were observed: rolling shear and tension failures in the major layer, with withdrawal effects being less prominent, while the latter one showed rolling shear with withdrawal effects. In

a parallel study, Zhang et al. [5] examined inclined STS with a steel spline plate, capable of transferring 60 kNm/m with a flexural rigidity of 1131 kNm^2/m.

T-joints, depending on their type variations, can leverage high STS withdrawal resistance to transfer tension and bending loads between two components [37]. T-joints resemble a root and serve as focal point where the heads of multiple STS from different directions installed at different angles converge (Figure 2-8). T-joints provide a flush surface with no protruding parts and offer easy positioning in the borehole, enhancing the practicality of their application.

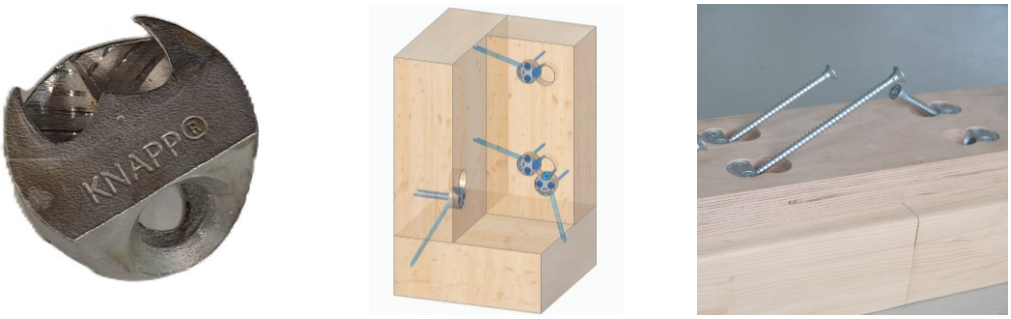

Figure 2-8: T-joint connection: (a) T-JOINT D40 W30, (b) and (c) example application of different variants [37]

*2.3.4 **Adhesive bonds***

Adhesive joints are a viable alternative to mechanical fasteners [38], [39]. However, there is no standardized design guidance [41-43]. The Timber Structures 3.0 (TS3) system permits the butt-joint bonding of fibres, (Figure 2-9) [43], using a two-component Polyurethane adhesive [44]. A bending strength up to 21 MPa was achieved for small-scale CLT panels with a width of 50 mm and thicknesses ranging from 100 to 180 mm [45]. The performance was affected by the joint thickness, temperature, humidity, and how the end grain was treated before they were joined.

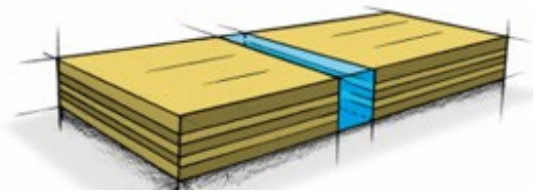

Figure 2-9: Butt-joint bonding technology (TS3) [43]

2.3.5 ***Hybrid connections***

Composite construction has seen significant advancements in recent years, with Timber-Concrete Composite (TCC) structural members garnering considerable attention [47-53]. Stieb et al. [53] created a bending-resistant edge connection between two CLT TCC elements, termed TC Fusion (Figure 2-10). STS are installed in the narrow faces of the CLT elements to create a lap splice, into which concrete is poured to form a reinforced connection. Experimental tests demonstrated high load-bearing capacity, with potential for further optimization by adjusting screw spacing or diameter. The study also indicated that rotational stiffness exceeding 5000 $kNmrad^{-1}m^{-1}$ has negligible effects on the structural performance of the floors.

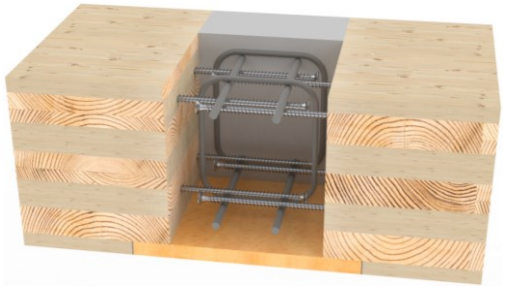

Figure 2-10: Schematic of TCC connection [53]

Serrated steel plates offer an alternative solution for ensuring continuity between CLT panels (Figure 2-11) [54]. These plates feature micro-teeth located along the narrow side of the panels, which embed into the solid wood when a threaded steel rod is rotated. Such connections provide both stiffness and a ductile failure mode [55].

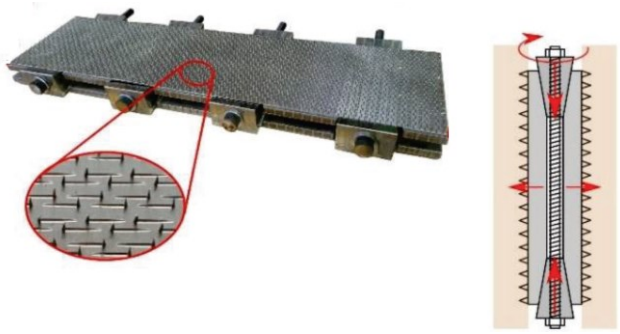

Figure 2-11: Edge connected panels with serrated steel plates [54]

2.4 **Modelling of CLT floors**

FEA offers the potential to minimize costly large-scale testing, provided that the model can be validated. However, modeling CLT may pose distinct challenges due to the layup configuration between major and minor layers, and gaps between boards, among others [56]. In the formulation of models for the out-of-plane of CLT floor, two prevalent assumptions are typically employed. Firstly, CLT panels are assumed to exhibit elastic behavior. Secondly, the non-linear behavior is concentrated at the connections. It is common practice to represent CLT panels using shell elements, while moment and shear connectors are represented using spring elements [57].

The selection between shell and solid elements is a crucial consideration. Solid elements provide a 3-D representation that requires more computational power but often delivers better accuracy, especially for thicker plates and higher shear deformation. Linear solid elements may suffer from shear-locking issues in geometries with significant bending deformations, leading to an overestimation of system stiffness due to unintended shear deformations. This issue can be addressed by using more elements through the thickness or employing quadratic solid elements, both of which increase computational effort. The choice of element type may also depend on the complexity of the geometry, with a fine mesh being necessary for detailed models with numerous features, favoring the use of shell elements [58], [59]. However, shell elements offer a

computationally efficient approach by transforming a 3D problem into a 2D, utilizing plate theory to estimate displacements across the plate thickness. While shell elements are generally suitable for thin plates with low shear deformation, their accuracy diminishes with thicker plates, increased shear deformation, and concentrated loadings [58], [59].

Muster and Frangi [60] analyzed the punching performance of continuous two-way CLT point-supported floors. The material of each layer was determined individually, and the interaction between these layers was assumed to be without any slippage. In the FE model, there was no gap between the lamellas, as it was determined that the precise definition of the gap between the boards does not have a significant impact on the rolling shear stresses. These models were successfully evaluated using RFEM [61] in 2D. Additionally, the 3D solid finite element model produced stresses of comparable magnitude to the 2D simplified model, supporting its accuracy. The shear stress verification presented a greater challenge. Due to the absence of nonlinearities in the simulations and the lack of a conclusive definition for an increase in rolling shear strength for CLT under concentrated loads, the calculated rolling shear stresses remain uncertain. Nonetheless, all models accurately predicted rolling shear failure when considering a 50% increase in resistance. Nevertheless, both distinct calculation methods demonstrated acceptable agreement [60].

Asselstine et al. [4] employed FEA for the two-way bending CLT panels utilizing 3D elements with 20 nodes to represent the major and minor layers separately. To reduce computational workload, symmetry was employed in the modeling of the beam bending setup. To address the impact of variations in ring orientation and other inconsistencies among the individual boards in the major and minor layers, a process of calibration was carried out. This involved the conversion of the orthotropic properties, as illustrated in Figure 2-12.

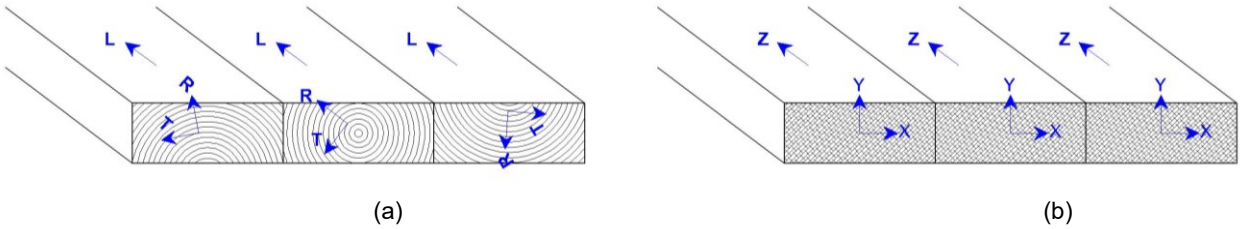

Figure 2-12: (a) Grain orientation in lamellas and (b) homogenized orthotropic model [4]

Mahdavifar et al. [13] employed a shell modelling approach that incorporated nonlinear interface elements to represent the combined effects of rolling shear and bonding of the layers. The chosen elements focused on capturing membrane and plate bending behavior while neglecting other deformation modes. To calibrate the elastic properties, an iterative process utilizing the shear analogy method described in CLT handbook [8] was employed. Initially, an assumed modulus of elasticity (MOE) was selected based on established values for Douglas-fir. Then, the apparent flexural rigidity (EI) was calculated using the shear-analogy method. Subsequently, the deflection at peak load was compared to experimental values, and iterations were conducted by adjusting the MOE until calculated and experimental deflections aligned. The remaining elastic properties, including the rolling shear stiffness assigned to the interface elements, were determined based on recommendations from the CLT handbook [8]. The linear elastic response of the model exhibited good agreement with experimental load-displacement curves [56].

2.5 **Summary of literature review**

CLT panels exhibit potential for two-way action. Given the dimensional constraints of such panels, ensuring continuity between adjacent panels, particularly in the minor direction, becomes imperative. STS are the most common type of connection in timber structures, known for their fast installation and cost-efficiency. In this regard, lap- and spline-joints are two common connections. Although most previous research focused on STS, there are some alternatives with limited

information on their structural performance. X-fix connectors can provide quick and secure connections without the need for additional metal. Adhesively bonded connections are also an option, providing mechanical integrity and aesthetic advantages. Assessing the out-of-plane behavior of connections in minor directions are particularly crucial, especially in point-supported CLT floors. However, the majority of studies to date have focused on the performance of connections in the major direction between CLT panels, and only some studies have focused on the out-of-plane performance of edge-connected CLT panels in the minor strength direction. Further studies are necessary to ensure continuity in the minor direction, as neglecting the minor direction capacity of CLT panels notably underestimates the resistance and displacement deflection capacities of these structural components.

3 Experimental investigation

3.1 Overview

This chapter presents the experimental investigations on edge-connections in the minor strength axis of 7-ply CLT panels. These connections were subjected to out-of-plane 4-point and 3-point bending loading. The work was carried out at Fast + Epp's concept lab in Vancouver, British Colombia. Five connection configurations were tested:

1) The first configuration (S1), screwed splines, entailed attaching plywood sheets with STS.

2) The second configuration (S2), glued splines, used glue for attachment instead of screws.

3) The third configuration, T-joints (S3), utilized the proprietary connector installed with STS.

4) The fourth connection (S4) was the X-fix, a wooden shear key with a dovetail shape.

5) Lastly, the fifth configuration (S5) involved attaching steel rebars at the bottom of the panels.

3.2 Materials

The experimental program employed CLT of V2M6 grade manufactured by Kalesnikoff in accordance with ANSI/APA PRG 320 [62]. In this V2 grade, both longitudinal and transverse layers were No.1/No. 2 SPF lumber. A 245 mm thick 7-layer CLT was selected for this study to provide solutions for large two-way spans in point-supported CLT floors. The layers were 35 mm thick, and the lamellas were 170 mm wide.

The study utilized Ø8×160 mm and Ø10×320 mm fully threaded ASSY plus VG screws with a countersunk (CSK) head, as depicted in Figure 3-1. These screws are specifically designed for wood-to-wood applications. SK Ø6×100 mm washer head screws were used in the glued spline samples to clamp the plywood onto the CLT panels during adhesive curing.

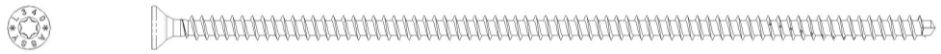

Figure 3-1: ASSY plus VG screws [63]

Two types of 18 mm (¾") thick Baltic birch plywood panels served as splines: high-quality grade B and low-quality grade C. Grade C permits patches, open knots, small veneer splits, veneer laps, and small core voids (Figure 3-2). For clarity, these were designated as type B and type C.

Figure 3-2: Plywood: (a) high-quality (grade B) and (b) low-quality (grade C)

Two adhesives were utilized: LePage PL Premium Max and Titebond III. PL Premium Max, formulated with a silane-modified polymer base, provides a compression shear strength of 9 MPa, with an open time of 20 minutes and a curing period of 24 to 48 hours [64]. Titebond III, a polymer-based wood glue, has an open time of approximately 3-5 minutes and a total assembly time of 10-15 minutes. Despite its quicker setting, it delivers a minimum bond strength of 5.5 MPa [65].

In this study, X-fix-C measuring 130 mm in length (L), 96 mm in width (w), and 90 mm in height (h) were utilized (Figure 3-3). According to the product European technical assessment (ETA-18/0254, 2020), the plywood employed in X-fix has a bending strength of 34.8 MPa, tension strength of 36.9 MPa, and shear strength of 9.5 MPa, with a mean density of 680 kg/m³ [66].

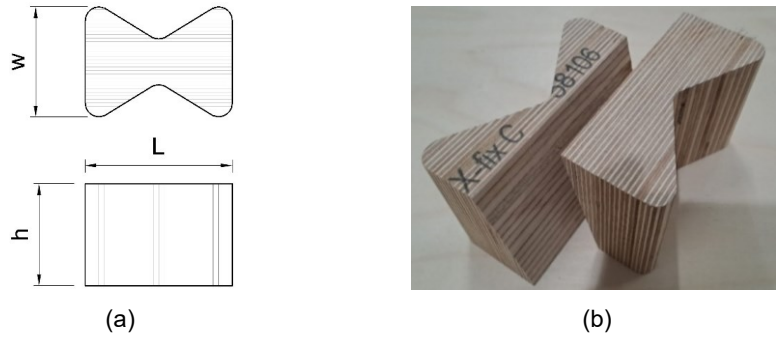

Figure 3-3: X-fix-Cm Connector; (a) schematic view, (b) actual view

For the T-joint connection, the D40 W30 variant was employed (Figure 2-8a), specifically designed to enable tension and bending joints between two wooden components through dual-angle screw fastening. This design utilizes three screws to directly transfer tensile forces from one component to the other, as illustrated in Figure 3-4.

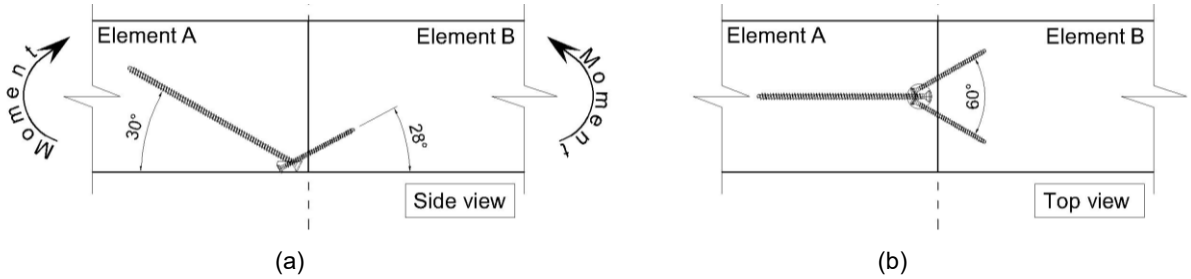

Figure 3-4: Schematic representation of a T-joint connection utilizing the D40 W30 variant

Two types of steel rebar were employed, both with a minimum yield strength of 400 MPa. The first type was #4 (Ø8 mm) carbon steel (A615) grade 60 rebar, marked as NU4S60; the second type was a Ø 10 mm epoxy rebar, labeled as grade 400W according to CSA G 30.18 [67].

3.3 Specimen description

3.3.1 S1 - spline plate with inclined STS

The screwed spline connection consisted of two plywood sheets attached at the bottom of the CLT panels, effectively providing a thickness equal to that of the removed CLT layer. In the minor strength direction, the bottom (7^{th}) layer does not transfer stresses in bending, yet the continuous spline plates do. The plywood sheet, measuring 400 mm in length in its major direction and 600 mm in width, was connected to the panels using 12 STS on each side, installed at a 45-degree angle, as shown in Figure 3-5. The plywood sheets were predrilled with holes for STS installation. Two series were prepared and subsequently tested: Grade C plywood was employed for the 4-point bending tests, whereas grade B plywood was used for the 3-point bending tests.

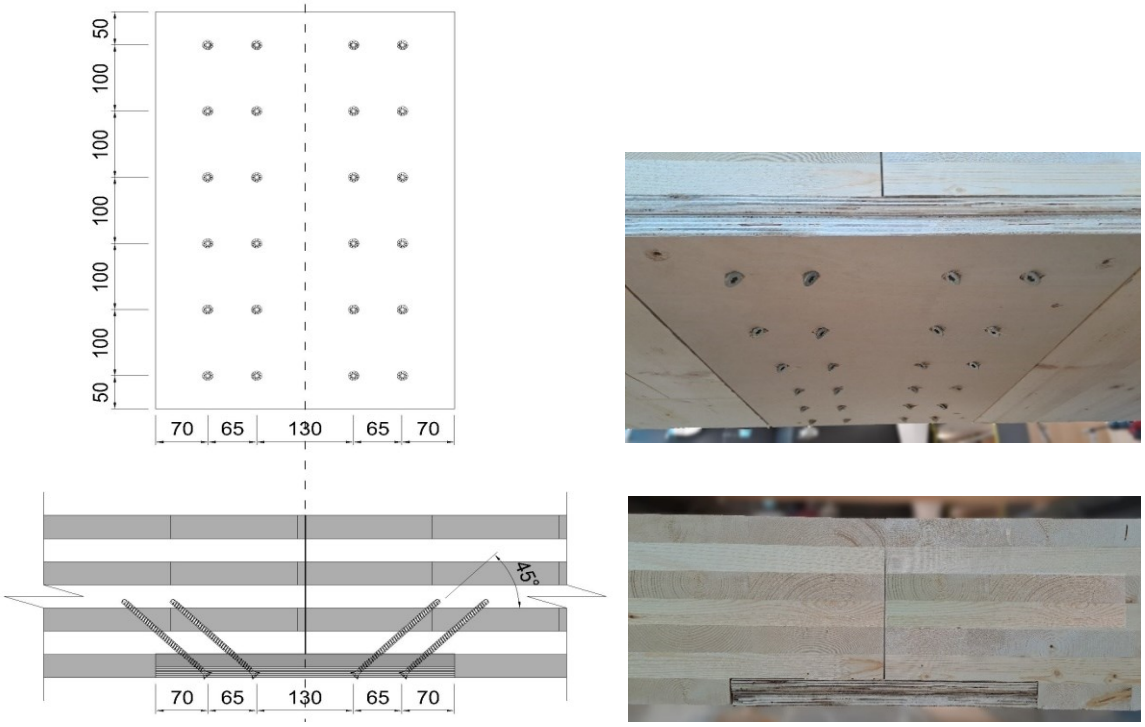

Figure 3-5: Spline connection with inclined STS: (a) schematic (b) photos side and bottom

3.3.2 ***S2 - glued spline plate***

Similar to the screwed spline, the 7th layer of the CLT panels was removed in the connection zone. Two 17 mm thick, 400 mm long and 600 mm wide plywood sheets were glued together using Titebond III wood glue, the resulting 35 mm thick sheet was then glued onto the CLT panels using PL Premium Max. The minimum curing time recommended by the manufacturer, at least 24 hours after fabrication, was met. For each specimen, approximately 175 ml of glue was applied in eleven parallel lines across the width of the panel, ensuring an approximate 1 mm thick glue line covered the spline and surfaces after pressing. To ensure proper compression between the CLT panel and plywood surface, 16 SK Ø6×100 mm STS, arranged in a 4×4 pattern, were installed to clamp the plywood onto the CLT panels. It is important to note that these STS were removed before testing. Grade B plywood was exclusively used for the 3-point bending tests, while both grades were used for the 4-point bending tests, with six samples from grade B and two from grade C.

3.3.3 ***S3 - T-joint***

In these connections, four T-joints were arranged in a zigzag pattern, with a center-to-center spacing of 120 mm along the CLT panel width, with two on the left side and two on the right side of the connecting line, as depicted in Figure 3-6. Each T-joint was attached with two Ø8×160 mm STS on one side at a 28˚ angle to the surface, and one Ø10 × 320 mm STS at a 30˚ angle on the other side. To achieve a flush surface, the T-joints were installed recessed into the 7th layer, approximately 18 mm based on the height of the T-joint.

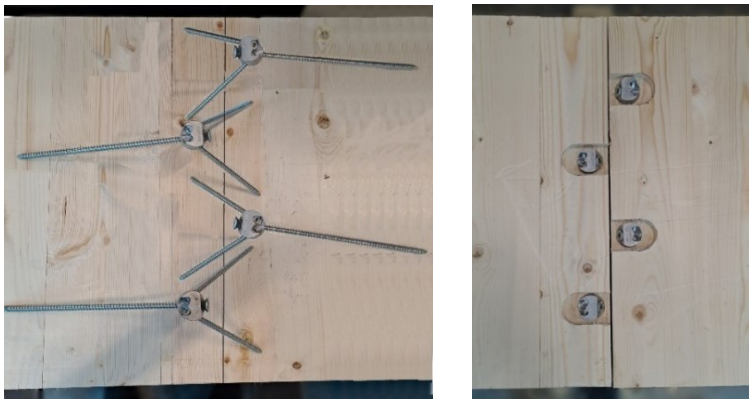

(a) (b)

Figure 3-6: T-joint: (a) layout before installation, (b) fully installed

*3.3.4 **S4 - X-fix***

This connection involved two X-fix-C shear keys to secure the panels to each other, as depicted in Figure 3-7. The X-fix connections were positioned with a spacing of 300 mm at the center of the panel width. Similar to spline connections, the 7th layer was removed; however, the X-fix engaged the 6th, 5th, and part of the 4th layers (Figure 3-7a).

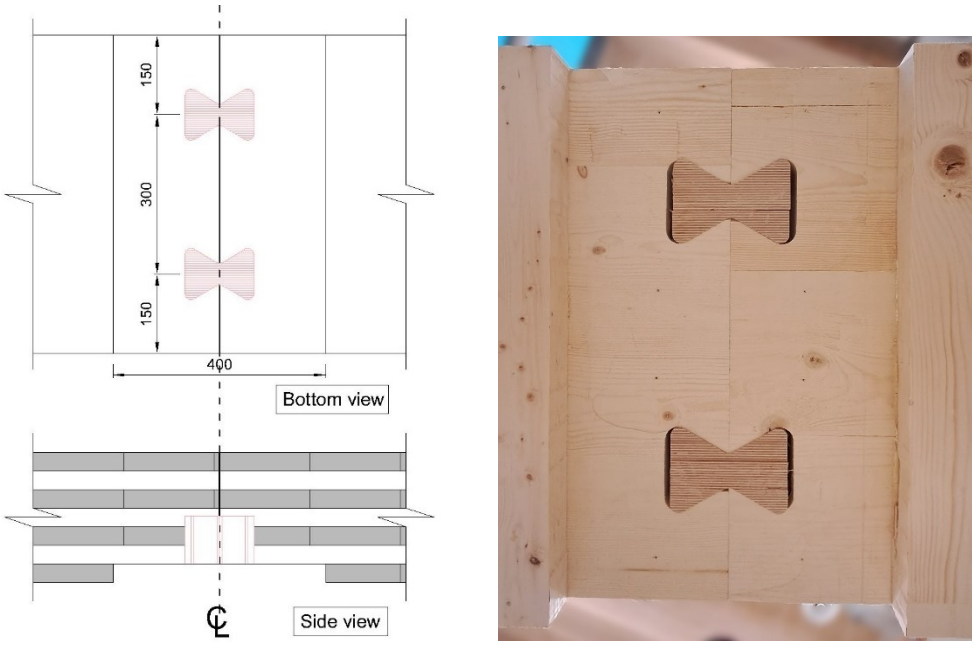

(a) (b)

Figure 3-7: X-fix connection: (a) schematic; (b) photo bottom face

3.3.5 ***S5 - Steel rebar***

In these connections, bent steel rebars were installed into slots at the bottom of the panels, positioned at the bottom of the 6th layer. These connections were evaluated in two variants: S5A utilized U-shaped rebars bent at a 90˚ angle, consisting of three Φ12 mm rebars spaced at 175 mm intervals. S5B involved four Φ10 mm rebars spaced at 120 mm bent at a 120˚ angle. To secure the rebars in position, both ends were fixed using two flat washers and a nut (Figure 3-8).

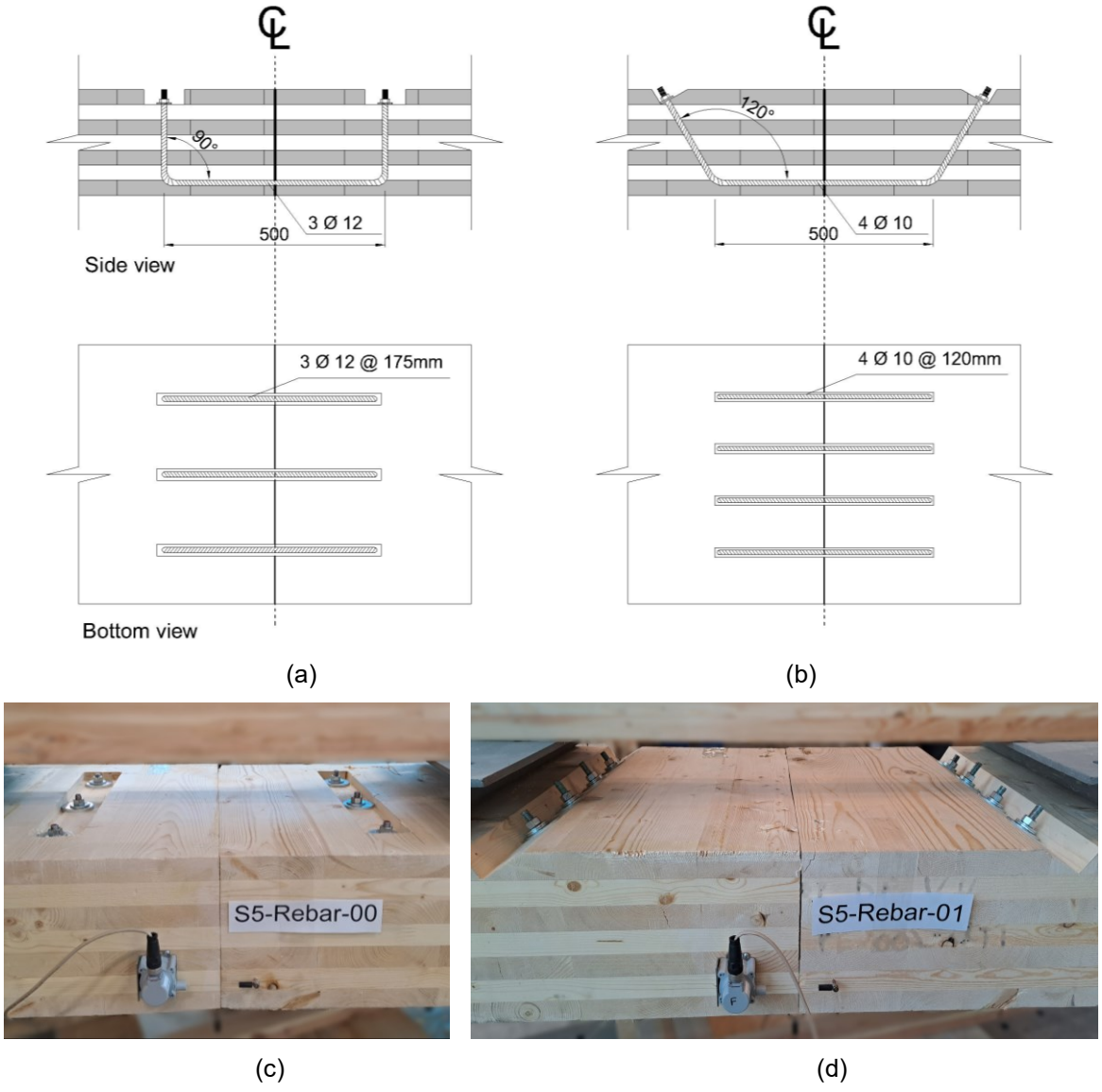

Figure 3-8: Steel rebar connection: (a) schematic S5A, (b) and S5B, (c); photo S5A, (d) and S5B

3.4 Test methods

3.4.1 4-point bending test

The 4-point bending tests, as shown in Figure 3-9, created a pure bending moment in a zero-shear zone at the connecting line. The length of the two connected panels was 3450 mm, and the span, representing the distance between two supports, was 2730 mm. The width of the panels (in the major direction) was 600 mm. The load was applied as two lines at a distance of 495 mm from the connection. Simple line supports without constraint of rotational movement were provided.

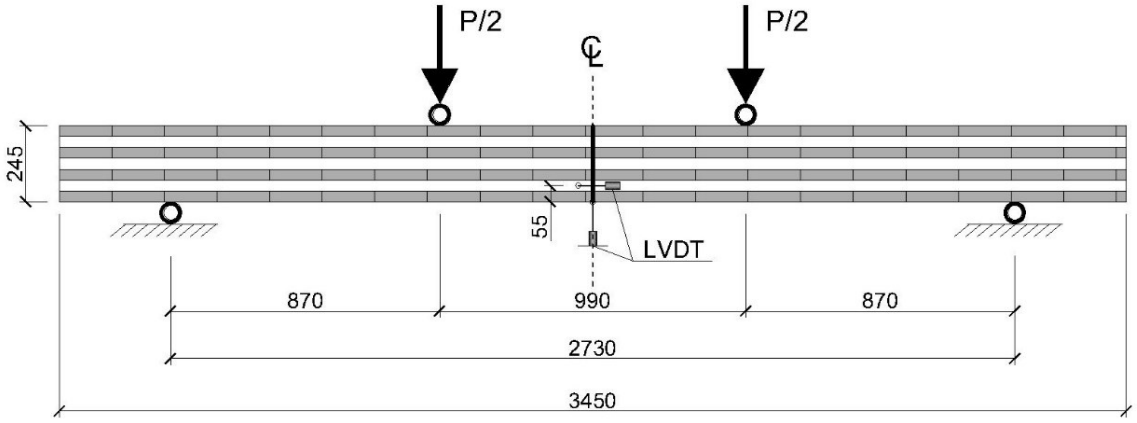

(a)

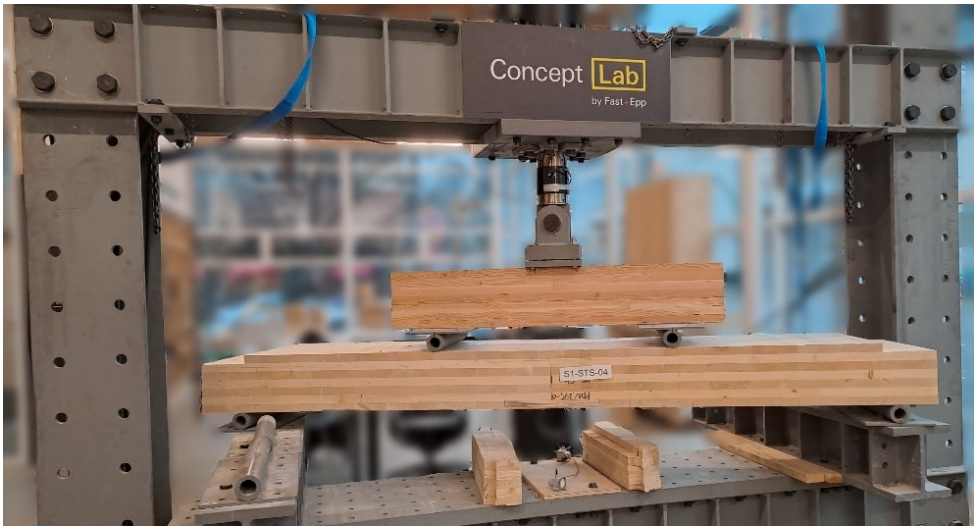

(b)

Figure 3-9: 4-point bending test: (a) schematic (dimensions in mm); (b) photo

Four linear variable differential transformers (LVDTs) were installed. One pair measured the mid-span deflection, and another pair measured the gap opening, with each pair positioned perpendicular to the contact surface of the two panels located 55 mm from the bottom surface.

The rotational stiffness (C_φ) was defined from the slope of the moment-rotation curve in the range of 10% to 40% of the peak load after the unloading cycle. The rotation is represented by the gap angle (arc) opening of the connection, where this angle is the ratio of the gap opening at the connection line (evaluated by two horizontal LVDTs on the panel sides) to the depth of the section. Ductility (μ) was defined as the ratio of ultimate displacement (δ_u) to yielding displacement (δ_y). The displacements δ_u and δ_y were determined using the procedure shown in Figure 3-10. Line 1 ($L1$) is the tangent to 10% and 40% of the peak load, with a slope α relative to the horizontal axis, while $L2$ passes through the peak load with a slope of α/6. The point of intersection between these lines defined δ_y, and δ_u represents the deflection corresponding to the point where the load drops to 80% of the peak load, as defined in section 3.5.2 [69-71].

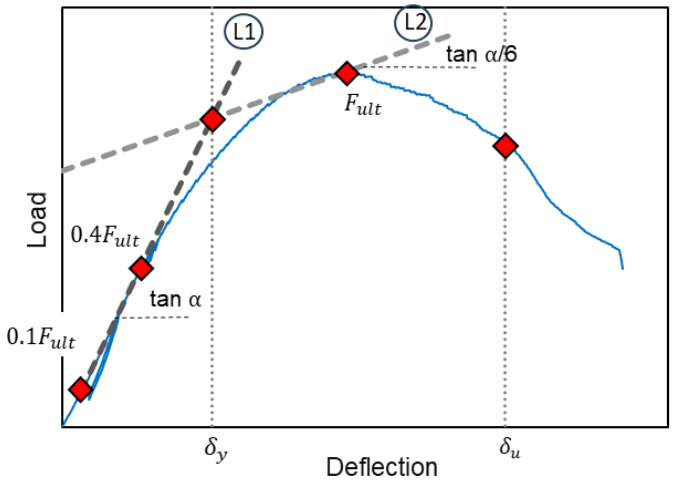

Figure 3-10: Procedure for calculating ductility index

3.4.2 ***3-point bending tests***

The 3-point bending test was employed to evaluate the performance of connections under simultaneous out-of-plane shear and out-of-plane bending moment loads, which is a scenario commonly encountered in floor applications. The X-fix connector and rebar joints were excluded from the 3-point bending tests because these connections are not designed to transfer out-of-plane shear. As illustrated in Figure 3-11, the connection was positioned off-centre, located at a distance equivalent to one-quarter of the floor span from the support.

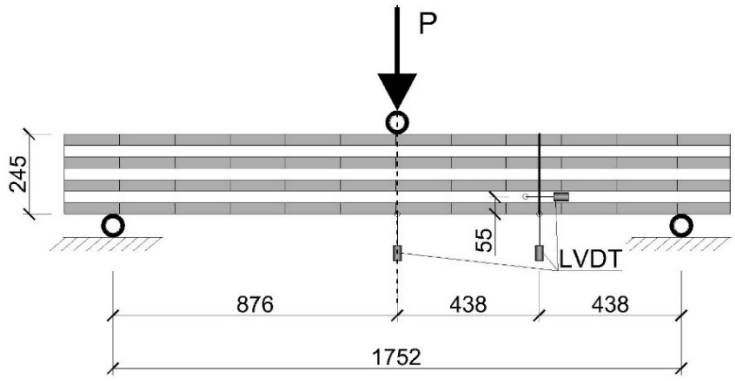

(a)

(b)

Figure 3-11: 3-point bending test: (a) schematic (dimensions in mm); (b) photo

The test span was 1752 mm, and the line load was applied at the midpoint of this span, extending along the entire width of the panel. (Note: a small series of 3-point tests of continuous CLT panels was conducted with a span of 1504 mm, and the load was applied in the centre of the span.) Five LVDTs were installed: one pair at the center span on both sides of the panel, one LVDT at the center of the connecting line to measure the maximum deflection of the specimens, and deflection at the connecting line, respectively. Additionally, one pair was positioned on both sides of the connecting line to measure the opening of the connection gap.

*3.4.3 **Loading protocol***

The testing apparatus included a hydraulic actuator with calibrated load cell with a capacity of 350 kN. All testing followed a modified EN-26891 [71] loading protocol, employing a displacement-controlled rate set at 8 mm/min. The specimens were subjected to loading up to 40% of load-carrying capacity, followed by unloading to 10% of this value. After each of these stages, the load was maintained at a constant level for 20 seconds. Subsequently, the loading was increased until failure, defined as a 20% drop from the maximum load. The load-carrying capacity was determined based on preliminary tests conducted for each connection series.

3.5 **Results and discussion**

*3.5.1 **Load-deflection of 4-point bending tests***

Representative load-displacement curves of specimens from each connection configuration are shown in Figure 3-12. The individual load-displacement curves are shown in Appendix A.

In the screwed spline samples (S1), generally ductile performance was observed, characterized by three stages: a linear part up to a load of approximately 55 kN (about 70% of peak load), at an

average deflection of 22 mm, a nonlinear part with reduced stiffness leading up to the peak load, and a gradual drop in load-carrying capacity towards the failure point. The average maximum load-carrying capacity of the samples was 77 kN with a Coefficient of Variation (CoV) of 4%, at an average displacement of 42 mm.

The load-deflection characteristics of glued spline connections (S2) exhibited linear behaviour up to peak loads, immediately followed by brittle failure. The results highlight the significant influence of the plywood grade. Specimens featuring grade B (S2B) exhibited an average load-carrying capacity and maximum deflection of 82 kN and 20 mm, respectively. These values substantially decreased for the two samples fabricated with grade C (S2C) to 34 kN and 11 mm on average.

The load-deflection curve of the T-joint (S3) can be divided into three distinct segments: an initial linear phase, a subsequent phase characterized by reduced stiffness leading up to peak loads, and a final segment characterized by a descent from peak loads that resulted in failure. The average load-carrying capacity was 39 kN, corresponding to an average displacement of approximately 30 mm. The linear range extended to a load of 19 kN equivalent to about 8 mm deflection. All samples demonstrated a ductile behavior and the ability to experience about a 50% drop in load-carrying capacity without experiencing any failures.

The load-deflection response of the X-fix (S4) was initially almost linear, continuing up to approximately 70% of the peak load which averaged about 19 kN, at a deflection of 32 mm. Subsequently, as the load-displacement curve slope gradually decreased, slight fluctuations in loading were observed. Overall, these samples demonstrated a moderately ductile performance.

The load-deflection behavior of the rebar joints revealed two phases. Initially, there was a stiff phase lasting until 6% and 20% of deflection (10 mm and 40 mm) for specimens S5A and S5B, respectively, followed by a decrease in slope. However, the load-carrying capacity remained nearly constant during both phases. At this point, S5A and S5B reached a load-carrying capacity of 50 kN and 67 kN, respectively, corresponding to approximately 185 mm of deflection.

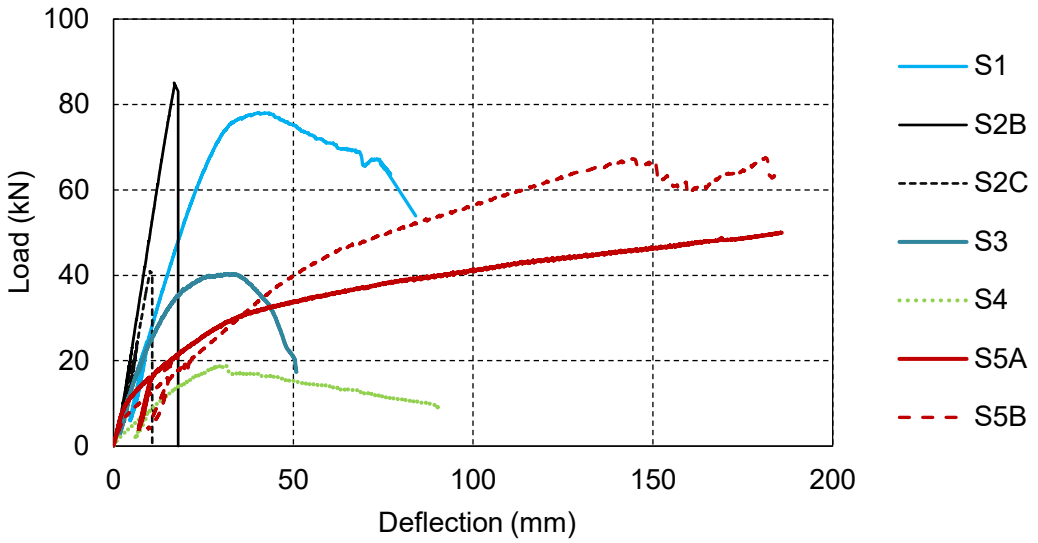

Figure 3-12: Typical load-deflection curves of 4-point tests

3.5.2 ***Failure modes in 4-point bending tests***

Failure in this study was characterized by the loss of functionality within the entire system. This occurred either when there was a 20% reduction in load-carrying capacity or when the deflection exceeded the test setup capacity, which was approximately 185 mm (L/15). Some typical failed specimens are shown in Figure 3-13. More photos are provided Appendix C.

The screwed spline samples (S1) displayed ductile behavior. Initial indications of damage were discernible through noises originating from the spline plate. Two distinct failure modes were identified: tension-induced failure in the plywood resulting in a sudden decrease in loading capacity

(Figure 3-13a), and screw withdrawal leading to a gradual reduction in loads without abrupt failure (Figure 3-13b). In tension failures, the gap between the spline plate surface and the 6th layer widened symmetrically, whereas withdrawal failures exhibited a localized increase in this gap.

In all glued spline samples (S2), failure was confined to the interface between the spline plate and the CLT panels. Samples using plywood grade B exhibited plywood failures (Figure 3-13c). Conversely, samples with grade C plywood had failure concentrated solely within the plywood lamella (see Figure 3-13d). Regardless of plywood type, failure was abrupt, without notable warnings and no slip between plywood and CLT panel before peak load.

T-joint connections (S3) exhibited three distinct failure modes: i) crushing perpendicular to the grain where T-joints meet the CLT interface; ii) withdrawal of the two short STS; and iii) bending of the STS close to the CLT surface due to the joint rotation, as depicted in Figure 3-13e through Figure 3-13g, respectively. Modes i) and iii) contributed to the ductility observed in the load-displacement response. Disassembling T-joint specimens posed considerable challenges, due to the bent STS. The T-joint components remained intact throughout the process.

The X-fix connection (S4) is depicted in Figure 3-13h and Figure 3-13j, exhibited shear failure parallel to the grain throughout the entire height of the X-fix. Additionally, shear failure perpendicular to the grain is observed in the 5th layer, leading to the rotation of this layer due to tension loads. Besides shear failure in the CLT panel layers, the X-fix itself experienced shear damage, with cracks developing parallel to the X-fix layer in the narrow part of the X-fix.

Figure 3-13: Failure modes series S1-S4 in 4-point tests; (a) S1 tension failure in the plywood, (b) S1 withdrawal effect in the spline plate, c) S2B, d) S2C, (e) S4 crushing perpendicular to the grain, (f) S4 Withdrawal effects, (g) S4 ductile failure in STS, (h) S3 bottom view, (i) S3 connecting section, (j) X-fix shear failure

In steel rebar joints (S5), the main failure mode was compression perpendicular to the grain at both ends of the rebar where washers pushed on the CLT (Figure 3-14a). S5B showed more damage due to smoother angles of the steel rebars, leading to larger tension loads. In contrast, S5A transferred tension loads through the vertex of the rebars, resulting in compressive loads on the wood surface. Failure was also evident at the bottom of the sixth layer. Imprints of the rebar ridges on the solid wood were visible along the entire slot length. Significant gap opening concentrated compressive forces on the first layer, leading to damage and crack formation between the first and second layers.

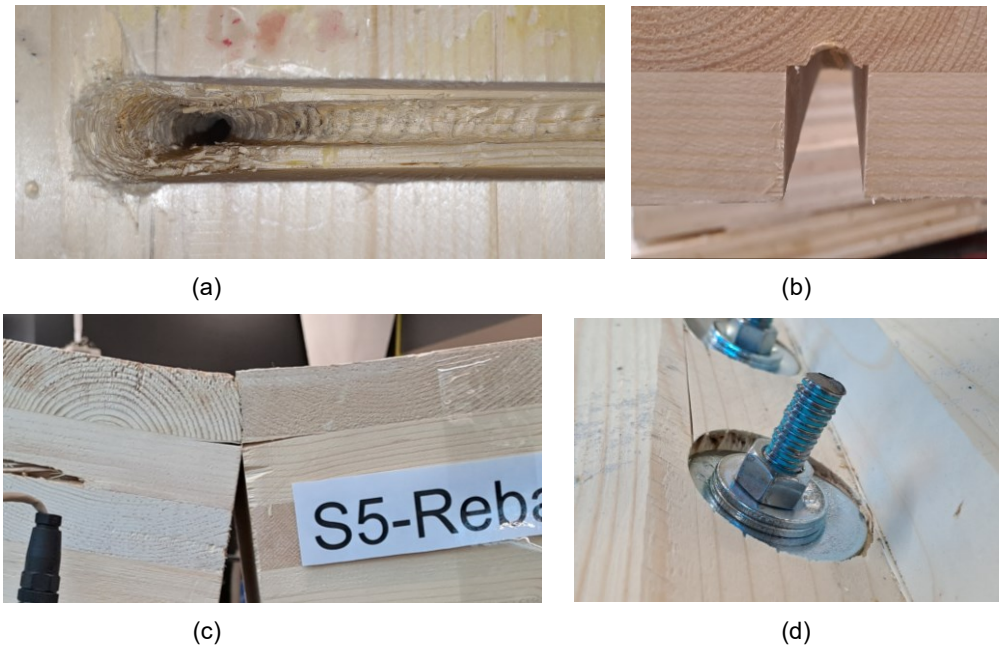

Figure 3-14: Failure modes series S5: (a) S5A slot view, S5, (b) connecting section, (c) CLT panel compression zone, (d) S5B rebar end compression zone

3.5.3 ***4-point bending test result analyses***

The results from the 4-point bending tests: loading carrying capacity (F_{ult}), deflection ($d_{@ult}$), connection gap opening ($g_{@ult}$), transferred bending moment (M_{ult}), rotational stiffness (C_{φ}), and ductility (μ) are summarized in Table 3-1.

Table 3-1: Results summary from 4-point bending tests

	Test series	S1-STS	S2-Glue		S3-Tjoint	S4-Xfix	S5-Rebar	
			Grade B	Grade C			A	B
F_{ult} [kN]	Mean	76.6	77.9	32.7	39.2	18.7	50.0	67.6
	Max	80.2	86.2	-	44.4	19.7	-	-
	Min	72.5	68.1	-	35.6	17.4	-	-
	CoV	4%	9%	-	8%	3%	-	-
M_{ult} [kNm]	Mean	33.3	35.5	15.0	17.1	8.1	21.8	29.4
	Max	34.9	39.0	-	19.3	8.6	-	-
	Min	31.5	30.8	-	15.5	7.5	-	-
	CoV	4%	9%	-	7%	7%	-	-
$d_{@Fult}$ [mm]	Mean	42.2	19.7	10.6	31.3	30.0	185	181
	Max	51.5	23.6	-	37.7	34.1	-	-
	Min	33.7	17.1	-	23.3	25.8	-	-
	CoV	14%	14%	-	14%	2%	-	-
$g_{@Fult}$ [mm]	Mean	5.2	0.5	0.5	3.2	6.4	48	38
	Max	5.7	0.6	-	7.0	6.8	-	-
	Min	4.2	0.3	-	5.0	5.8	-	-
	CoV	11%	20%	-	29%	8%	-	-
C_{φ} [kNmrad^{-1}]	Mean	3,555	47,834	24,085	2,476	853	847	486
	Max	5,644	83,581	-	3,830	1,062	-	-
	Min	2,347	12,900	-	1,563	533	-	-
	CoV	34%	54%	-	32%	33%	-	-
μ	Mean	2.3	≈ 1	≈ 1	3.2	2.2	10.1	2.7
	Max	2.9	≈ 1	-	3.9	2.6	-	-
	Min	1.8	≈ 1	-	2.3	1.9	-	-
	CoV	21%	-	-	20%	15%	-	-
	Replicates	6	6	2	6	3	1	1

The glued spline connection (S2B) exhibited the highest bending moment capacity, followed by the screwed spline (S1), steel rebar joint (S5), T-joint (S3), and X-fix (S4) , as depicted in Figure 3-15, with capacities at 94%, 83%, 47%, and 23% respectively, relative to series S2B. Notably, the coefficient of variation (CoV) in bending moment capacity remained small (<10%) for all series.

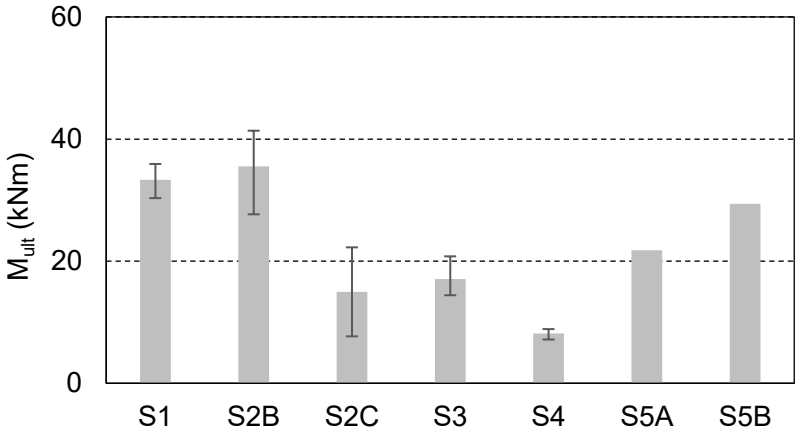

Figure 3-15: Moment resistance of connection configurations in 4-point tests

Samples in the S2B series demonstrated the least amount of deflection at peak load, with approx. 20 mm. In contrast, specimens in the S5 series exhibited notably higher deflection, reaching 185 mm. This deflection trend corresponded to the degree of gap opening within the connections, with S5 samples exhibiting the widest gaps, measuring 48 mm and 38 mm for S5A and S5B, respectively, whereas S2 registered less than 1 mm. Further, S1 exhibited an average deflection of approximately 42 mm, while S3 and S4 displayed deflections around 31 mm at the peak load. Variability of deflection was around 14% within most test series.

Figure 3-16 shows the typical moment-rotation curve of these connections, in which the slope of each series represents the rotational stiffness value. As can be seen series S2 samples (glued splines) exhibited superior rotational stiffness with 47,800 kNmrad^{-1}. Screwed connections S1 and S3 reached roughly 3,500 kNmrad^{-1} and 2,500 kNmrad^{-1}, respectively. Conversely, S4 (X-fix) and S5 (rebar) connections reached rotational stiffness values less than 1,000 kNmrad^{-1} (Figure 3-17). However, it has to be noted, that due to the very small displacements, even minor differences created a large variability in the rotational stiffness of the glued joints (CoV = >50%), while CoVs for the other connection configurations were around 30%.

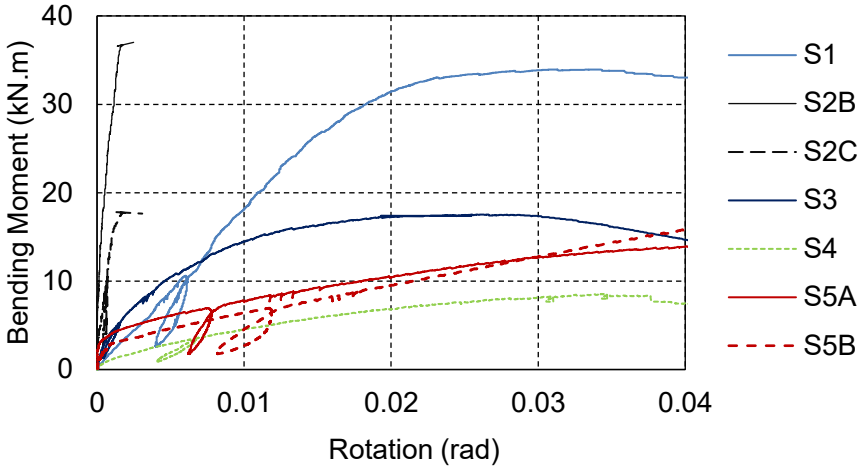

Figure 3-16: Typical moment-rotation curves of 4-point tests

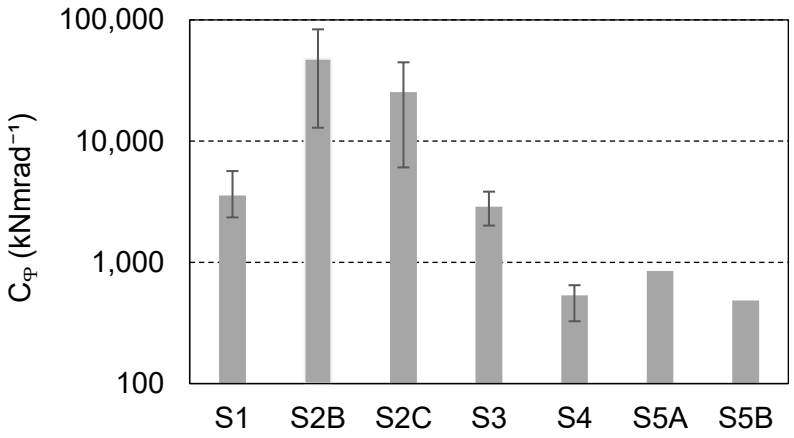

Figure 3-17: Rotational stiffness of connection configurations in 4-point bending tests

In terms of ductility, S2 exhibited a completely brittle behavior, with the yielding and failure points coinciding. S5A demonstrated ductile performance, reaching approximately 10. Following this, S3, S1, and S4 exhibited limited ductility of 3.2, 2.3, and 2.2, respectively. However, for S5B, the type of failure mode and maximum deflection in the experiment prevented an accurate representation of its ductility value, despite its deflection being almost equal to that of S5A.

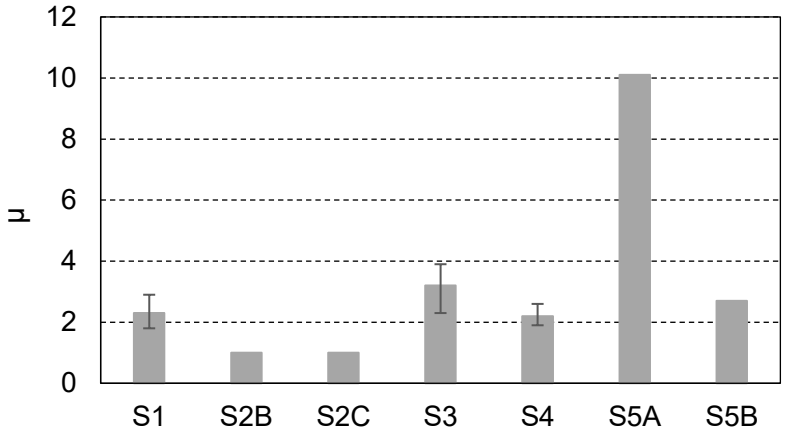

Figure 3-18: Connection ductility in 4-point tests

3.5.4 ***Load-displacement behavior of 3-point bending tests***

Figure 3.16 depicts the typical load-deflection characteristics resulting from 3-point bending tests on screwed spline (S1), glued spline (S2), and T-joint (S3) connections. The individual load-displacement curves are shown in Appendix B.

The spline plate with inclined STS had an initially linear response, extending up to approximately 85 kN (57% of peak load), at an average mid-span deflection of about 10 mm. Subsequently, a nonlinear part developed up to peak load, averaging 150 kN, with an associated deflection of approximately 26 mm. The glued spline plates exhibited a purely linear behavior until reaching an average load-carrying capacity of 115 kN, equivalent to a deflection of 13 mm coinciding with a sudden and abrupt failure. The T-joints encompassed a linear segment up to 50 kN and 7 mm displacement, a second segment with reduced stiffness up to peak load of approximately 67 kN, and a gradual decline with the capability of experiencing a 50% drop in load-carrying capacity.

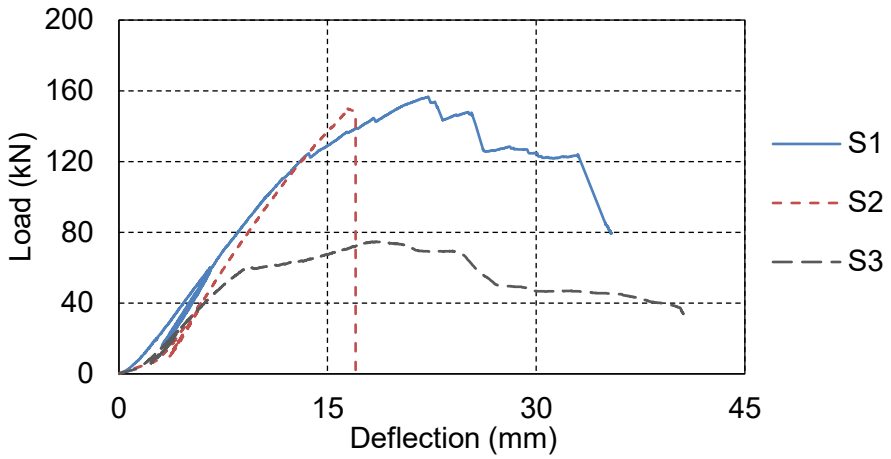

Figure 3-19: Load-deflection curves of 3-point bending tests

3.5.5 ***Failure modes of 3-point bending tests***

Some typical failed specimens are shown in Figure 3-20. More photos are provided in Appendix D. For spline plate with inclined STS connections (S1), the first audible signs of damage were detected around 70 kN, corresponding to an average mid-span deflection of 8 mm. The typical initial damages often included separation at the second layer, occurring within or at the top or bottom of this layer. This was followed by rolling shear failure emerging on the panel surface between the loading point and the connecting line (Figure 3-20a).

In the glued spline connections (S2), upon reaching the peak load at approximately 115 kN, equivalent to an average deflection of 12.6 mm, a sudden failure occurred. This failure point was concentrated in the area where the plywood comes into contact with the CLT, involving a combination of failures in solid wood, and plywood (Figure 3-20b).

In T-joint connections (S3), a horizontal crack appeared on the compression side of the second layer of the right panel at the connecting line, under a load of approximately 55 kN (Figure 3-20c), attributable to the low out-of-plane shear resistance of the connection. As the loading increased, it

resulted in an unleveled surface at the bottom of the connecting line and a leveled surface at the top of the sample, due to friction preventing sliding at the compression side between the two panels, (Figure 3-20d). Furthermore, sliding caused the tearing from the corner of the seventh layer due to the rotation of STS and T-joint, applying tension load perpendicular to the grain.

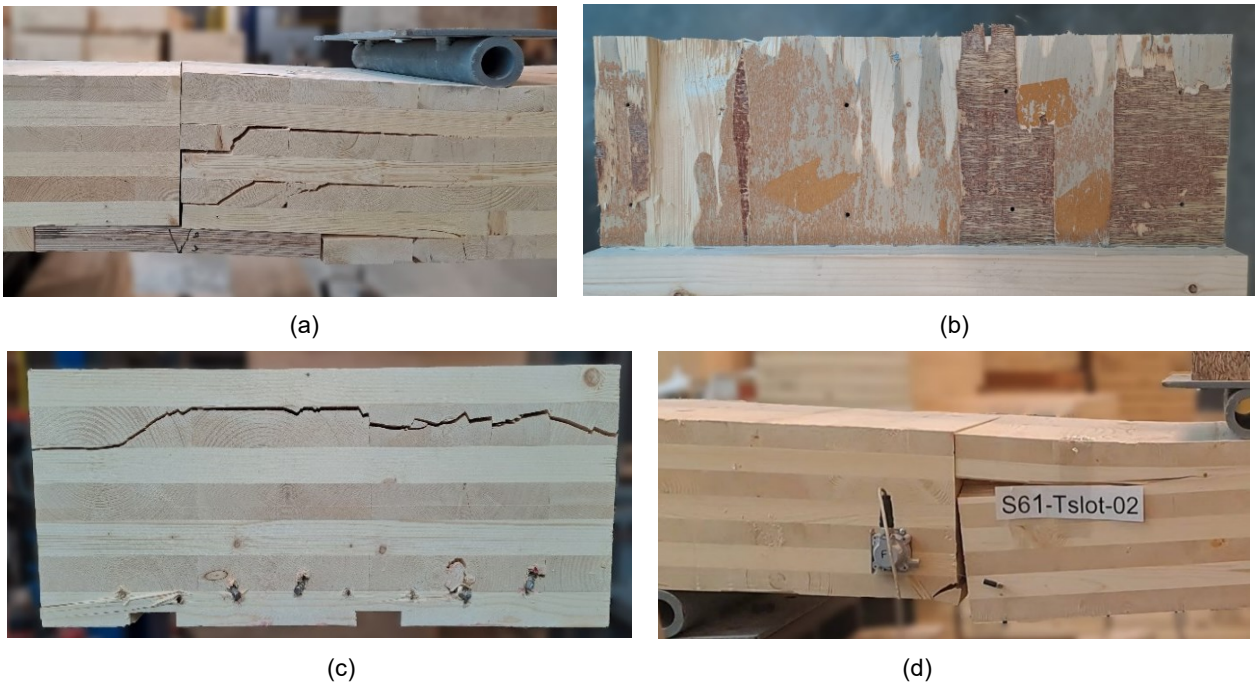

Figure 3-20: Failure modes in 3-point tests: a) S1, b) S2 plywood surface c) S3 cross section at connecting line, d) S3 side view

3.5.6 ***3-point bending test result analyses***

The results from 3-point bending tests on series S1, S2, S3, and S0 (solid panel) are summarized in Table 3-2, including $M_{ult,joint}$ (connection bending moment capacity), $d_{@Fult}$, $d_{j@Fult}$ (displacement at the connecting line), $g_{@Fult}$, V_{ult} (out-of-plane shear resistance), and $C\varphi$.

Series S1 reached the highest loading carrying capacity, shear and bending moment resistance, exceeding that of S2 and S3 by approximately 77% and 47%, respectively (Figure 3-21 a and b).

Concerning deflection, S2 exhibited the least deflection at about 13 mm, followed by S3 and S1, with average deflections of 18 mm and 28 mm, respectively.

Table 3-2: Results summary from 3-point bending tests

	Test series	S1-STS	S2-Glue	S3-Tjoint	S0-Full
V_{ult} [kN]	Mean	75.0	57.5	19.6	108.3
	Max	83.2	74.9	22.2	111.3
	Min	66.3	47.7	17.8	105.0
	CoV	8%	17%	9%	3%
$M_{ult,joint}$ [kNm]	Mean	32.8	26.2	15.4	-
	Max	36.4	34.8	17.1	-
	Min	29.03	22.1	13.3	-
	CoV	8%	18%	9%	-
$d_{@Fult}$ [mm]	Mean	27.8	12.6	18.0	14.9
	Max	43.7	16.4	25.0	15.6
	Min	16.1	10.9	10.0	14.5
	CoV	33%	16%	24%	4%
$d_{joint@Fult}$ [mm]	Mean	19.8	10.9	21.9	-
	Max	23.4	13.5	31.3	-
	Min	13.7	10.1	10.8	-
	CoV	18%	13%	32%	-
$g_{@Fult}$ [mm]	Mean	4.1	0.17	5.0	-
	Max	6.55	0.25	8.2	-
	Min	2.18	0.1	2.1	-
	CoV	37%	34%	41%	-
$C\varphi$ [kNmrad^{-1}]	Mean	6590	32533	2869	-
	Max	8522	55733	4383	-
	Min	4223	17335	2104	-
	CoV	22%	56%	30%	-
	Replicates	6	6	6	3

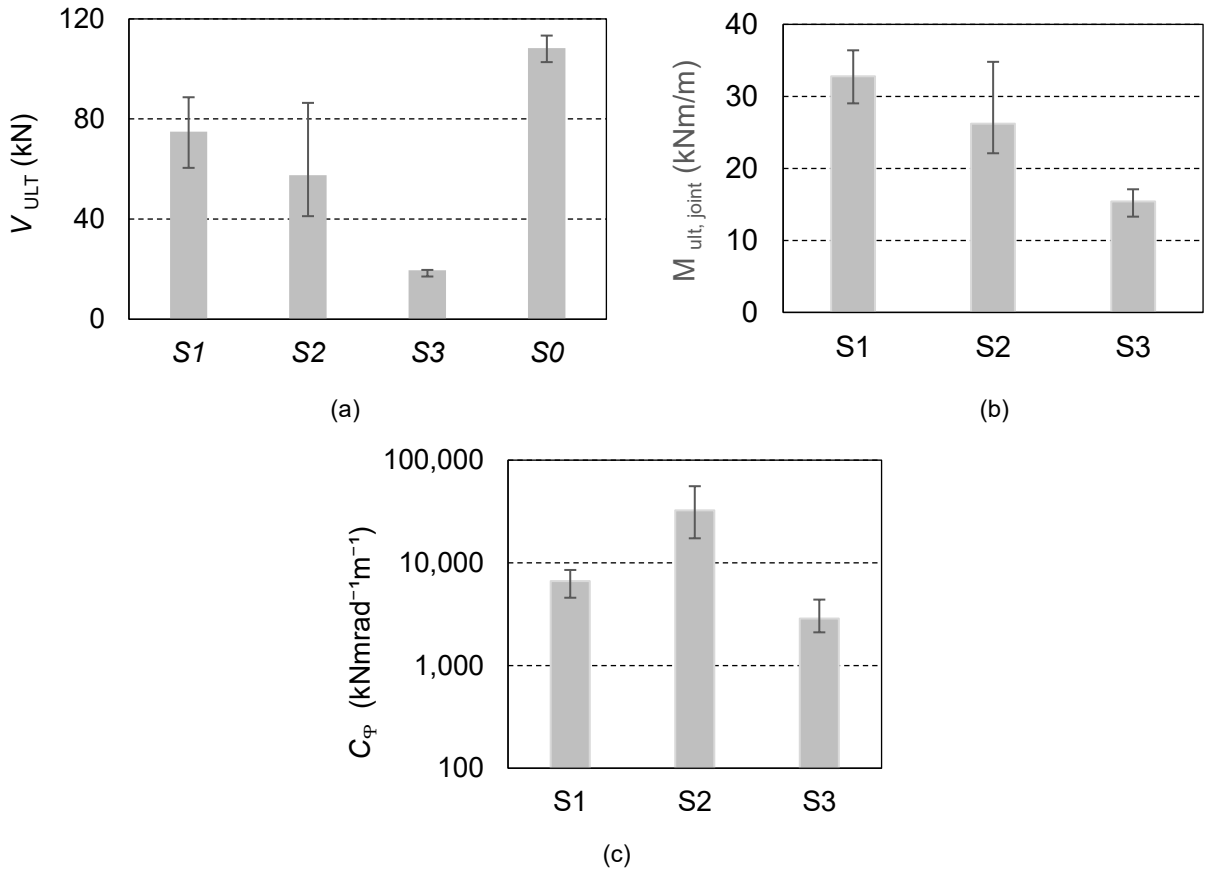

Figure 3-21: 3-point bending tests: (a) shear resistance, (b) moment resistance and (c) rotational stiffness

The gap opening within the S2 series was less than 1 mm, whereas S1 and S4 both exhibited values of approximately 5 mm. The rotational stiffness, $C\varphi$, for series S1 and S3 was about 20% and 9% of S2, respectively (Figure 3-21c). It is noteworthy that the variability in $C\varphi$ for S2 was notably higher, with a CoV of 56%. Examining the CoV for shear resistance, S2 displayed the highest value with 17%. S3, with a CoV of 9%, demonstrated a moderate degree of variability. In contrast, S0-Full and S1, with CoVs of 3% and 8%, respectively, showcased lower levels of variability compared to their means.

3.5.7 ***Reference specimen***

Three CLT panels without connection were tested. The load-deflection curves, shown in Figure 3-22a, reveal an initial stage, characterized by an almost linear behavior up to the peak load (on average 217 kN at an average deflection of 15 mm), followed by a sudden drop in load-carrying capacity. The first sign of damage at a load of 85 kN was manifested by audible cracking noises. Initial small rolling shear cracks emerged at a load of 195 kN. As the sample approached the peak load, rolling shear failures transpired, succeeded by delamination, as shown in Figure 3-22b.

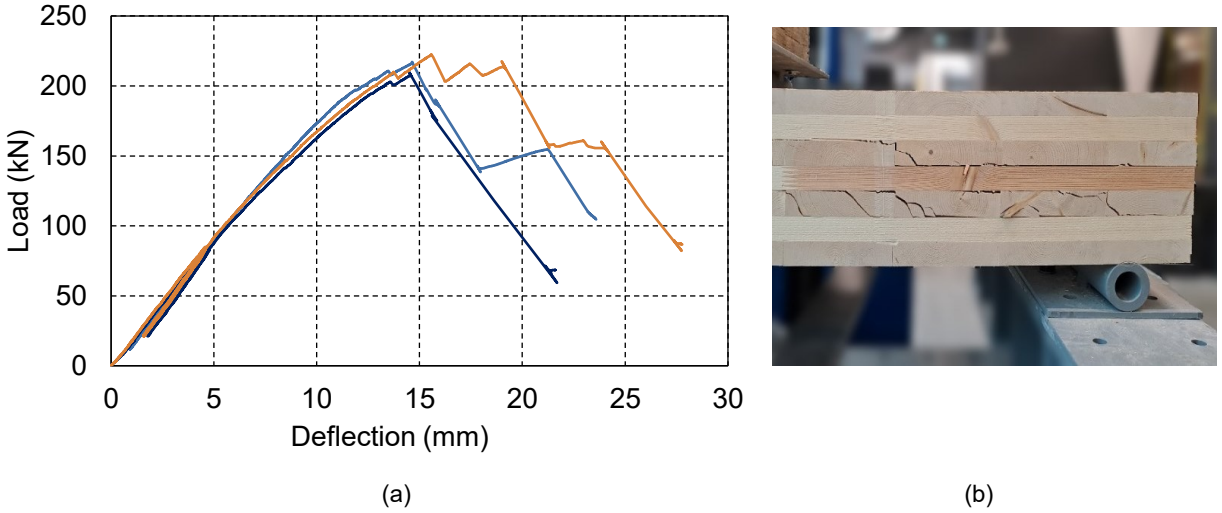

Figure 3-22: 3-point test of continuous panel: (a) load-displacement curve and (b) failure mode

4 Numerical investigations

4.1 Overview

The numerical investigation aimed to determine: i) the demand on the joints between adjacent CLT panels in various floor scenarios; and ii) the maximum bending moment capacity that can be transferred in the minor direction as a function of joint rotational stiffness.

In Figure 4-1, a floor consisting of three CLT panels, each with dimensions of $b.L$ is displayed. The three panels were connected along the minor direction throughout the length of the panels (L), as indicated by the dashed lines. The points indicated rectangular point supports, each 300 mm × 300 mm in size. These supports were located in the center line of the side panels along the major direction at a distance (e) from the edges in the major direction. Consequently, the span between point supports was $L\text{-}2{\cdot}e$ in the major direction and $2{\cdot}b$ in the minor direction (Table 4-1).

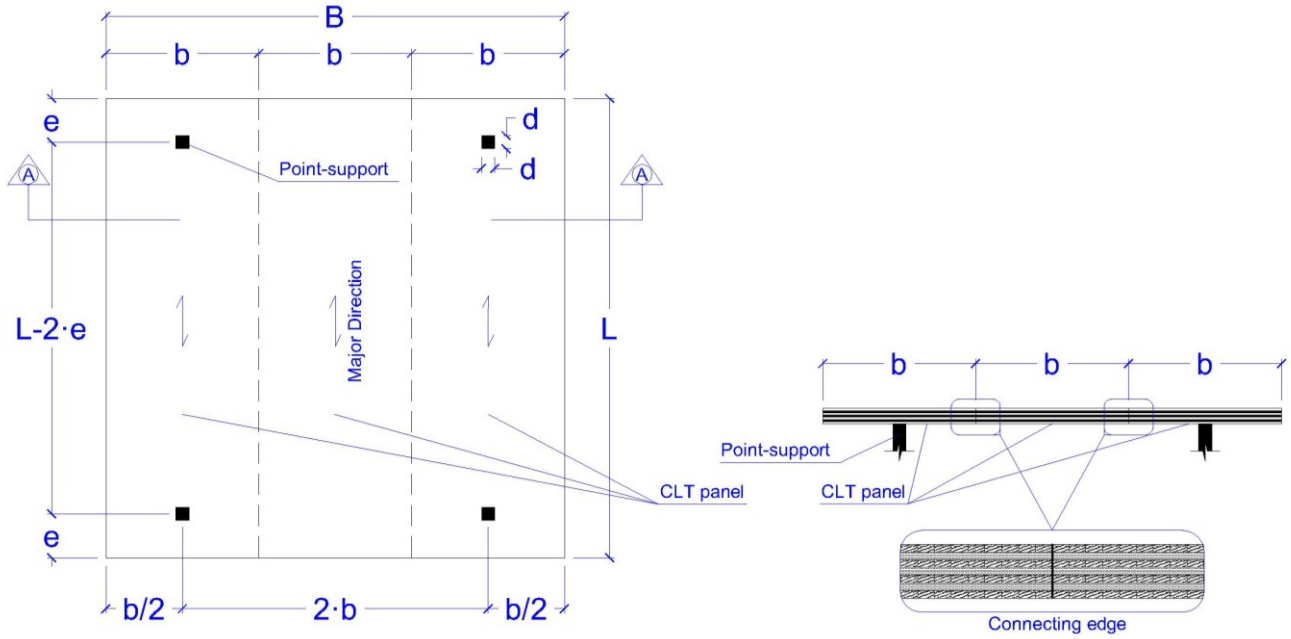

Figure 4-1: Geometry of point-supported floor: (a) top view, (b) cross section A-A along minor direction

Uniform dead (*DL*) and live loads (*LL*) were applied to the floors, with the load combinations for the ultimate limit state (ULS) and serviceability limit state (SLS), referring to the maximum load-carrying capacity and allowable deflection, respectively [72]. Two levels of uniform live load of, 1.9 kPa and 2.4 kPa, were considered for residential and office buildings, respectively. These loads were accompanied by a uniformly applied dead load of 1.0 kPa, excluding the self-weight of the CLT panels, which was also considered in the analysis. The floors were designed to meet deflection limits: $L/180$ for total loads and $L/360$ for live loads as outlined in the National Building Code of Canada (NBCC) [73]. Additionally, the critical load combination for ULS design was $1.4 \cdot DL + 1.25 \cdot LL$.

The selection of rotational stiffness was based on the previous experimental findings presented in Chapter 3, ranging from 500 to 5,000 $kNmrad^{-1}m^{-1}$. Stieb et al. [55] observed that changes in rotational stiffness up to around 5,000 $kNmrad^{-1}m^{-1}$ were found to have a more significant impact on floor structural performance. This observation was corroborated by initial analyses, indicating that 500 $kNmrad^{-1}m^{-1}$ satisfies the SLS. Consequently, this study selected stiffness values of 500, 1,000, 1,500, 2,000, and 5,000 $kNmrad^{-1}m^{-1}$, and a continuous panel representing an infinite value.

Table 4-1: Model parameters floor dimensions (m)

b	$B = 3 \cdot b$	L	e
2.4	7.2	7.2	0.5 and 1.0
2.4	7.2	9.5	0.5, 1.0, and 1.5
3.0	9.0	9.0	1.5

4.2 **Model development**

The numerical models were developed utilizing the RFEM 6 software [61], employing the RF-Laminate module for CLT. Following a sensitivity analysis, a 150 mm mesh size was chosen. The

floor was modeled as a plate element with three degrees of freedom at each node, comprising one translation and two rotations, as illustrated in Figure 4-2.

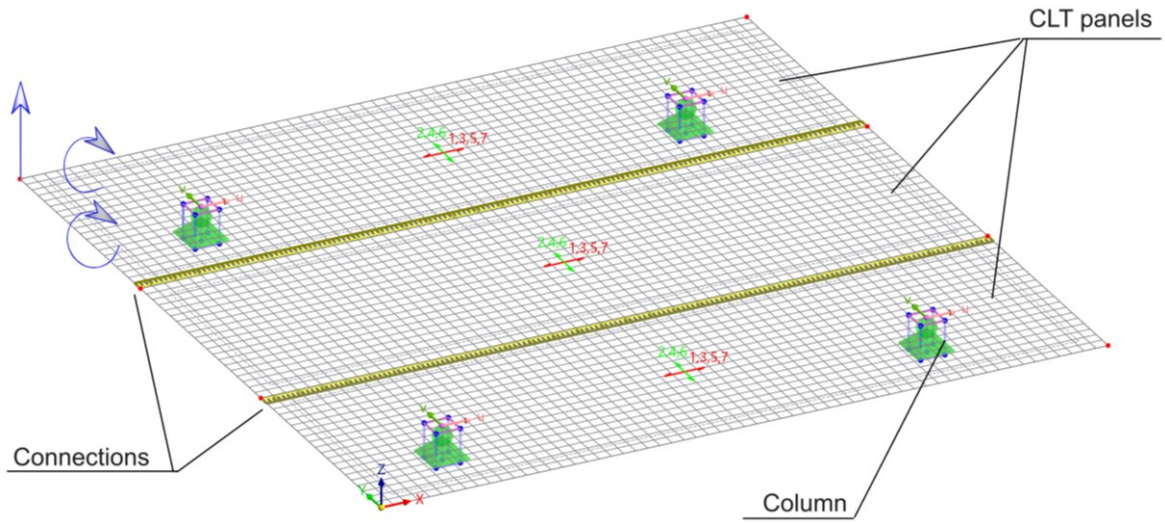

Figure 4-2: RFEM model of point-supported CLT floor

The point supports' boundary conditions had their translation constrained in all directions and all rotational degrees of freedom. The floor was treated as a single isolated unit, with no constraints applied at the surrounding ends. The predefined surface stiffness type had the capability to transfer both moments and membrane forces [74]. Figure 4-2 depicts an isometric view of the floor model.

To attain a precise depiction of the stress distribution at support areas, adjustments to the surface results were specified for connection zones between columns and the floor. This involves establishing areas that match the dimensions of the columns, simulating column performance by averting stress concentration at the support area [75], depicted as virtual columns in Figure 4-2.

Wood was modelled as a linear elastic transverse isotropic material, accounting for the parallel and perpendicular to the grain directions. CLT properties of grades E1 and V2 were employed in accordance with PR-L332(C) [62]. The panels had a thickness of 245 mm, with seven 35 mm thick

layers. The stiffness and strength parameters for these panels are provided in Table 4-2. Figure 4-3 illustrates the nomenclature employed, elucidating the CLT grade, the floor spans, the live load, and the distance from the support centreline to the panel edge.

Table 4-2: Material properties for the FEM simulation (MPa) [76]

CLT Grade	Major strength direction					Minor strength direction				
	Grade & Species	f_b	E	f_t	f_s	Grade & Species	f_b	E	f_t	f_s
E1	1950f-1.7E SPF	28.2	11700	15.4	0.5	No. 3 SPF	7.0	9000	3.2	0.5
V2M6	No. 1/No. 2 SPF	11.8	9500	5.5	0.5	No. 1/No. 2 SPF	11.8	9500	5.5	0.5

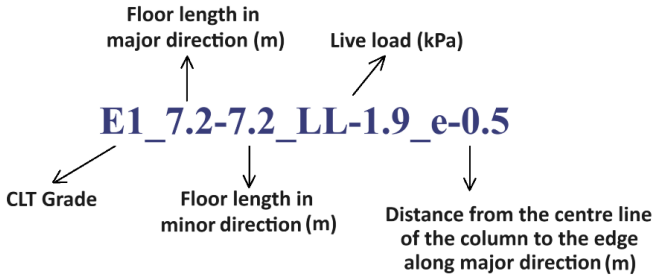

Figure 4-3: Models labelling convention

4.3 **Model validation**

The model was validated by comparing the numerical and experimental load–deflection curves. The reference specimens (S0 series, see Figure 4-4a) represent the characteristics of CLT panels, along with support and loading conditions, without considering any connection behavior. Additionally, the S1 series was selected for both 4-point bending tests (Figure 4-4b) and 3-point bending tests (Figure 4-4c). Rotational stiffness was simulated using connection test results within the ranges of 10% to 40% and 40% to 80%. All dimensions and boundary conditions were aligned with those employed in the experimental setup. The line supports had no rotational restrictions, and loads were applied as line loads. When ignoring the initial alignment behaviour, the model and

experiments align reasonably well, demonstrating the validity of the numerical model for the present experiments within the linear range.

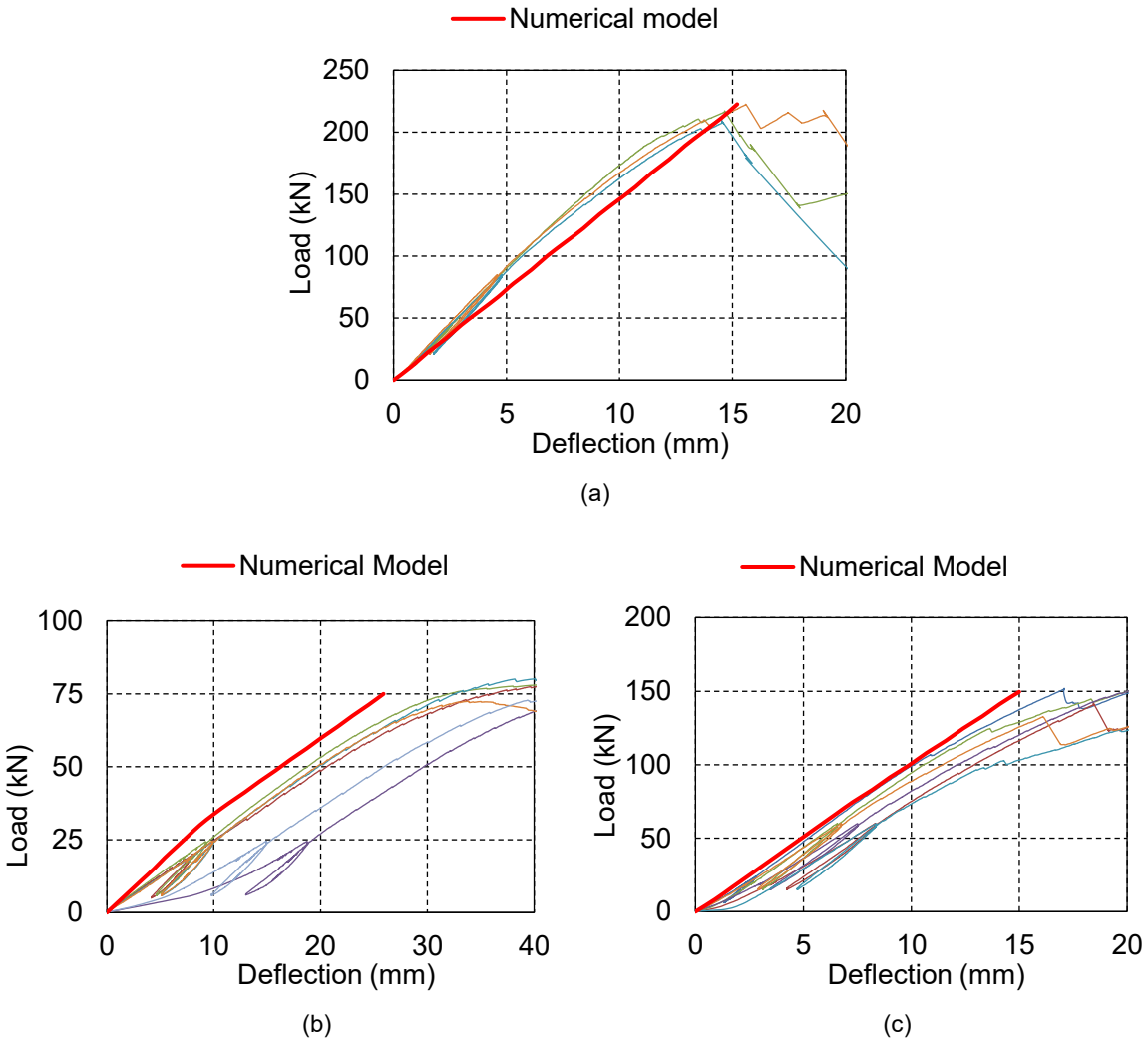

Figure 4-4: Numerical validation of experiments; (a) 3-point bending tests of solid panels, (b) 4-point bending tests of S1 series, (c) 3-point bending tests of S1 series

4.4 Results and discussion

4.4.1 Impact of rotational stiffness on bending moment

Figure 4-5 and Figure 4-6 depict the distribution of bending moment and shear force along the connecting line. Consistently for all floor configurations, larger bending moments and shear forces are observed at the ends of the connecting line compared to the midpoint. Reducing the rotational stiffness leads to a more balanced distribution of bending moment along the connecting line. For a floor with a $C\varphi$ of 500 kNmrad^{-1}m^{-1}, the bending moment ranges from 8.4 to 10.8 kNm/m, while for a continuous floor (with infinite $C\varphi$), it varies from 5.7 to 14.3 kNm/m. The smaller value of rotational stiffness leads to a reduction at the ends of the connecting line and an increase at the midpoint, but the average value remains constant as shown in Figure 4-5b, rotational stiffness does not affect the internal out-of-plane shear force.

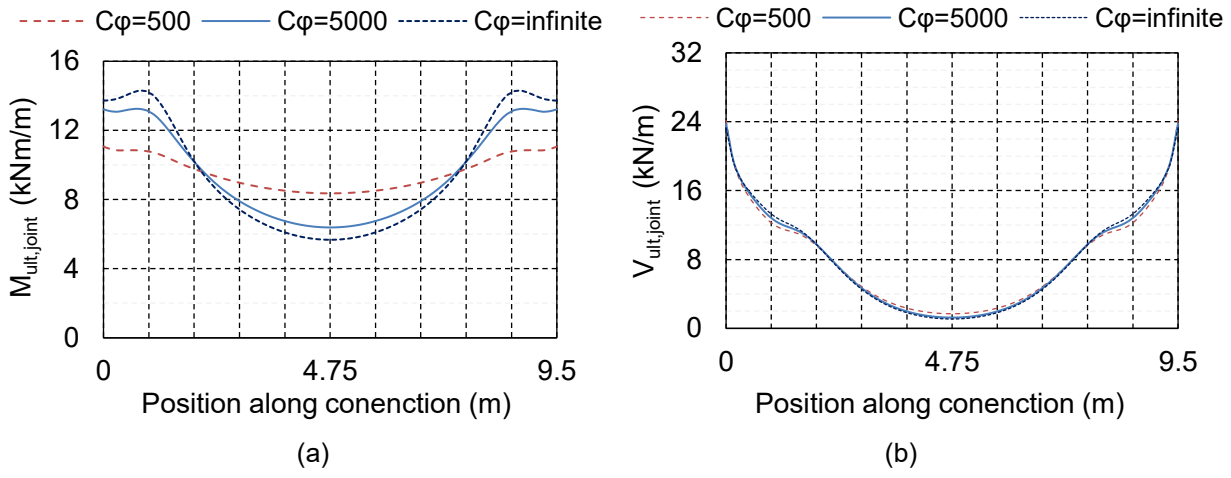

Figure 4-5: Impact of C_φ on internal loads at the connecting line for floor V2_9.5-7.2_LL 1.9_e 1.0; (a) bending moment diagram, (b) shear force diagram

Increasing the column edge distance (e) promotes a more uniform distribution of bending moments along the connecting line, as depicted in Figure 4-6. Large e brings higher and lower bending moment values closer to the average.

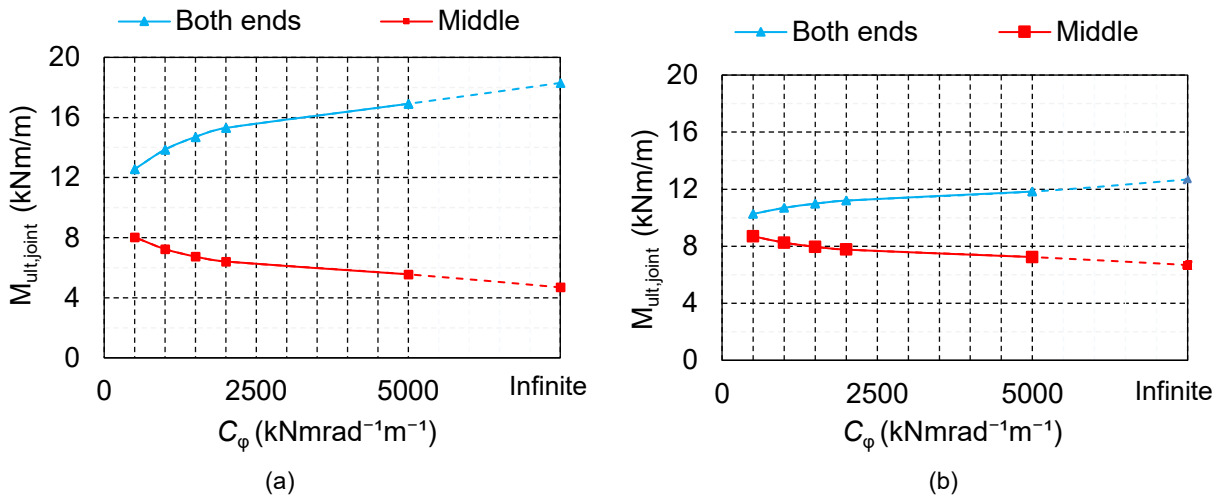

Figure 4-6: Bending moment at connecting line V2_9.5-7.2_LL 1.9 for (a) e=0.5 m, (b) e=1.5

Figure 4-7 and Figure 4-8 display the impact of rotational stiffness (C_φ) and column edge distance (e) on the internal bending moment distribution in the minor and major directions, respectively. For the minor direction, an inverse relationship between rotational stiffness and uniformity of bending moment is confirmed. As rotational stiffness decreases, the stress gradients become smoother compared to a continuous floor. Furthermore, it can be inferred that in floors with higher rotational stiffness, the connections located at both ends of the connecting line exert a more significant impact on internal bending moment transmission. In continuous floors, the blue area representing the highest bending moment is concentrated at the free edge of the middle panel.

In the major direction (Figure 4-8), transitioning from a continuous panel to 500 kNmrad^{-1}m^{-1} increases the bending moment by only 4% at the column strip in the major direction. It is also noteworthy that in the middle panel, the primary factor influencing the maximum bending moment is positive bending moments along the minor direction, while in the side panels, the maximum bending moment is usually due to negative bending moments along the same direction. The variations in the bending moment in the major direction due to changes in rotational stiffness are approximately one-third of those observed in the minor direction.

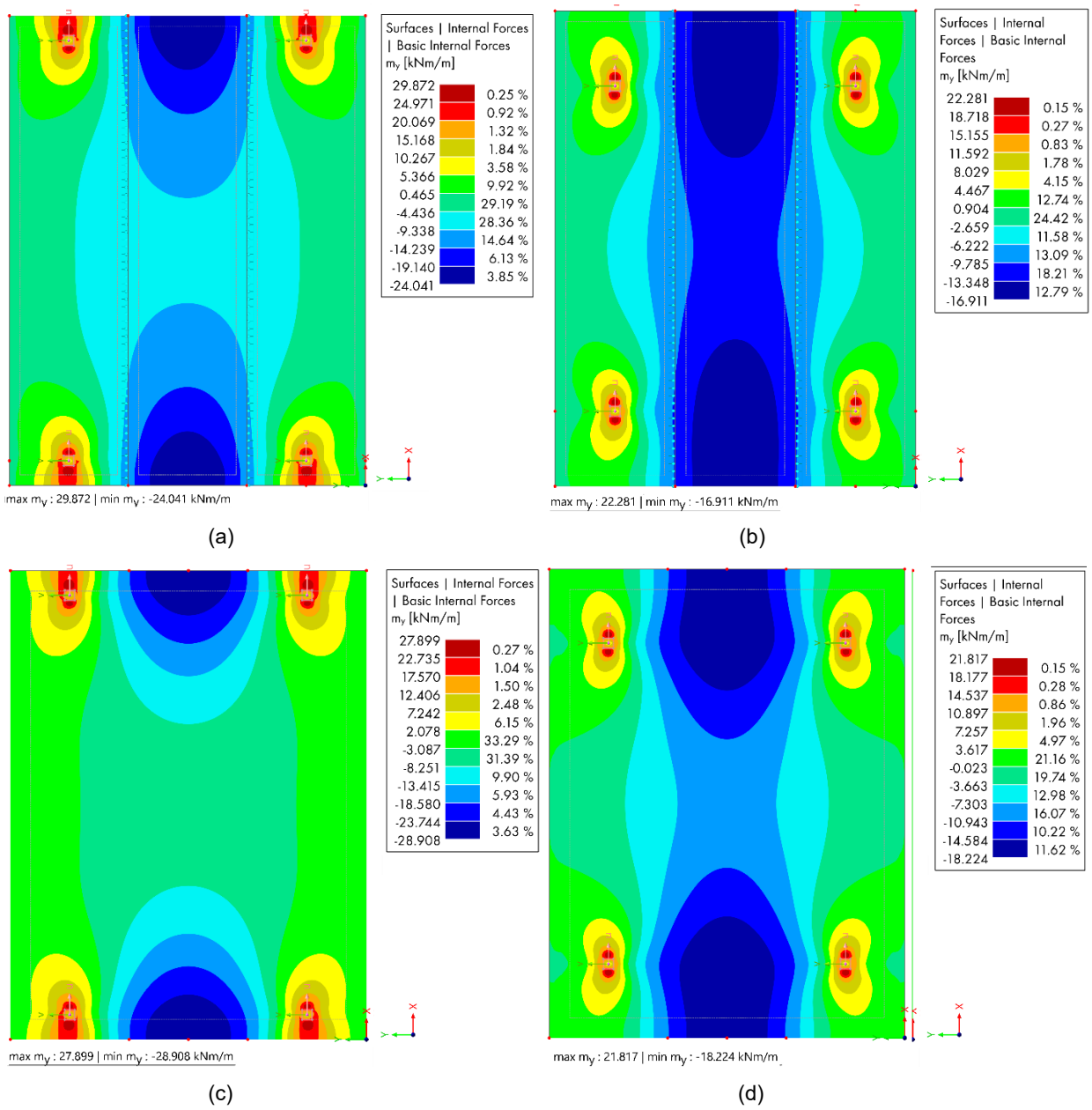

Figure 4-7: Impact of Cφ and e on bending moment along minor direction for floor V2_9.5-7.2_LL 1.9; (a) e=500 mm, Cφ = 500, (b) e=1500 mm, Cφ = 500, (c) e=500 mm, Continuous floor, (d) e=1500 mm, Continuous floor

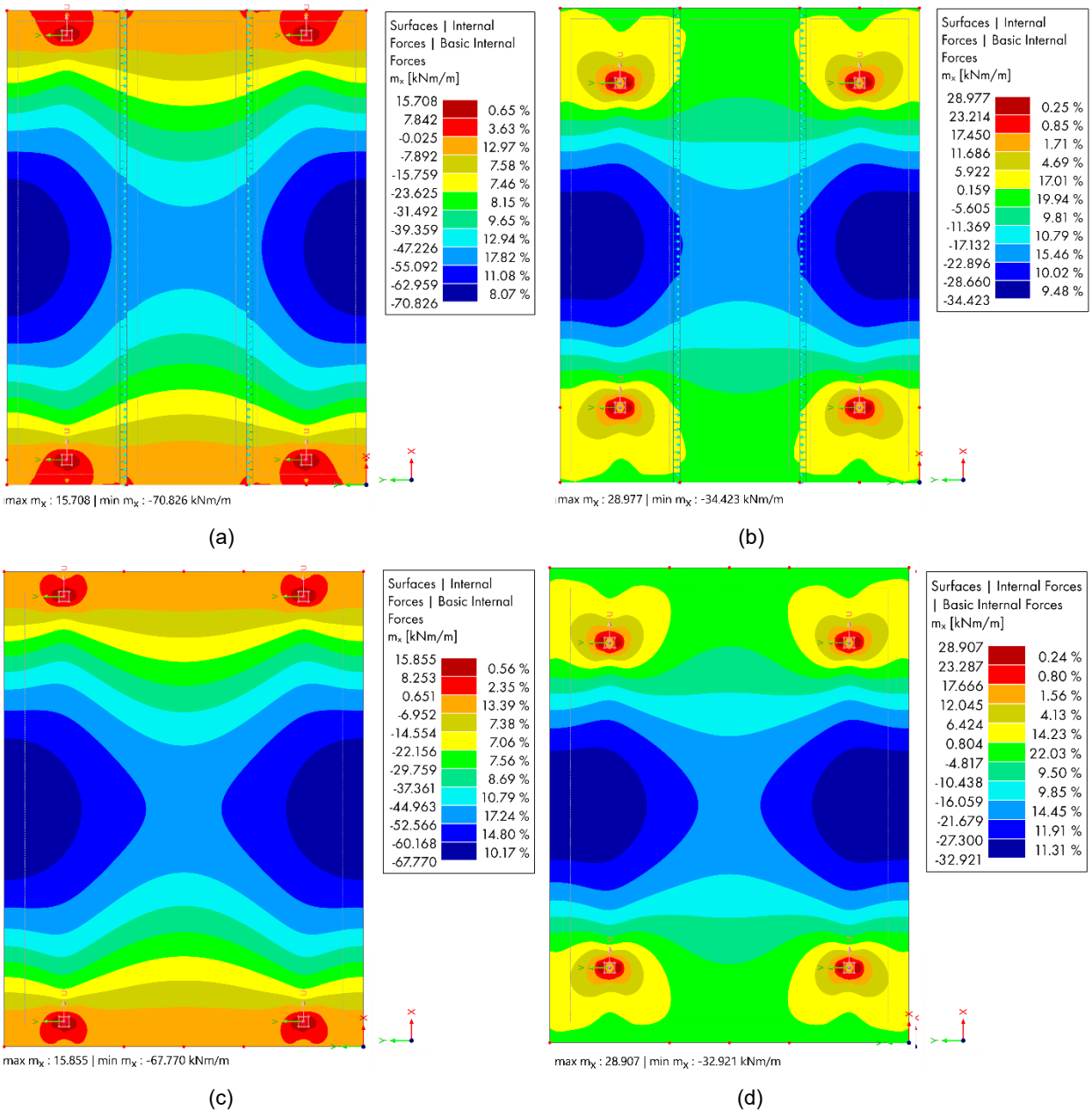

Figure 4-8: Impact of Cφ and e on bending moment along minor direction for floor V2_9.5-7.2_LL 1.9; (a) e=500 mm, Cφ = 500, (b) e=1500 mm, Cφ = 500, (c) e=500 mm, Continuous floor, (d) e=1500 mm, Continuous floor

4.4.2 Impact of rotational stiffness on the ULS and SLS panel utilisation

The impact of rotational stiffness on the ULS utilization (ratio of load to capacity) for bending moment in both major and minor directions is depicted in Figure 4-9, while the SLS utilization (ratio of deflection to deflection limit) is shown in Figure 4-10. The ULS ratio pertains to the out-of-plane bending moment resistance according to CSA O86 [76]. Across all scenarios, an increase in rotational stiffness leads to a slight reduction in the maximum ULS ratio for the major direction, while a minor increase is discerned for the minor direction, ranging from 3% to 8%.

Comparatively, the SLS ratio exhibits heightened sensitivity to rotational stiffness, particularly at lower values. Even slight increments in rotational stiffness result in substantial enhancements in the SLS ratio. However, as evidenced in Figure 4-10, this effect gradually diminishes once a rotational stiffness of around 5000 kNmrad^{-1}m^{-1} is reached. After surpassing this point, the influence of rotational stiffness becomes inconsequential on the floor SLS ratio (Figure 4-10).

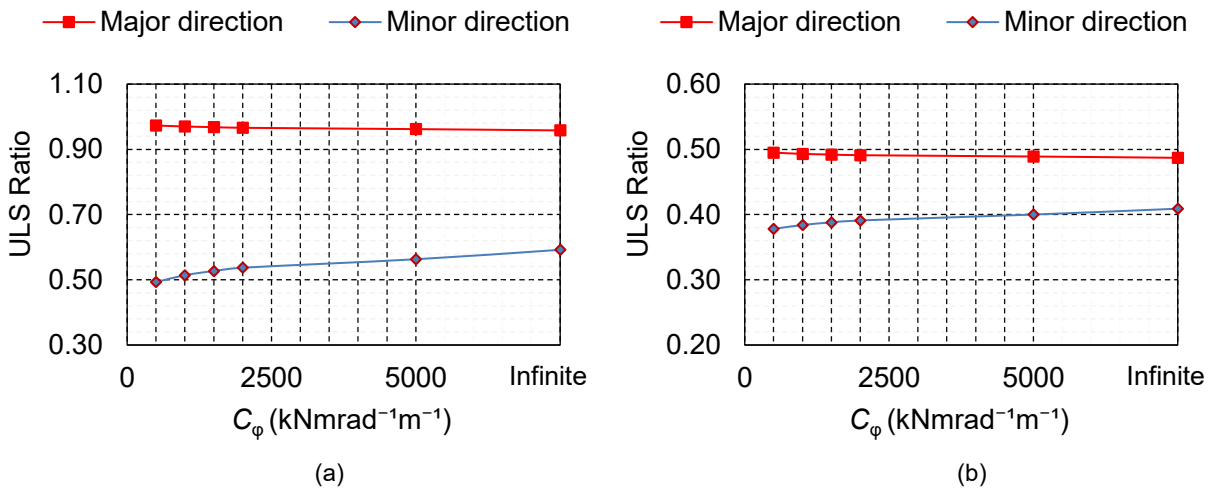

Figure 4-9: Impact of Cφ on the ULS V2_9.5-7.2_LL 1.9; for (a) e=0.5, (b) e=1.5

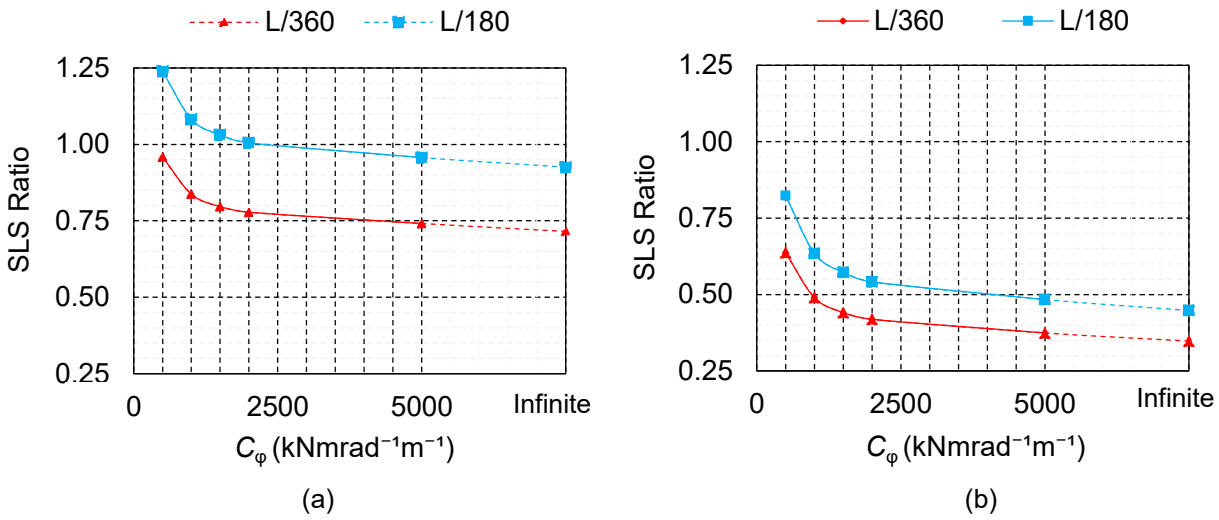

Figure 4-10: Impact of Cφ on the SLS ratio for V2_9.5-7.2_LL 1.9; (a) e=0.5, (b) e=1.0, (c) e=1.5

*4.4.3 **Impact of rotational stiffness on floor deflection***

The sensitivity of floor deflection to rotational stiffness at various floor span aspect ratios is illustrated in Figure 4-11. The vertical axis represents the ratio of edge-connected floor deflection ($U_{z,ec}$) to continuous floor deflection ($U_{z,c}$), while the horizontal axis represents changes in rotational stiffness. Consequently, each line on this graph demonstrates the impact of rotational stiffness on floor deflection, scaled against a continuous floor, for each analyzed floor scenario. The results underscore the significance of floor aspect ratio: floors with smaller span ratios exhibit much higher sensitivity to rotational stiffness, particularly at lower levels of rotational stiffness. For example, considering 500 kNmrad^{-1}m^{-1} rotational stiffness, the maximum deformation for floors with span aspect ratios of 1.0 and 1.8 is 2.2 and 1.3 times higher than the maximum deformation of a continuous floor, respectively.

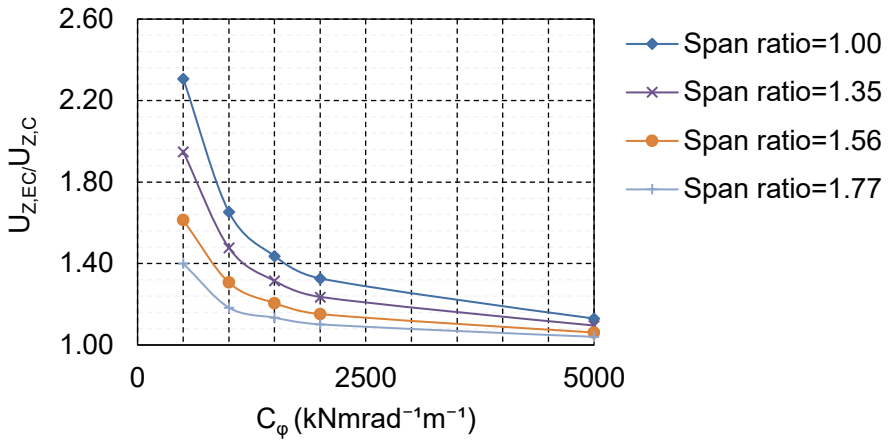

Figure 4-11: Influence of floor span ratio on floor deformation sensitivity for CLT grade V2

In Figure 4-12, the influence of rotational stiffness and the floor span ratio on the deformation pattern shape of the floor is depicted. In Figure 4-12d, for the continuous floor, the two-way performance is enhanced, especially when the floor span ratio approaches 1:1. In contrast, in Figure 4-12c, the continuous floor deflects similarly to a one-way floor due to the larger span ratio. For edge-connected floors, as shown in Figure 4-12a and Figure 4-12b, reducing the rotational stiffness significantly impacts the floor deformation shape, resulting in opposite outcomes to those seen in continuous floors. Consequently, while the distinction between two-way and one-way action in floor behavior depends on the floor aspect ratio, influencing the floor's deformation pattern and load distribution direction, for edge-connected floors, the significance of the floor aspect ratio can be diminished or rendered less effective based on the value of rotational stiffness. Consequently, it can be asserted that edge-connected floors with a lower value of rotational stiffness tend to exhibit cranking in two directions, indicating a proclivity towards one-way action characterized by a cylindrical deformation shape, even when the aspect ratio of these floors falls within the range typical of two-way floors.

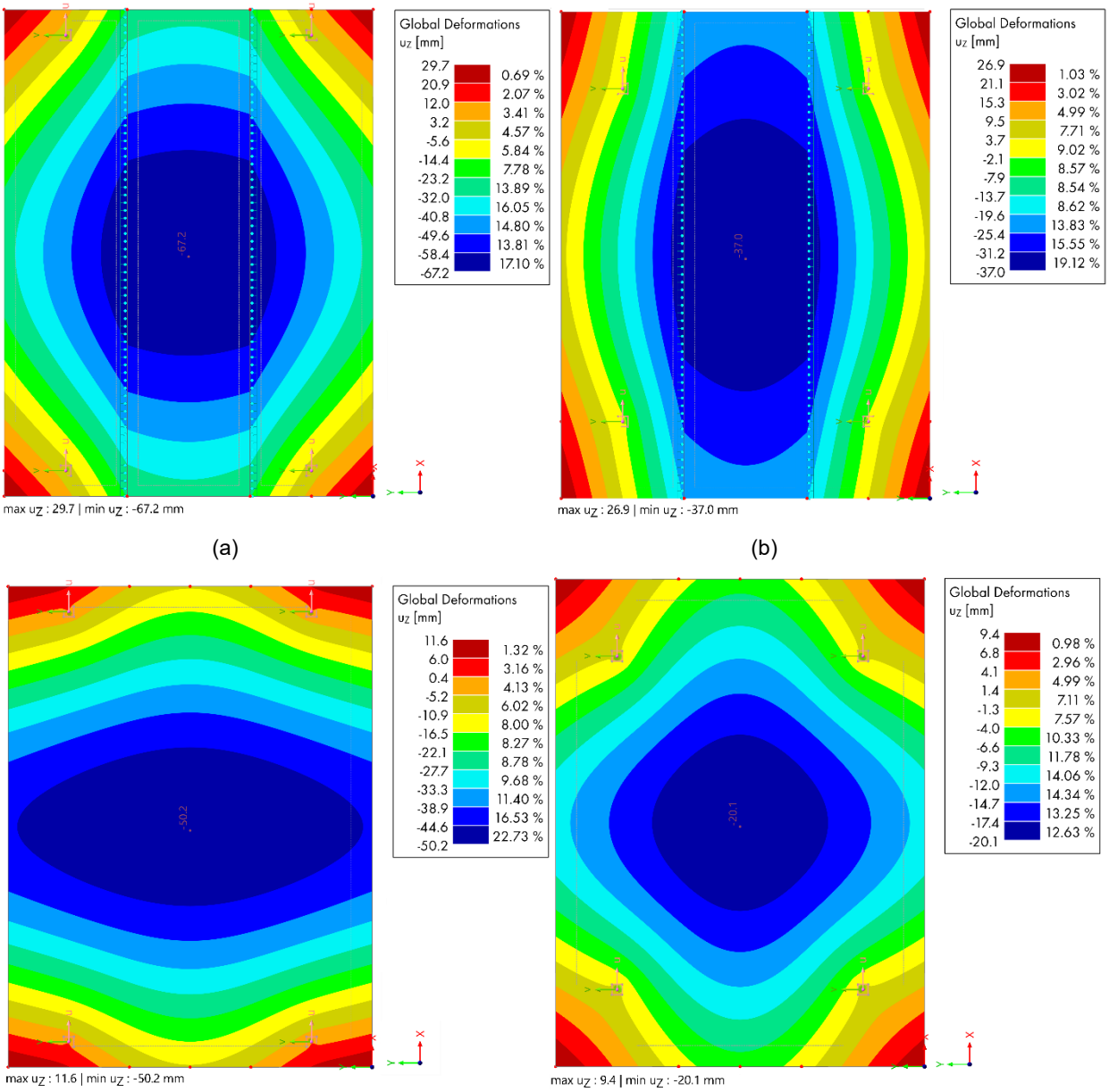

Figure 4-12: Impact of Cφ and e on the floor deformation for floor V2_9.5-7.2_LL 1.9; (a) e=500 mm, Cφ = 500, (b) e=1500 mm, Cφ = 500, (c) e=500 mm, Continuous floor, (d) e=1500 mm, Continuous floor

5 Recommendations for floor connection design

In addressing the need for continuity in the minor direction, the required numbers of connections to satisfy both ULS and SLS criteria, pertaining to load-carrying capacity and stiffness respectively, need to be determined. Achieving a floor behavior closely resembling continuity is paramount. Through the present numerical evaluations, it was established that enhancing rotational stiffness up to 5000 kNmrad^{-1}m^{-1} significantly enhances floor performance, reducing deflection by approximately 50%. However, further increasing rotational stiffness to attain a fully rigid connection (continuous floor) only marginally decreases deflection by 15%. Hence, a target rotational stiffness of 5000 kNmrad^{-1}m^{-1} is deemed appropriate to approach continuous floor behavior. As an example, two critical floors with longer possible spans including V2_9-9_LL 2.4_e 1.5, and V2_9.5-7.5_LL 1.9_e 0.5 were evaluated.

Screwed splines (S1), with 20 screws per meter (test result), achieved a bending moment capacity (M_{ult}) of roughly 55 kNm/m and a rotational stiffness (C_{Φ}) of close to 6,000 kNmrad^{-1}m^{-1} in the 4-point bending test. In the 3-point bending test, the S1 reached M_{ult}=53 kNm/m, a shear capacity (V_{ult}) of 125 kN/m, and a rotational stiffness of 11,000 kNmrad^{-1}m^{-1}. While plywood splines failed in the 4-point bending tests, CLT shear strength governed failure in the 3-point bending tests and the connection element remained undamaged. Therefore, for evaluating floor demand, the results of the 3-point bending test are deemed critical, even though the rotational stiffness surpassed the target in the 4-point bending test, with approximately 36% of the connection bending moment capacity satisfying the floor demand. Based on the experimental data, using 17 screws per m still meets the target rotational stiffness, with 40% utilization of the connection bending moment capacity fulfilling the floor demand. Employing only nine screws per m still satisfies both the ULS and SLS criteria, utilizing approximately 80% of the connection capacity to meet these

requirements. However, it is noteworthy that utilizing 80% of the connection capacity, while technically feasible, is not recommended due to the mean values utilized for this connection design.

For the glued splines (series S2), the outcome of the 3-point bending test serves as the primary design criterion. Under simultaneous out-of-plane bending moment and shear load, M_{ult} decreased by 26% (M_{ult} = 44 kNm/m, V_{ult} = 96 kN/m) compared to the 4-point bending tests. Despite variations in plywood grade, the rotational stiffness of the connection consistently remained significantly higher than $C_{\Phi,t}$. For the S2B series, which incorporates plywood measuring 220 mm/m long along the CLT panel's minor direction, utilizing 80% of the capacity allows the connection to meet floor demands while ensuring $C_{\Phi} > 5000$ kNmrad^{-1}m^{-1}. However, based on the tested connections configuration (400 mm/m long), satisfying the floor demand requires utilizing only 45% of the connection bending moment capacity.

Utilizing six T-joints per meter in the S3 series allows for meeting floor demands by utilizing 78% and 64% of the bending moment and shear capacity of the connection, respectively (M_{ult} = 23 kNm/m, V_{ult} = 29 kN/m, C_{Φ} = 3700 kNmrad^{-1}m^{-1}). Increasing the number of T-joints to nine per meter results in M_{ult} = 35 kNm/m, V_{ult} = 44 kN/m, and C_{Φ} = 5500 kNmrad^{-1}m^{-1}, which represents the maximum number of T-joints that can be utilized in a zigzag position within one meter [37]. However, increasing the length of the two STS that connect the panels would increase the withdrawal resistance. It is important to note that the spacing of T-slots depends on the length of the STS, as this spacing prevents intersecting of the STS.

As for the S4 series, according to the ETA-18/0254 [66] by considering a minimum edge distance of 150 mm and a connector spacing of 300 mm, maximum of three X-fix connectors can be

installed per meter, providing M_{ult} = 12.1 kNm/m, $C_{Φ}$ = 1275 kNmrad^{-1}m^{-1} which does not meet the ULS and SLS requirements.

Regarding floor V2_9.5-7.2_LL 1.9_e 0.5 the connection should be capable of providing M_{ult} = 15.5 kNm/m, V_{ult} = 27.5 kN/m, which is the average value within one meter of the critical area of the connecting line (connecting line edges) due to the uneven distribution of forces and minimum rotational stiffness of $C_{Φ,min}$=2000 kNmrad^{-1}m^{-1} to satisfy SLS ratio. In this way, for connection S1 series with minimum eight STS per meter (M_{ult} = 21.8 kNm/m, V_{ult} = 50 kN/m, $C_{Φ}$ = 4400 kNmrad^{-1}m^{-1}) the connection utilizes 71% of the connection bending moment capacity. However, by utilizing fifteen STS per meter (M_{ult} = 41.0 kNm/m, V_{ult} = 93.7 kN/m, $C_{Φ}$ = 7950 kNmrad^{-1}m^{-1}) the floor behavior can be much closer to a continuous floor as 38% of the connection capacity meets the demand.

For the S2B series, featuring plywood measuring 180 mm/m long in its major direction, utilizing 80% of the capacity enables the connection to meet floor demands while maintaining $C_{Φ}$ > 5000 kNmrad^{-1}m^{-1}. However, with a plywood measuring 360 mm/m long in its major direction, the floor demand is satisfied by $C_{Φ}$, utilizing 40% of the connection capacity meets the floor demand.

Regarding S3 series utilizing five T-joints per meter in the S3 series allows for meeting floor demands while utilizing 78% and 64% of the bending moment and shear capacity of the connection, respectively (M_{ult} = 19.2 kNm/m, V_{ult} = 24.5 kN/m, $C_{Φ}$ = 3100 kNmrad^{-1}m^{-1}). By utilizing nine T-joint per meter resulting in M_{ult} = 35 kNm/m, V_{ult} = 44 kN/m, and $C_{Φ}$ = 4900 kNmrad^{-1}m^{-1}, which meets the floor demand by utilizing 45% and 63% of the connection bending and shear capacity, respectively.

Table 5-1 presents the summary results for design recommendations. For example, in the case of floor V2_9-9_LL 2.4_e 1.5 which is one of the evaluated critical scenarios suggests that connection series S1 and S2 have the capability to achieve rotational stiffness close to or higher than the target rotational stiffness, utilizing up to 80% of their connection capacity, although about 40% of their capacity meets the floor demand. In comparison, using 9 T-joints per meter with the same STS detailing can achieve higher than target rotational stiffness by utilizing approximately 40% of the connection capacity. However, meeting the floor demand would require utilizing about 55% of the connection capacity.

Table 5-1: Design recommendation for floor V2_9-9_LL 2.4_e 1.5

Connection series	Connection detailing	$C\varphi$ (kNmrad^{-1}m^{-1})		Connection capacity utilization (%)
		10%-40%	40%-80%	
S1 (Screwed spline)	20 STS	10900	4660	36
	17 STS	9300	3980	40
	9 STS	4950	2110	80
S2 (Glued spline)	400×600 mm / 175 ml	54200	23380	45
	220×600 mm / 96 ml	29800	12850	80
S3 (T-joint)	9 T-joint	6190	2130	55
	6 T-joint	4120	1420	78

6 Conclusions

6.1 Summary of experimental work

The research conducted in this thesis delves into the out-of-plane behavior of connections in the minor direction of edge-connected CLT floor segments. The structural performance of five distinct connections was assessed: glued-on plywood spline, plywood spline attached with inclined screws, wooden X-fix, T-joints, and steel rebar.

1. Utilizing glued splines with a rotational stiffness exceeding 5000 $kNmrad^{-1}m^{-1}$, approaches the bending stiffness of a solid panel, making it an appropriate choice to meet SLS requirements.
2. The plywood quality significantly influences the structural performance of glued spline connections within the S2 series. In comparison to the S2B series, the S2C samples exhibited approximately 50% lower values for F_{ult}, M_{ult}, $d_{@ult}$, and C_{φ}. Moreover, C_{φ} remained significantly superior to other connection types even after the S2B series.
3. Screw spline connections are less sensitive to the quality of plywood. This observation is supported by the fact that both the S1 series (screwed spline plate) and S2C utilized the same grade of plywood. Despite this, the load-bearing capacity and moment resistance of the S1 series are comparable to those of the S2B series.
4. The T-joint (S3) remained intact and reusable. Compared to screwed joints, T-joints exhibited about half the out-of-plane bending moment and one-fourth the shear capacity. In the 3-point bending tests, the T-joints exhibited sliding along the connecting line.
5. The X-fix connector (S4) exhibited ductile performance. However, its rotational stiffness was very small; its bending moment capacity was only about half of the S2C series.

6. Steel rebars were able to transfer 74% of the maximum bending moment compared to screwed and glued splines. However, owing to their lower rotational stiffness, their deformation capacity is multiple times greater than that of the screw splines. Therefore, they could be considered a solution to add robustness of the connections between floor panels.

6.2 Summary of numerical work

The secondary objective was to evaluate the impact of rotational stiffness on floor performance using numerical modeling. A range of scenarios for point-supported CLT floors, considering variations in rotational stiffness, span, and loading conditions was explored.

1. While higher rotational stiffness can enhance floor structural performance, particularly in terms of serviceability, the impact of rotational stiffness gradually diminishes. Based on the results, up to about 5000 $kNmrad^{-1}m^{-1}$ could be considered as the upper limit (target rotational stiffness), beyond which the results become less sensitive to changes in rotational stiffness. An increase in rotational stiffness resulted in higher bending moments being transferred at both ends of the connection compared to the middle. Consequently, depending on the stiffness of the connection, additional connectors at both ends of the connecting line may be required.
2. Increasing the rotational stiffness results in the transfer of a major portion of the bending moment to both ends of the connecting line. Therefore, when utilizing a stiffer connection to approach continuous flooring, the detailing of the joints at both ends of the connecting line may require more attention.
3. In edge-connected floor systems, the floor aspect ratio is not the predominant factor determining the transition to two-way action. The magnitude of rotational stiffness also exerts a direct influence on the shift between one-way and two-way action.

4. Based on the floor analysis and experimental results, the tested connection configurations screwed spline (S1) and glued spline (S2) were capable of providing values close to or higher than the target rotational stiffness (5000 $kNmrad^{-1}m^{-1}$), while utilizing approximately 40% of the connection capacity to meet the required demand. T-joint can meet the target demands; however, more research is needed to define the optimum compromise between number of connectors and length of STS used to install them. The X-fix connector exhibited moderately ductile performance; however, its rotational stiffness and bending moment capacity is insufficient for out-of-plane moment connections.

6.3 **Future Research**

Drawing upon the findings of this research, further experimental and numerical investigations focusing on edge-connected CLT floors should aim to advance the development of connections that address a broader spectrum of structural performance, constructability, and cost-effectiveness.

1. Testing of hybrid connections combining glued spline with screws or steel rebar is recommended. This combination could add the ductile performance of steel rebar to complement the stiffness of the glued joint. Such experiments provide insights into their behavior, aiding in the development of resilient structural solutions for CLT floor applications.
2. Assessing the structural performance of the connection under simultaneous out-of-plane and in-plane loads since the connections are subjected to the biaxial loading.
3. Conducting experiments on a larger scale, capable of simulating real two-way action scenarios.
4. Evaluating the long-term loading performance, particularly for glued spline joints, is crucial.

References

[1] A. Hossain, M. Popovski, and T. Tannert, “Group Effects for Shear Connections with Self-Tapping Screws in CLT,” *Journal of Structural Engineering*, vol. 145, no. 8, May 2019, doi: 10.1061/(ASCE)ST.1943-541X.0002357.

[2] A. Hossain, I. Danzig, and T. Tannert, “Cross-Laminated Timber Shear Connections with Double-Angled Self-Tapping Screw Assemblies,” *Journal of Structural Engineering*, vol. 142, no. 11, Jun. 2016, doi: 10.1061/(ASCE)ST.1943-541X.0001572.

[3] M. Subhani, S. K. Shill, S. Al-Deen, M. Anwar-Us-Saadat, and M. Ashraf, “Flexural Performance of Splice Connections in Cross-Laminated Timber,” *Buildings 2022, Vol. 12, Page 1124*, vol. 12, no. 8, p. 1124, Jul. 2022, doi: 10.3390/BUILDINGS12081124.

[4] J. Asselstine, F. Lam, and C. Zhang, “New edge connection technology for cross laminated timber (CLT) floor slabs promoting two-way action,” *Eng Struct*, vol. 233, p. 111777, Apr. 2021, doi: 10.1016/J.ENGSTRUCT.2020.111777.

[5] C. Zhang, G. Lee, and F. Lam, “Connection and performance of two-way CLT plates,” Vancouver, Apr. 2018. [Online]. Available: https://research.thinkwood.com/en/permalink/catalogue1482

[6] E. Macpherson, P. Papastavrou, T. Wallwork, S. Smith, and A. Mcrobie, “The rotational stiffness of cross-laminated timber half-lap joints,” in *WCTE 2018 - World Conference on Timber Engineering*, Seoul, Republic of Korea, Aug. 2018. doi: 10.17863/CAM.34857.

[7] M. He, X. Sun, Z. Li, and W. Feng, “Bending, shear, and compressive properties of three- and five-layer cross-laminated timber fabricated with black spruce,” *Journal of Wood Science*, vol. 66, no. 1, pp. 1–17, Dec. 2020, doi: doi.org/10.1186/s10086-020-01886-z.

[8] FPInnovations, *CLT Handbook*, Canadian edition. Quebec City, 2019. Accessed: Nov. 29, 2022. [Online]. Available: https://web.fpinnovations.ca/clt/

[9] S. Breneman, “Cross-Laminated Timber Structural Floor and Roof Design,” *Structural Design*, 2016.

[10] Y. Yang, X. Cao, Z. Wang, Z. Liang, and J. Zhou, “Evaluation of the Out-of-Plane Shear Properties of Cross-Laminated Timber,” *J Renew Mater*, vol. 7, no. 10, pp. 957–965, Mar. 2019, doi: 10.32604/JRM.2019.07558.

[11] A. Sandoli and B. Calderoni, “The Rolling Shear Influence on the Out-of-Plane Behavior of CLT Panels: A Comparative Analysis,” *Buildings 2020, Vol. 10, Page 42*, vol. 10, no. 3, p. 42, Mar. 2020, doi: 10.3390/BUILDINGS10030042.

[12] M. Poulin, C. Viau, D. N. Lacroix, and G. Doudak, “Experimental and Analytical Investigation of Cross-Laminated Timber Panels Subjected to Out-of-Plane Blast Loads,” *Journal of Structural Engineering*, vol. 144, no. 2, p. 04017197, Nov. 2017, doi: 10.1061/(ASCE)ST.1943-541X.0001915.

[13] V. Mahdavifar, A. R. Barbosa, and A. Sinha, “Nonlinear Layered Modelling Approach for Cross Laminated Timber Panels Subjected to Out-of-plane Loading,” in *41st IAHS World Congress on Housing Sustainability and Innovation for the Future*, Algarve, Sep. 2016.

[14] J. D. Bowick, “Mass Timber Primer.” Accessed: Nov. 07, 2023. [Online]. Available: https://www.canadianarchitect.com/mass-timber-primer/

[15] “X-fix - The timber-to-timber connection system.” [Online]. Available: https://www.hasslacher.com/en/X-fix-c

[16] “X-fix metallfreie Holz Verbinder Brettsperrholz Holzdübel / no metal wood CLT connectors wooden dowel.” Accessed: Jan. 05, 2023. [Online]. Available: https://www.X-fix.at/

[17] H. Li, F. Lam, and H. Qiu, “Feasibility of the analytical model for the splice beam with half-lap joints reinforced with different cross-sections and layout of self-tapping screws,” *Structures*, vol. 28, pp. 120–126, Dec. 2020, doi: 10.1016/J.ISTRUC.2020.08.061.

[18] M. Sadeghi, M. Ballerini, I. Smith, and E. Pedrotti, “Bending properties of connections in cross laminated timber,” *IABSE Conference, Nara 2015: Elegance in Structures - Report*, pp. 366–367, 2015, doi: 10.2749/222137815815775402.

[19] Zhang Chao, Asselstine Julian, Lee George, and Lam Frank, “Connection and performance of two-way CLT plates Phase II,” Jun. 2019. [Online]. Available: https://research.thinkwood.com/en/permalink/catalogue2086

[20] E. Mills and H. Kalman, “Architectural History of Indigenous Peoples in Canada | The Canadian Encyclopedia.” Accessed: Nov. 22, 2022. [Online]. Available: https://www.thecanadianencyclopedia.ca/en/article/architectural-history-early-first-nations

[21] B. Stafford Smith and A. Coull, “Tall building structures : analysis and design,” p. 537, 1991, Accessed: Feb. 23, 2023. [Online]. Available: https://www.wiley.com/en-us/Tall+Building+Structures%3A+Analysis+and+Design-p-9780471512370

[22] R. J. Ross, “Wood handbook: Wood as an engineering material,” *FPL-GTR-282*, vol. 282, pp. 1–543, 2021, Accessed: Oct. 26, 2022. [Online]. Available: http://www.fs.usda.gov/research/treesearch/62200

[23] D. W. Green, “Wood: Strength and Stiffness,” *Encyclopedia of Materials: Science and Technology*, pp. 9732–9736, Jan. 2001, doi: 10.1016/B0-08-043152-6/01766-6.

[24] “Engineered wood and mass timber, 2020.” Accessed: Feb. 23, 2023. [Online]. Available: https://www.naturallywood.com/topics/mass-timber/

[25] P. Quintana Gallo, D. M. Carradine, and R. Bazaez, “State of the art and practice of seismic-resistant hybrid timber structures,” *European Journal of Wood and Wood Products*, vol. 79, no. 1, pp. 5–28, Jan. 2021, doi: 10.1007/S00107-020-01556-3/METRICS.

[26] N. Doyle, R. Emberley, and J. L. Torero, “Fire Behavior of Cross-Laminated Timber (CLT) Slabs: Two-Way Action,” *Fire Science and Technology 2015*, pp. 281–288, 2017, doi: 10.1007/978-981-10-0376-9_28.

[27] M. Shahnewaz *et al.*, “Experimental Research on Point-supported CLT Panels: Phase 1: Rolling Shear Strength,” *13th World Conference on Timber Engineering, WCTE 2023*, vol. 1, pp. 352–357, 2023, doi: 10.52202/069179-0048.

[28] M. Popovski, Z. Chen, and B. Gafner, “Structural Behaviour of Point-Supported CLT Floor Systems | Research Library | Think Wood,” in *World Conference on Timber Engineering*,

Vienna, Aug. 2016. Accessed: May 08, 2024. [Online]. Available: https://research.thinkwood.com/en/permalink/catalogue1476

[29] P. Mestek and P. Dietsch, “Design concept for CLT -reinforced with self-tapping screws,” in *Focus Solid Timber Solutions - European Conference on Cross Laminated Timber*, Graz: University of Bath, May 2013.

[30] T. Bogensperger, R. Joebstl, and M. Augustin, “Concentrated Load Introduction in CLT Elements Perpendicular to Plane – Experimental and Numerical Investigations,” in *World Conference on Timber Engineering*, Vienna: TU Verlag Wien, Aug. 2016, pp. 2341–2349. Accessed: Nov. 25, 2022. [Online]. Available: https://research.thinkwood.com/en/permalink/catalogue1613

[31] “EN 13986 : 2004 +A1:2015, Wood-based panels for use in construction – Characteristics, evaluation of conformity and marking,” 2004.

[32] G. S. Ayansola and T. Tannert, “High capacity wooden connector for CLT shear walls,” in *World Conference on Timber Engineering (WCTE 2021)*, Santiago, Aug. 2021. Accessed: May 17, 2023. [Online]. Available: www.proceedings.com

[33] Jack. Porteous and Abdy. Kermani, *Structural timber design to Eurocode 5*. Wiley-Blackwell, 2013. Accessed: Feb. 24, 2023. [Online]. Available: https://www.wiley.com/en-us/Structural+Timber+Design+to+Eurocode+5%2C+2nd+Edition-p-9780470675007

[34] I. Bejtka and H. Blass, “Reinforcements perpendicular to the grain using self-tapping screws,” in *Proceedings of the 8th world conference on timber engineering*, Lahti, Finland, 2004.

[35] P. Dietsch and R. Brandner, “Self-tapping screws and threaded rods as reinforcement for structural timber elements – A state-of-the-art report,” *Constr Build Mater*, vol. 97, pp. 78–89, Oct. 2015, doi: 10.1016/J.CONBUILDMAT.2015.04.028.

[36] M. Milojević, V. Racic, M. Marjanović, and M. Nefovska-Danilović, “Influence of inter-panel connections on vibration response of CLT floors due to pedestrian-induced loading,” *Eng Struct*, vol. 277, p. 115432, Feb. 2023, doi: 10.1016/J.ENGSTRUCT.2022.115432.

[37] “T-JOINT - Screw connector made of cast steel - Knapp Connectors.” Accessed: Mar. 22, 2024. [Online]. Available: https://www.knapp-verbinder.com/en/produkt/t-joint/

[38] L. F. M. da Silva, A. Öchsner, and R. D. Adams, “Handbook of Adhesion Technology ,” *Handbook of Adhesion Technology*, 2011, doi: 10.1007/978-3-642-01169-6_1.

[39] L. Blyberg *et al.*, “Glass, timber and adhesive joints – Innovative load bearing building components,” *Constr Build Mater*, vol. 55, pp. 470–478, Mar. 2014, doi: 10.1016/J.CONBUILDMAT.2014.01.045.

[40] D. Otero Chans, J. E. Cimadevila, and E. M. Gutiérrez, “Glued joints in hardwood timber,” *Int J Adhes Adhes*, vol. 28, no. 8, pp. 457–463, Dec. 2008, doi: 10.1016/J.IJADHADH.2008.04.008.

[41] T. Vallée, T. Tannert, and S. Fecht, “Adhesively bonded connections in the context of timber engineering – A Review,” *http://dx.doi.org/10.1080/00218464.2015.1071255*, vol. 93, no. 4, pp. 257–287, Mar. 2016, doi: 10.1080/00218464.2015.1071255.

[42] V. Di Maria and A. Ianakiev, “Adhesive connections in timber: a comparison between rough and smooth wood bonding surfaces,” 2015, Accessed: Feb. 24, 2023. [Online]. Available:

http://waset.org/Publication/adhesive-connections-in-timber-a-comparison-between-rough-and-smooth-wood-bonding-surfaces/10000603

[43] S. Franke and S. Zöllig, "TS3 – A New Technology for Efficient Timber Structures," *Current Trends in Civil & Structural Engineering*, vol. 4, no. 4, 2020, doi: 10.33552/CTCSE.2020.04.000592.

[44] S. Zöllig, A. Frangi, S. Franke, and M. Muster, "Timber Structures 3.0 - New Technology for Multi-Axial, Slim, High Performance Timber Structures | Research Library | Think Wood," in *World Conference on Timber Engineering*, J. Eberhardsteiner, W. Winter, A. Fadai, and M. Pöll, Eds., Vienna, Austria: TU Verlag Wien, 2016, pp. 1290–1297. Accessed: Dec. 22, 2022. [Online]. Available: http://hdl.handle.net/20.500.12708/172

[45] A. 'Bühlmann, "Brandverhalten von stirnseitig verklebten Brettsperrholzplatten," Master Thesis, ETH Zürich, 2014.

[46] M. S. Mungwa, J. F. Jullien, A. Foudjet, and G. Hentges, "Experimental study of a composite wood–concrete beam with the INSA–Hilti new flexible shear connector," *Constr Build Mater*, vol. 13, no. 7, pp. 371–382, Oct. 1999, doi: 10.1016/S0950-0618(99)00034-3.

[47] S. Loebus and S. Winter, "Two-Way Spanning CLT-Concrete-Composite Slab," in *World Conference on Timber Engineering*, Vienna, Austria, 2016, pp. 4950–4956. Accessed: Dec. 21, 2022. [Online]. Available: http://hdl.handle.net/20.500.12708/172

[48] M. A. H. Mirdad, Y. H. Chui, and D. Tomlinson, "Capacity and Failure-Mode Prediction of Mass Timber Panel–Concrete Composite Floor System with Mechanical Connectors,"

Journal of Structural Engineering, vol. 147, no. 2, p. 04020338, Dec. 2020, doi: 10.1061/(ASCE)ST.1943-541X.0002909.

[49] M. A. H. Mirdad and Y. H. Chui, "Load-slip performance of Mass Timber Panel-Concrete (MTPC) composite connection with Self-tapping screws and insulation layer," *Constr Build Mater*, vol. 213, pp. 696–708, Jul. 2019, doi: 10.1016/J.CONBUILDMAT.2019.04.117.

[50] S. J. Pang, K. S. Ahn, S. man Jeong, G. C. Lee, H. S. Kim, and J. K. Oh, "Prediction of bending performance for a separable CLT-concrete composite slab connected by notch connectors," *Journal of Building Engineering*, vol. 49, p. 103900, May 2022, doi: 10.1016/J.JOBE.2021.103900.

[51] S. Lamothe, L. Sorelli, P. Blanchet, and P. Galimard, "Engineering ductile notch connections for composite floors made of laminated timber and high or ultra-high performance fiber reinforced concrete," *Eng Struct*, vol. 211, p. 110415, May 2020, doi: 10.1016/J.ENGSTRUCT.2020.110415.

[52] P. Clouston, L. A. Bathon, and A. Schreyer, "Shear and Bending Performance of a Novel Wood–Concrete Composite System," *Journal of Structural Engineering*, vol. 131, no. 9, pp. 1404–1412, Sep. 2005, doi: 10.1061/(ASCE)0733-9445(2005)131:9(1404).

[53] T. Stieb, R. Maderebner, and P. Dietsch, "A Timber–Concrete–Composite Edge Connection for Two-Way Spanning Cross-Laminated Timber Slabs—Experimental Investigations and Analytical Approach," *Buildings 2023, Vol. 13, Page 3004*, vol. 13, no. 12, p. 3004, Dec. 2023, doi: 10.3390/BUILDINGS13123004.

[54] R Maderebner, “Flächenhafte mechanische Verbindungsmittel. In 25.,” Innsbruck, Austria, 2019.

[55] T. Stieb, B. Maurer, M. Bestler, P. Dietsch, and R. Maderebner, “SOLUTIONS FOR EDGE CONNECTIONS TO BUILD TWO-WAY SPANNING CROSS LAMINATED TIMBER SLABS,” in *World Conference on Timber Engineering 2023*, Oslo, Jun. 2023, pp. 1322–1329. doi: 10.52202/069179-0180.

[56] J. H. Asselstine, “Edge connection technology for cross laminated timber (CLT) floor slabs promoting two-way action,” University of British Columbia, Vancouver, 2020. doi: 10.14288/1.0392448.

[57] S. L. Sultana, “Numerical modelling of CLT shear walls with hyperelastic hold-downs,” University of Northern British Columbia, 2023. doi: 10.24124/2023/59370.

[58] R. Stürzenbecher, K. Hofstetter, and J. Eberhardsteiner, “Cross Laminated Timber: A Multi-Layer, Shear Compliant Plate and its Mechanical Behavior,” in *Proceedings of ther World Conference on Timber Engineering*, CNR-IVALSA, 2010.

[59] W. Syed, *All Models are Wrong*. 2022. Accessed: Jun. 06, 2023. [Online]. Available: https://featips.com/ebook-on-fea-all-models-are-wrong/

[60] M. Muster and A. Frangi, “Experimental analysis and structural modelling of the punching behaviour of continuous two-way CLT flat slabs,” *Eng Struct*, vol. 205, p. 110046, Feb. 2020, doi: 10.1016/J.ENGSTRUCT.2019.110046.

[61] “Dlubal Software, RFEM 6.” 2022. Accessed: May 31, 2023. [Online]. Available: https://www.dlubal.com/en-US/products/rfem-fea-software/what-is-rfem

[62] APA, “PR-L332-Kalesnikoff Cross-Laminated Timber,” Aug. 2022. [Online]. Available: www.kalesnikoff.com

[63] MTC solutions, “Structural Screw Design Guide Formerly MyTiCon,” Feb. 2020, Accessed: Feb. 25, 2024. [Online]. Available: www.mtcsolutions.com

[64] “LEPAGE® PL® PREMIUM MAX Construction Adhesive, A brand of the Henkel Corporation,” 2022, Accessed: Feb. 25, 2024. [Online]. Available: http://www.lepage.ca/

[65] “Titebond.” Accessed: Mar. 04, 2024. [Online]. Available: http://www.titebond.com/product/glues/e8d40b45-0ab3-49f7-8a9c-b53970f736af

[66] ETA-18/0254, “European Technical Assessment,” 2020.

[67] Canadian Standards Association (CSA), *carbon steel bars for concrete reinforcement. CSA G30.18*. 2021. Accessed: Mar. 04, 2024. [Online]. Available: https://www.csagroup.org/store/product/2700248/

[68] R. Tomasi, M. A. Parisi, and M. Piazza, “Ductile Design of Glued-Laminated Timber Beams,” *Practice Periodical on Structural Design and Construction*, vol. 14, no. 3, pp. 113–122, Jul. 2009, doi: 10.1061/(ASCE)1084-0680(2009)14:3(113).

[69] “EN 1995-1-1: Eurocode 5: Design of timber structures - Part 1-1: General - Common rules and rules for buildings,” Brussels, 2004.

[70] ISO TR 21141:2022, “Timber structures-Timber connections and assemblies-Determination of yield and ultimate characteristics and ductility from test data,” May 2022. Accessed: Apr. 14, 2024. [Online]. Available: www.iso.org

[71] “EN 26891:1991 - Timber structures - Joints made with mechanical fasteners - General principles for.” Accessed: Mar. 04, 2024. [Online]. Available: https://standards.iteh.ai/catalog/standards/cen/e897b650-7198-4edc-9065-e3ae45738cdd/en-26891-1991

[72] Canadian Wood Council., *Wood design manual, 2020 : the complete reference for wood design in Canada*. Ottawa: Canadian Wood Council, 2021.

[73] Canadian Commission on Building and Fire Codes, *National Building Code of Canada 2020*, Fifteenth edition. Ottawa, 2020.

[74] “Surfaces | Dlubal Software.” Accessed: Nov. 05, 2023. [Online]. Available: https://www.dlubal.com/en-US/downloads-and-information/documents/online-manuals/rfem-6/000040

[75] “Surface Results Adjustments | Dlubal Software.” Accessed: Nov. 05, 2023. [Online]. Available: https://www.dlubal.com/en-US/solutions/online-services/glossary/000382

[76] Canadian Standards Association, *CSA O86 engineering design in wood*. Toronto: CSA Group, 2019.

Appendix A: Load-deflection response for 4-point bending tests

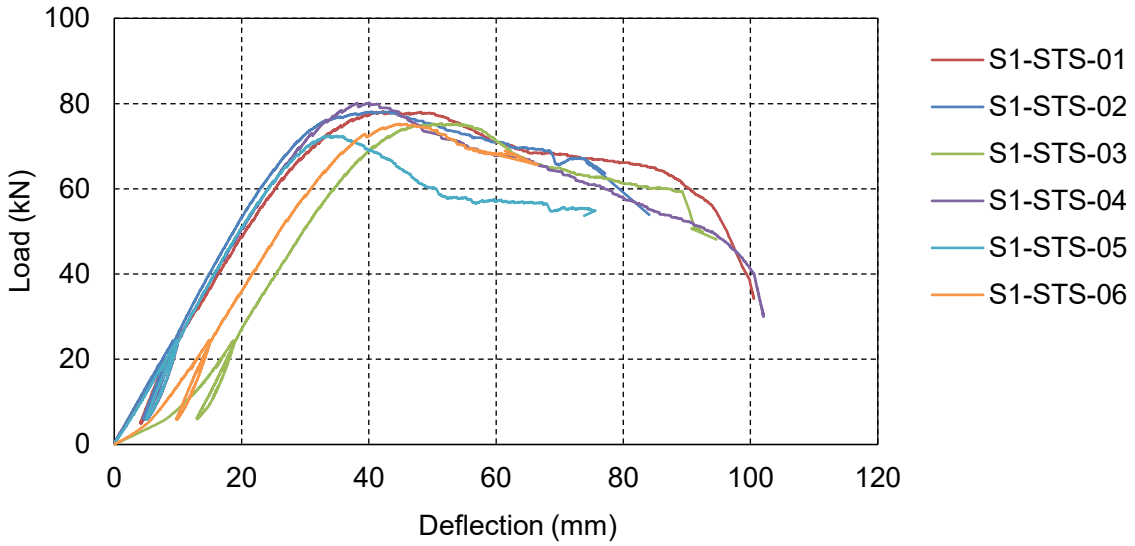

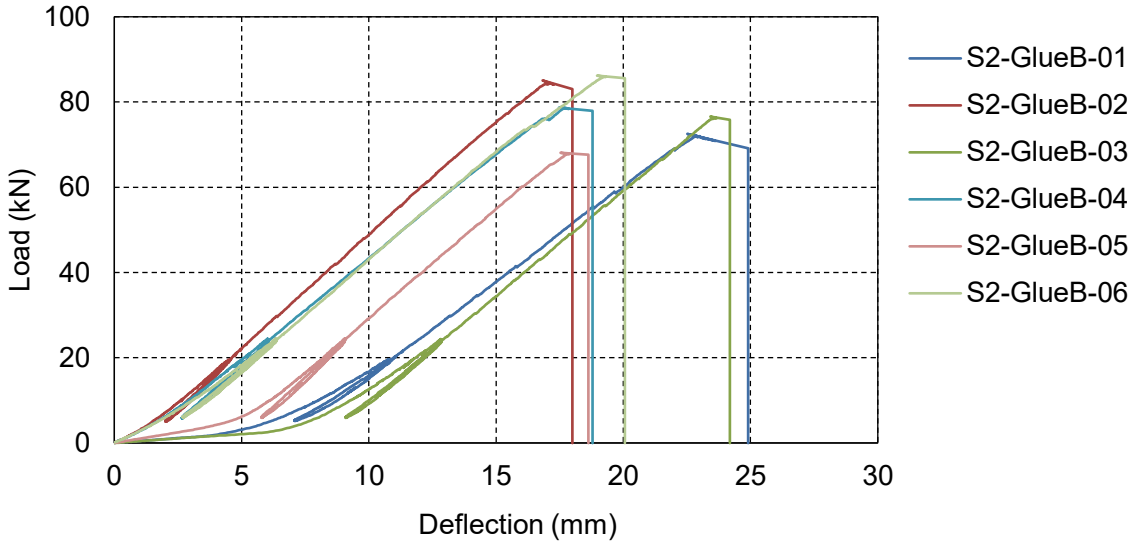

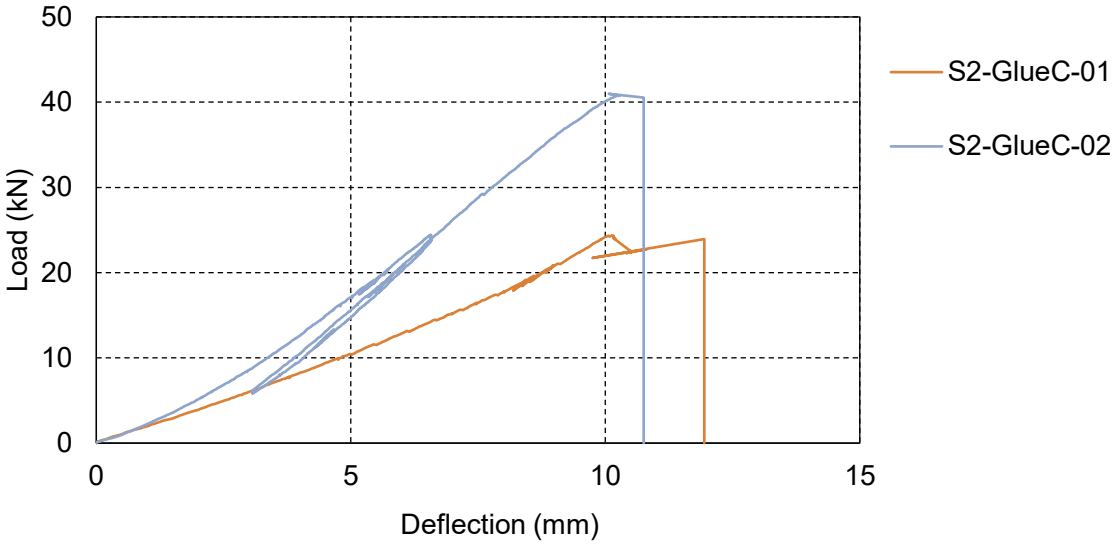
50
40
30
20
10
0
Load (kN)
0
5
10
15
Deflection (mm)
S2-GlueC-01
S2-GlueC-02

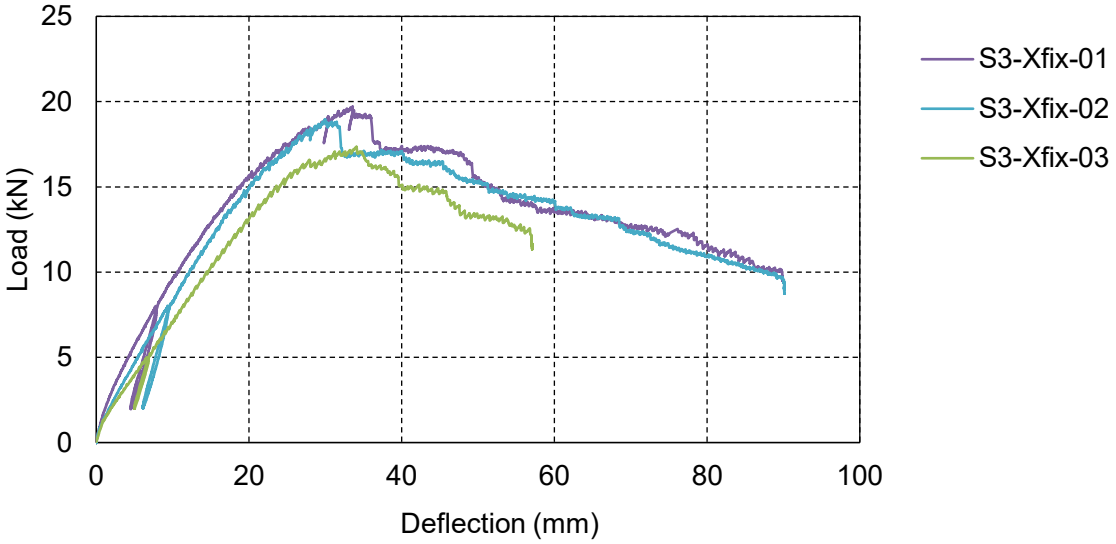
25
20
15
10
5
0
Load (kN)
0
20
40
60
80
100
Deflection (mm)
S3-Xfix-01
S3-Xfix-02
S3-Xfix-03

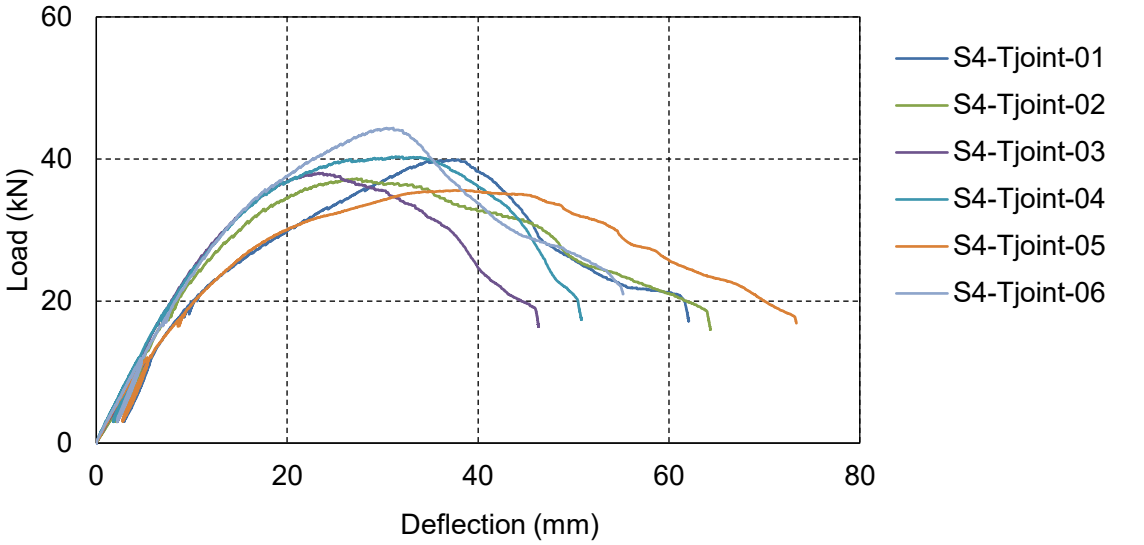
60
40
20
0
Load (kN)
0
20
40
60
80
Deflection (mm)
S4-Tjoint-01
S4-Tjoint-02
S4-Tjoint-03
S4-Tjoint-04
S4-Tjoint-05
S4-Tjoint-06

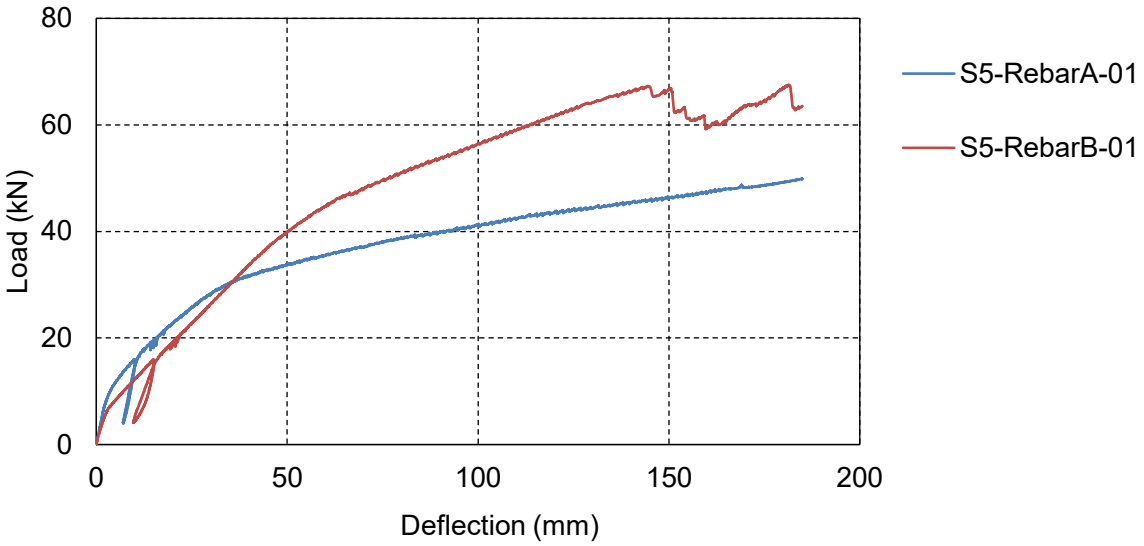
80
60
40
20
0
Load (kN)
0
50
100
150
200
Deflection (mm)
S5-RebarA-01
S5-RebarB-01

Appendix B: Load-deflection response for 3-point bending tests

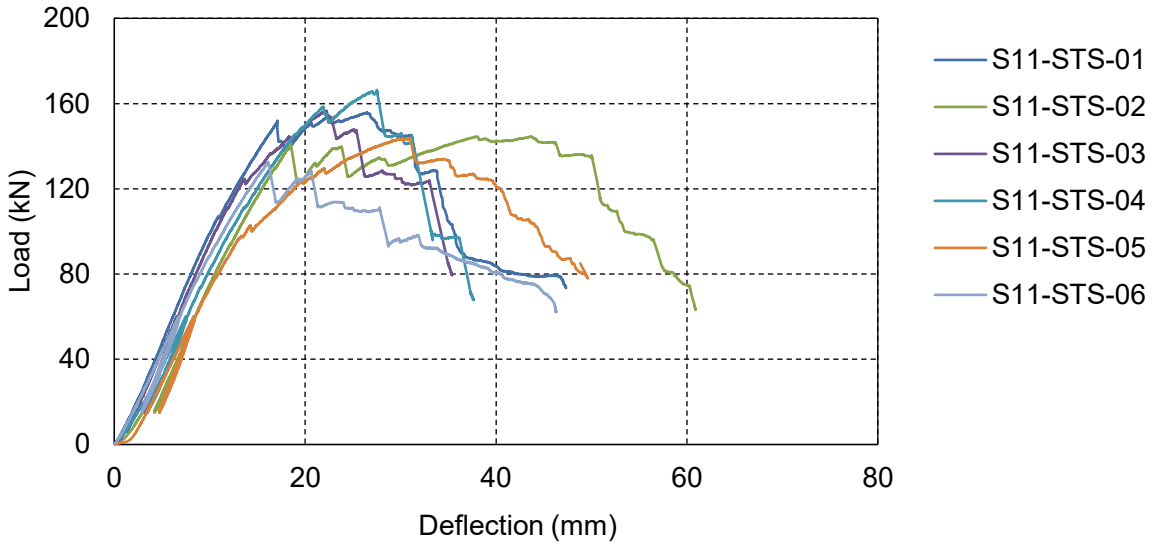

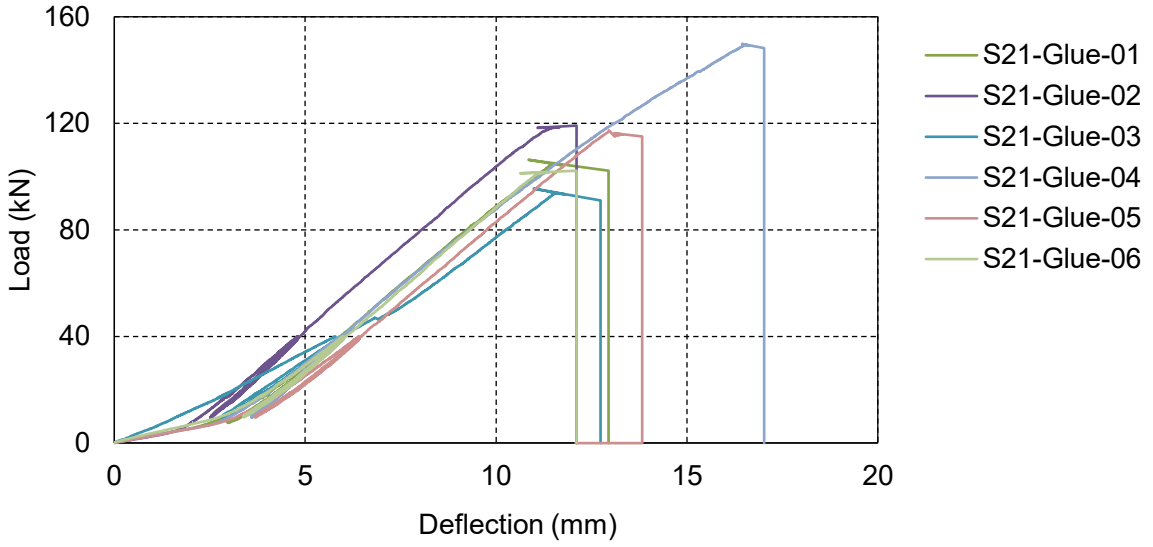

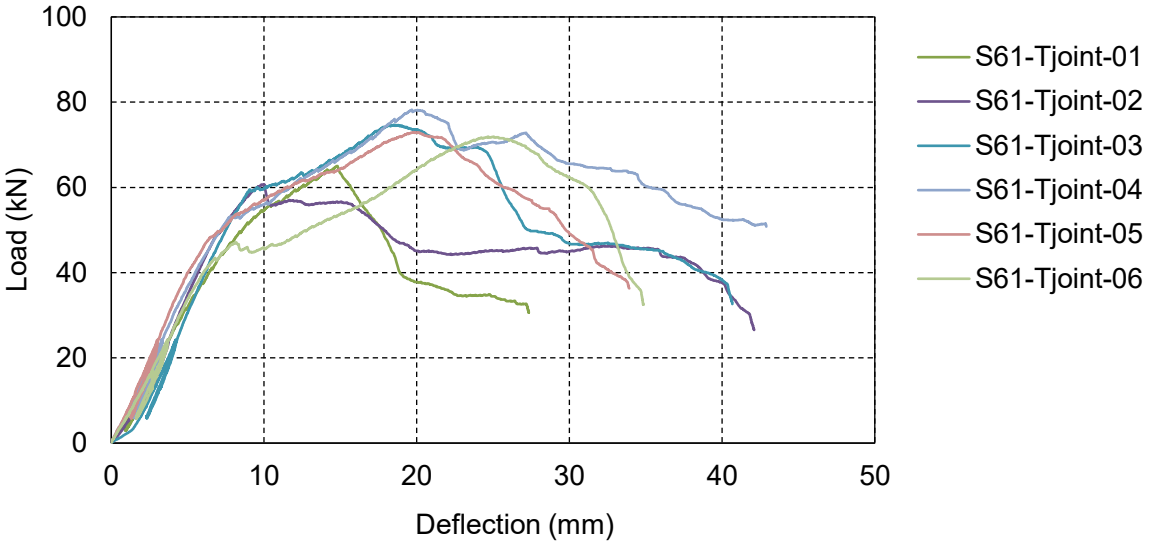
100
80
60
40
20
0
Load (kN)
0
10
20
30
40
50
Deflection (mm)
S61-Tjoint-01
S61-Tjoint-02
S61-Tjoint-03
S61-Tjoint-04
S61-Tjoint-05
S61-Tjoint-06

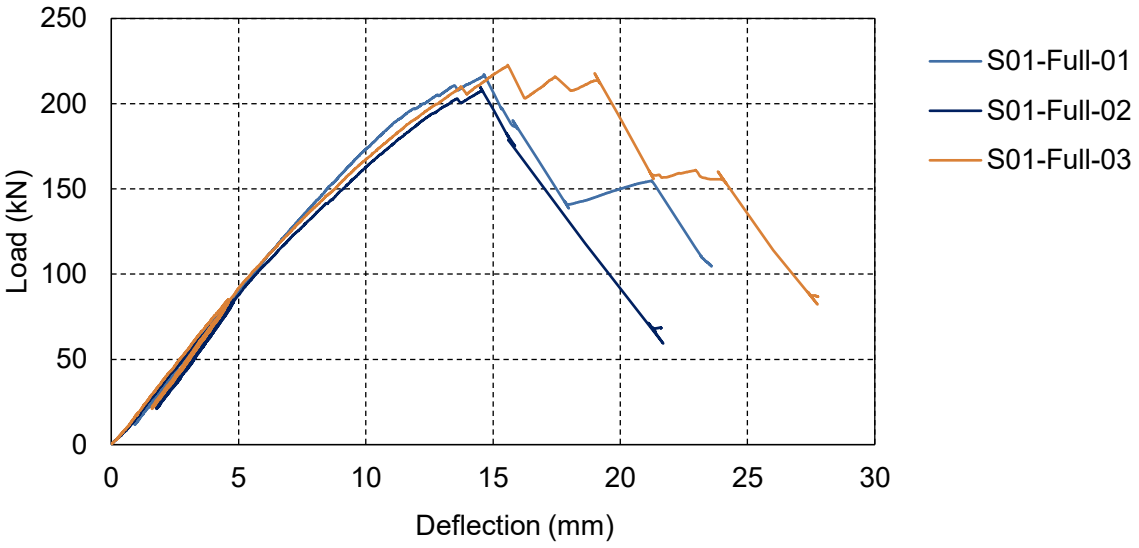
250
200
150
100
50
0
Load (kN)
0
5
10
15
20
25
30
Deflection (mm)
S01-Full-01
S01-Full-02
S01-Full-03

Appendix C: Failure modes from 4-point bending tests

S2B-1

S2B-2

S2B-3

S2B-4

S2B-5

S2B-6

S2C-1

S2C-2

Appendix C: Failure modes from 3-point bending tests

S1-1

S1-2

S1-3

S1-4

S1-5

S1-6

S2-1

S2-2

S2-3

S2-4

S2-5

S2-6

S3-1

S3-2

S3-3

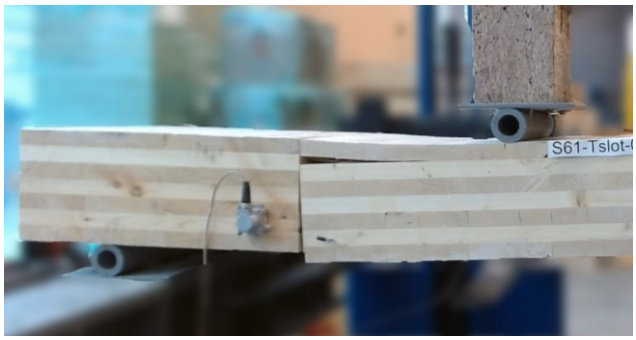

S3-4

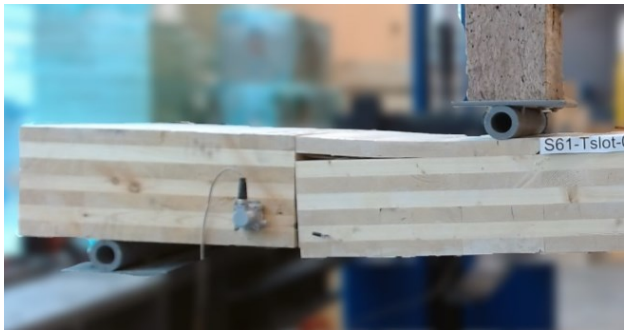

S3-5

S3-6

Appendix D: Numerical results

D1: Transferred bending moment at the connecting line

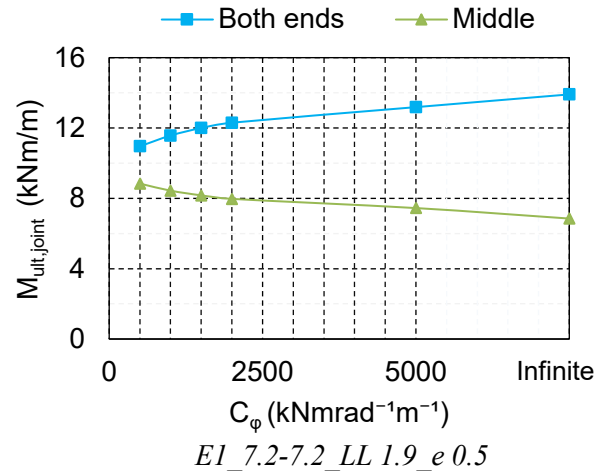

E1_7.2-7.2_LL 1.9_e 0.5

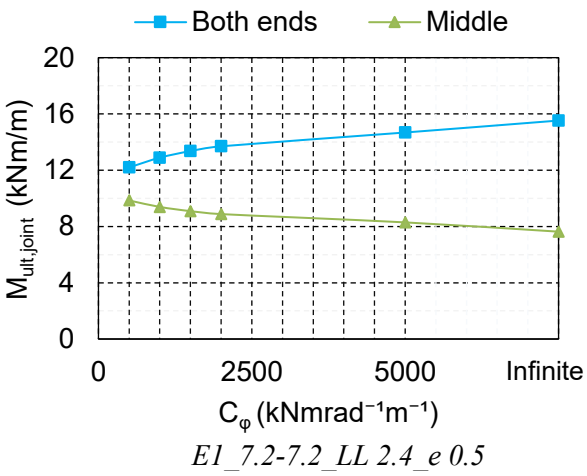

E1_7.2-7.2_LL 2.4_e 0.5

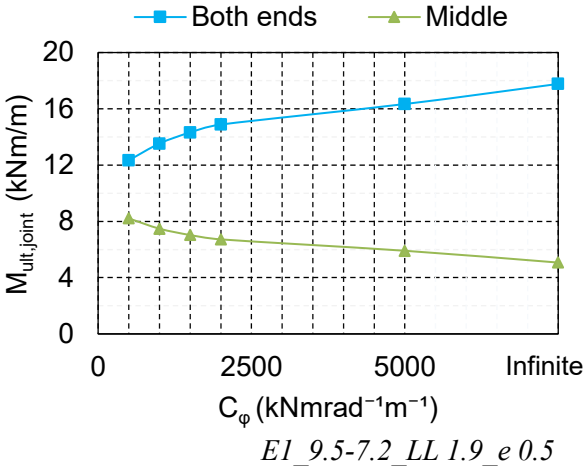

E1_9.5-7.2_LL 1.9_e 0.5

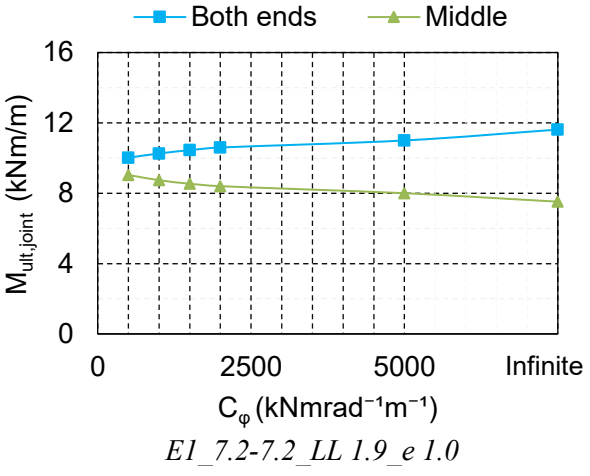

E1_7.2-7.2_LL 1.9_e 1.0

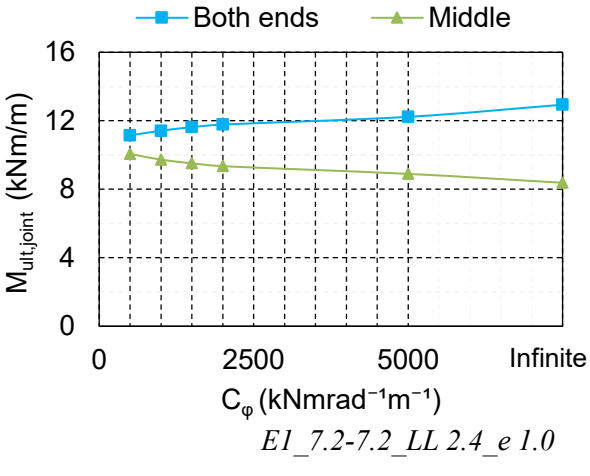

E1_7.2-7.2_LL 2.4_e 1.0

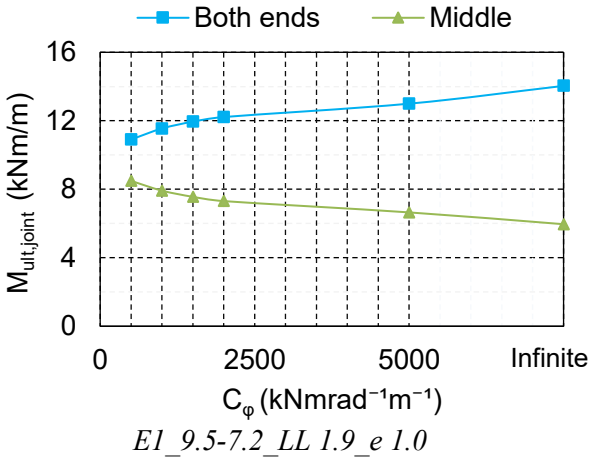

E1_9.5-7.2_LL 1.9_e 1.0

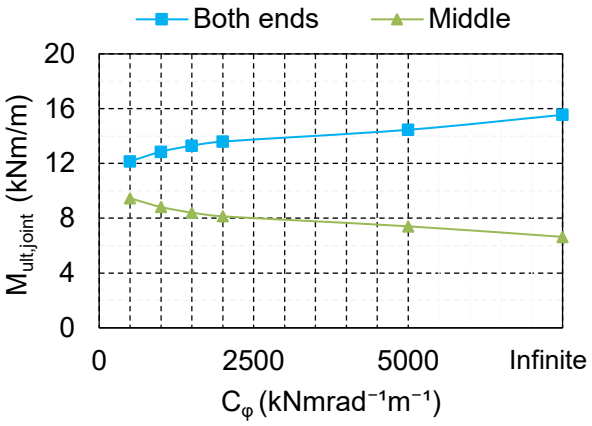

E1_9.5-7.2_LL 2.4_e 1.0

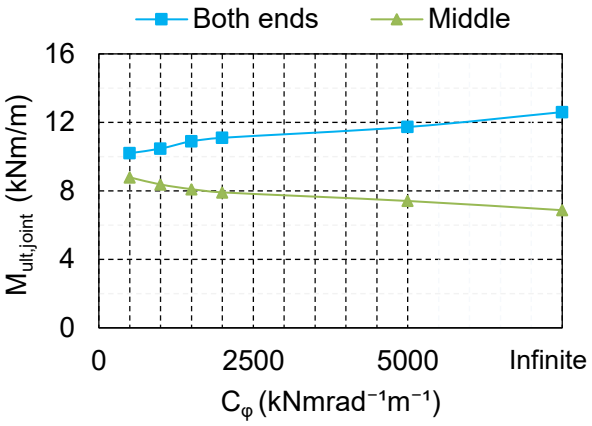

E1_9.5-7.2_LL 1.9_e 1.5

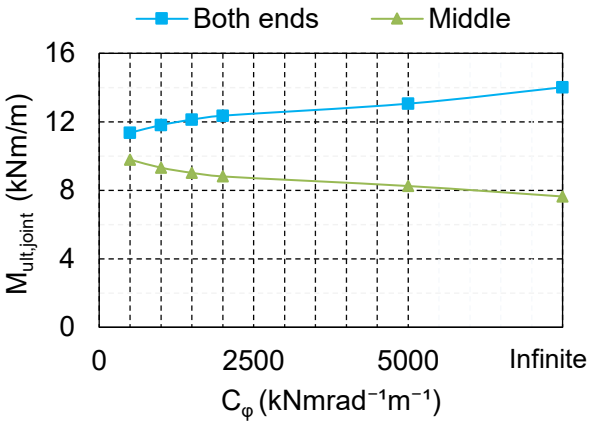

E1_9.5-7.2_LL 2.4_e 1.5

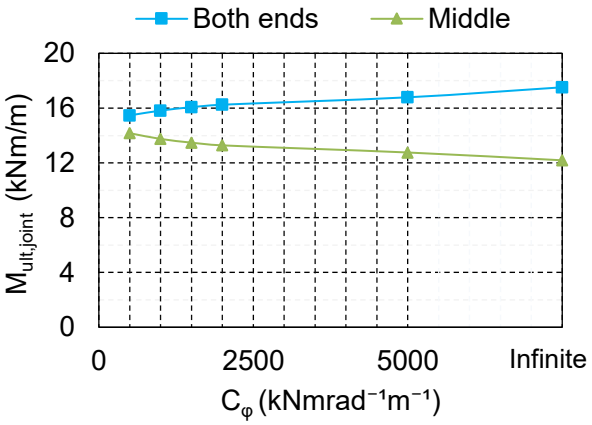

E1_9.0-9.0_LL 1.9_e 1.5

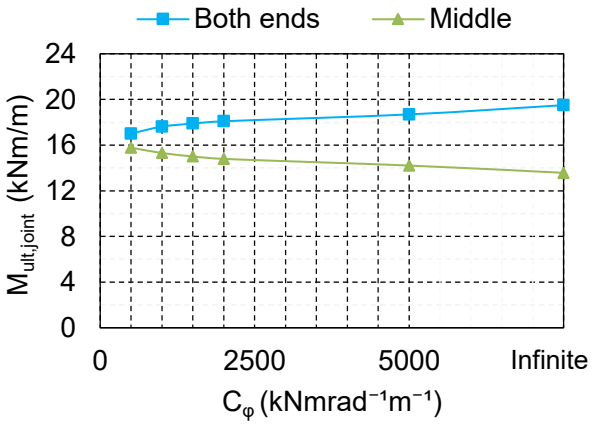

E1_9.0-9.0_LL 2.4_e 1.5

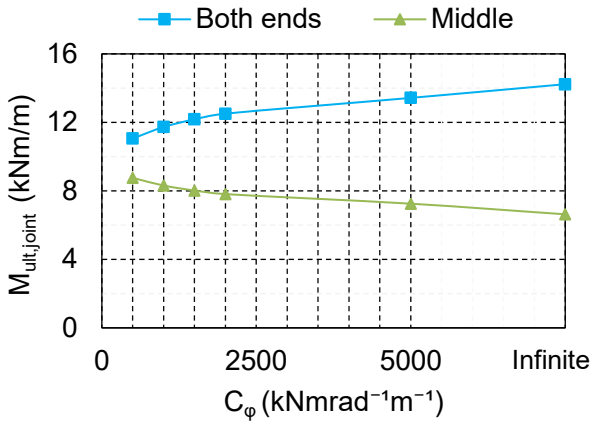

V2_7.2-7.2_LL 1.9_e 0.5

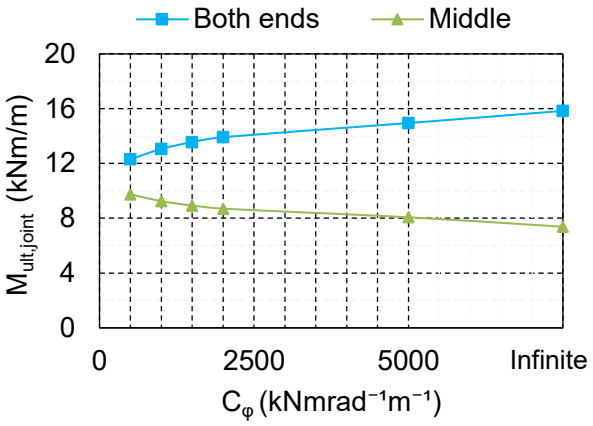

V2_7.2-7.2_LL 2.4_e 0.5

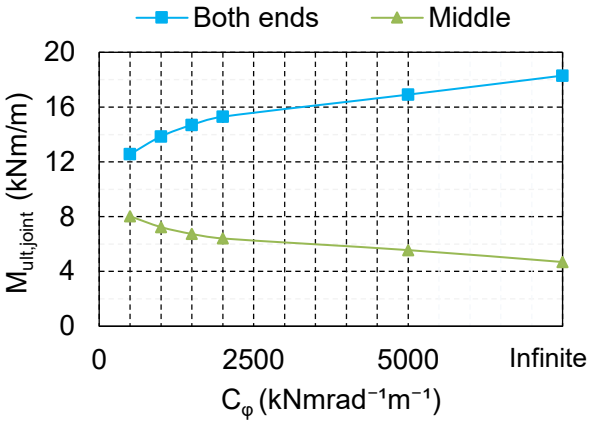

V2_9.5-7.2_LL 1.9_e 0.5

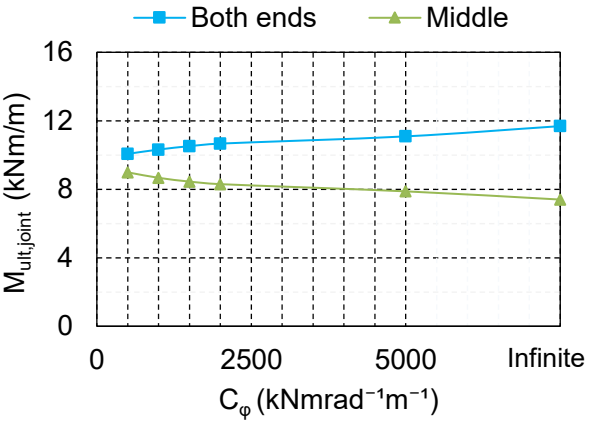

V2_7.2-7.2_LL 1.9_e 1.0

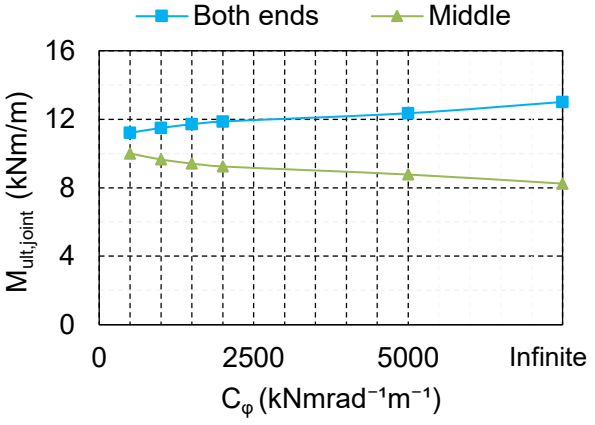

V2_7.2-7.2_LL 2.4_e 1.0

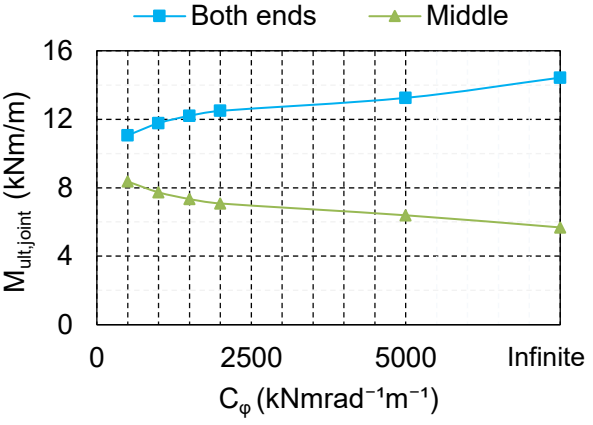

V2_9.5-7.2_LL 1.9_e 1.0

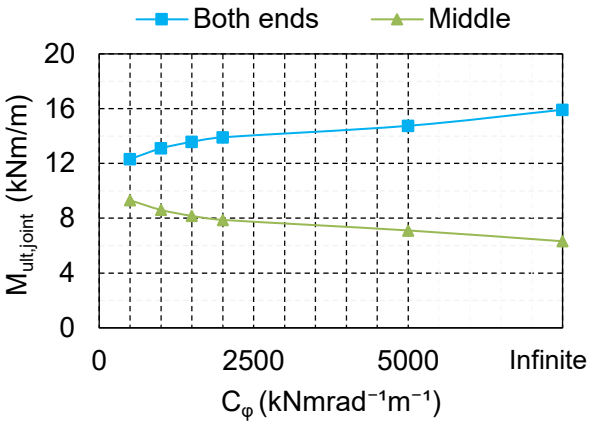

V2_9.5-7.2_LL 2.4_e 1.0

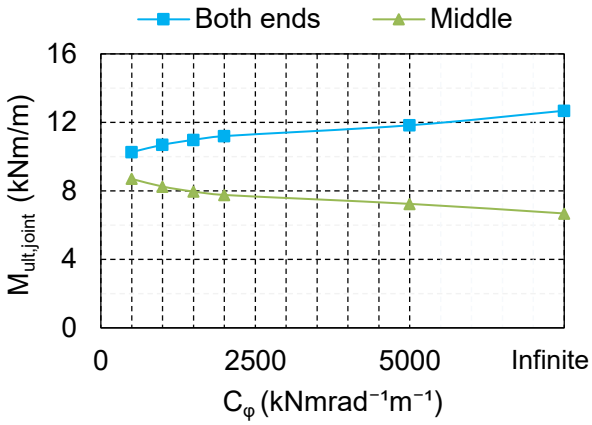

V2_9.5-7.2_LL 1.9_e 1.5

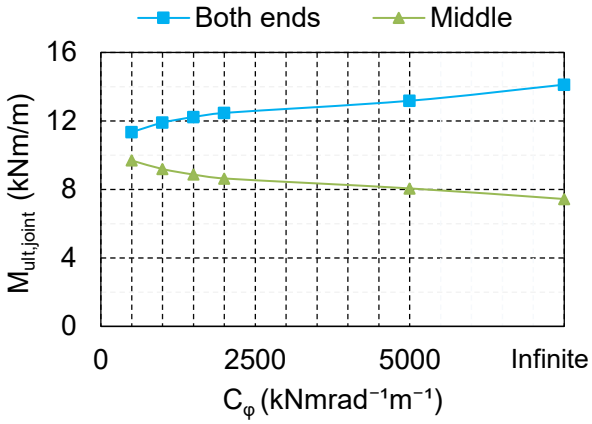

V2_9.5-7.2_LL 2.4_e 1.5

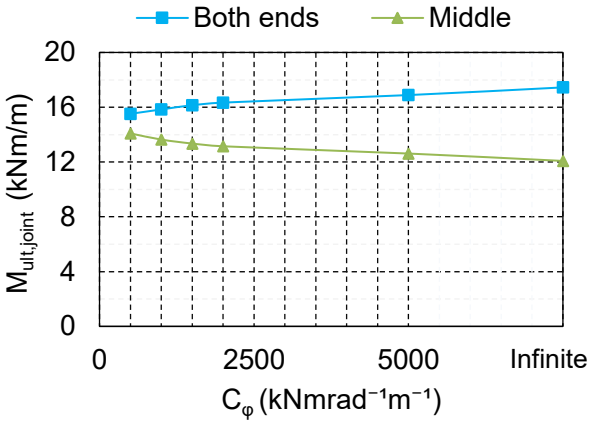

V2_9.0-9.0_LL 1.9_e 1.5

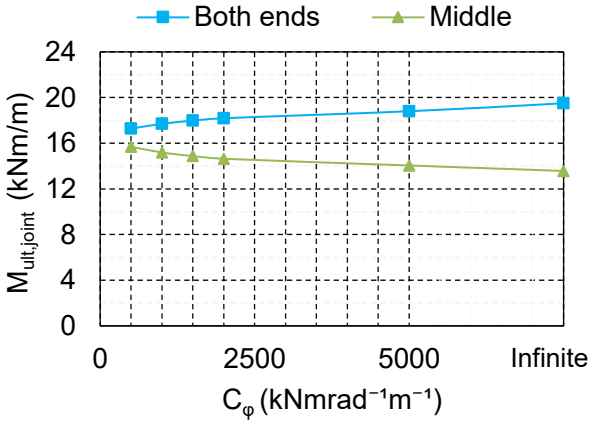

V2_9.0-9.0_LL 2.4_e 1.5

D2: Floor deflections

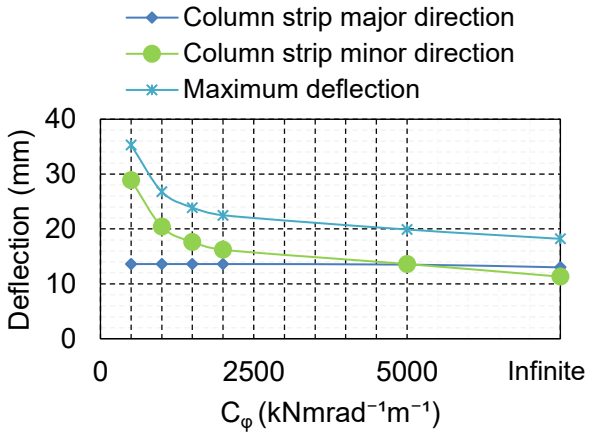

E1_7.2-7.2_LL 1.9_e 0.5

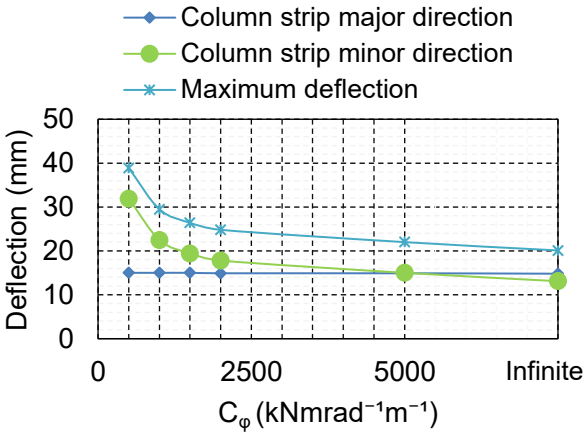

E1_7.2-7.2_LL 2.4_e 0.5

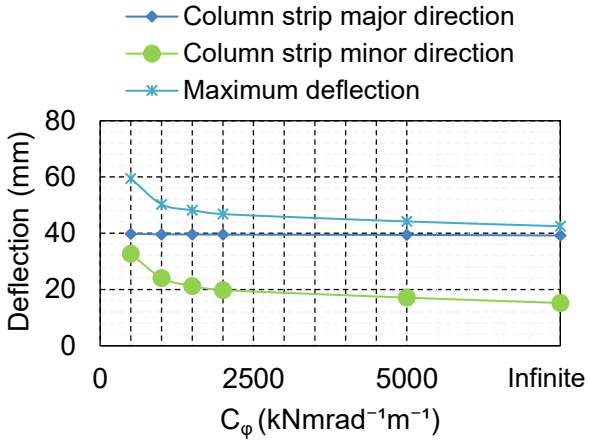

E1_9.5-7.2_LL 1.9_e 0.5

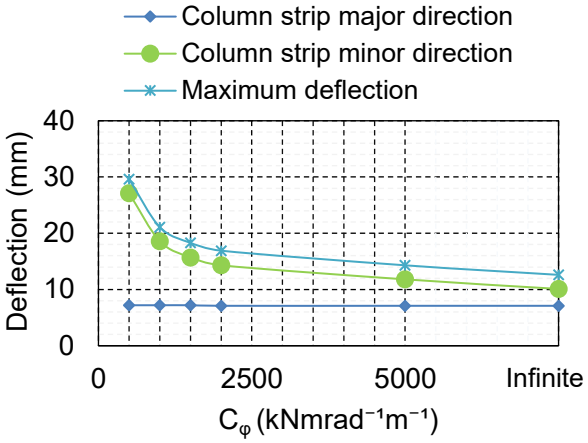

E1_7.2-7.2_LL 1.9_e 1.0

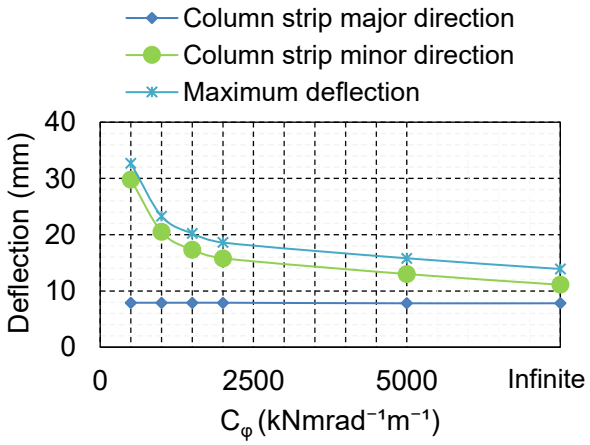

E1_7.2-7.2_LL 2.4_e 1.0

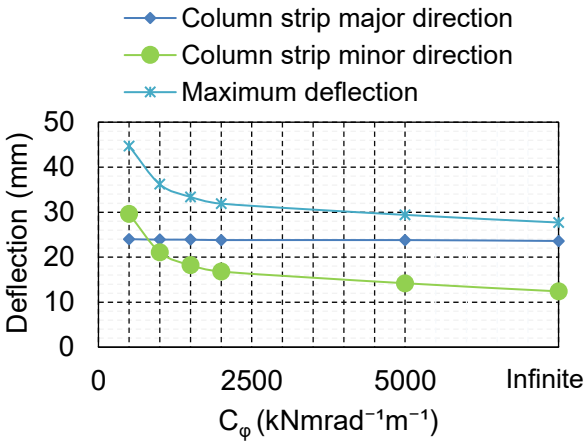

E1_9.5-7.2_LL 1.9_e 1.0

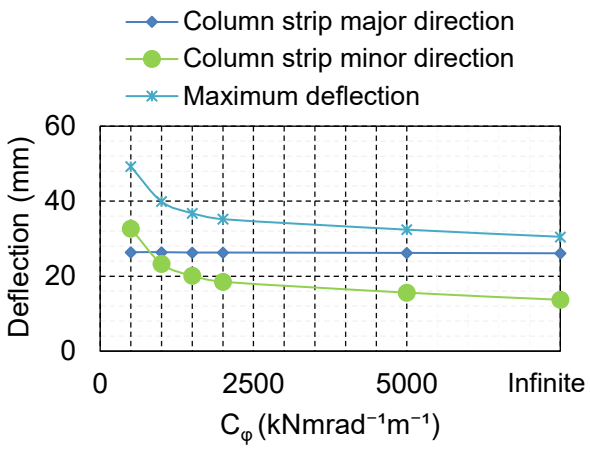

E1_9.5-7.2_LL 2.4_e 1.0

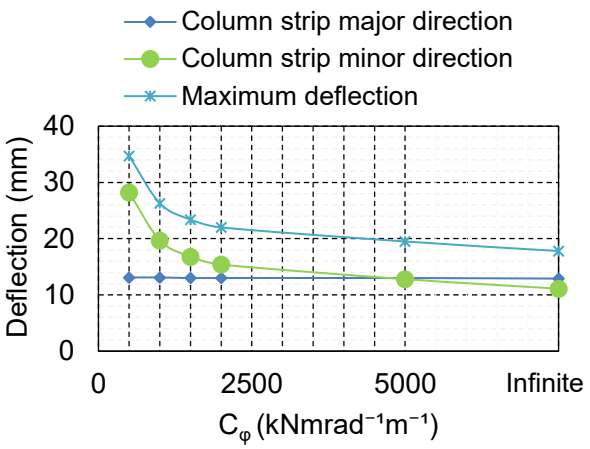

E1_9.5-7.2_LL 1.9_e 1.5

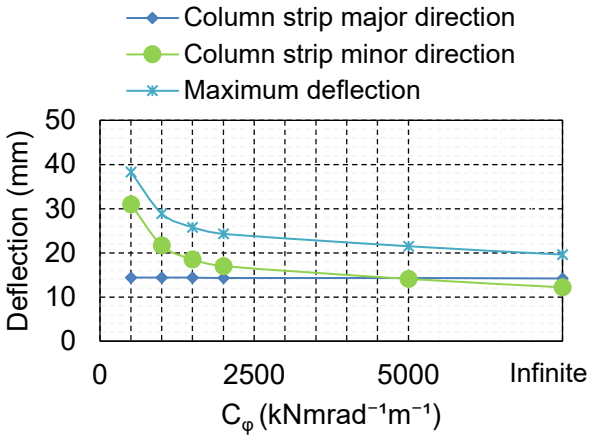

E1_9.5-7.2_LL 2.4_e 1.5

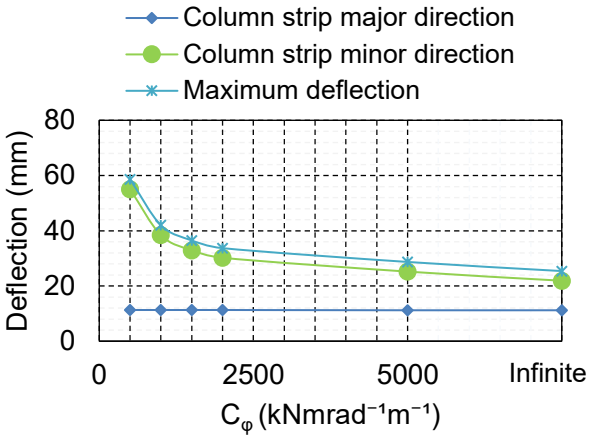

E1_9.0-9.0_LL 1.9_e 1.5

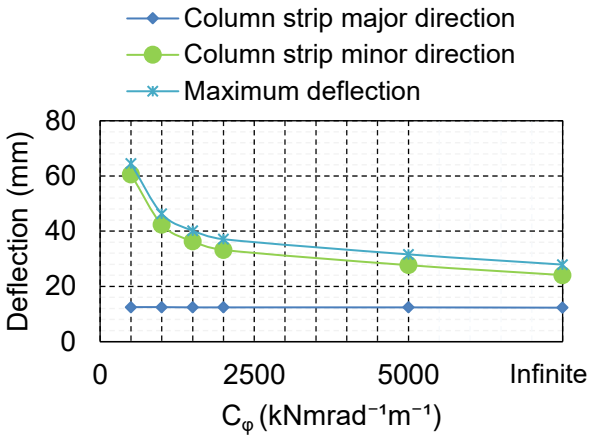

E1_9.0-9.0_LL 2.4_e 1.5

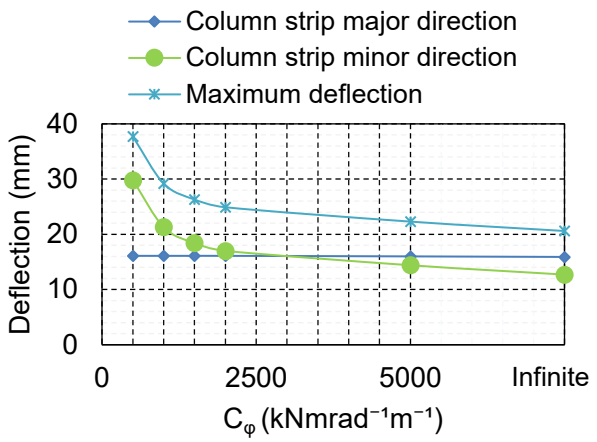

V2_7.2-7.2_LL 1.9_e 0.5

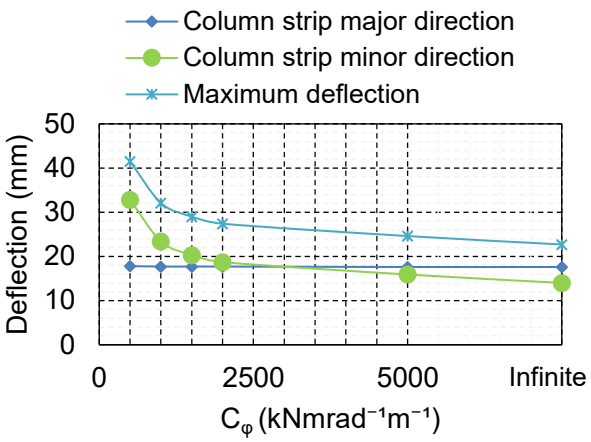

V2_7.2-7.2_LL 2.4_e 0.5

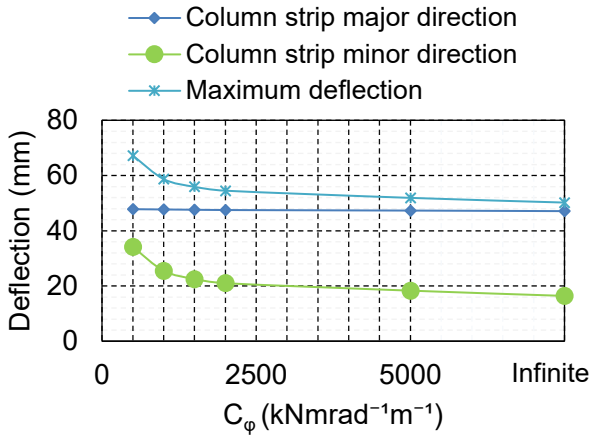

V2_9.5-7.2_LL 1.9_e 0.5

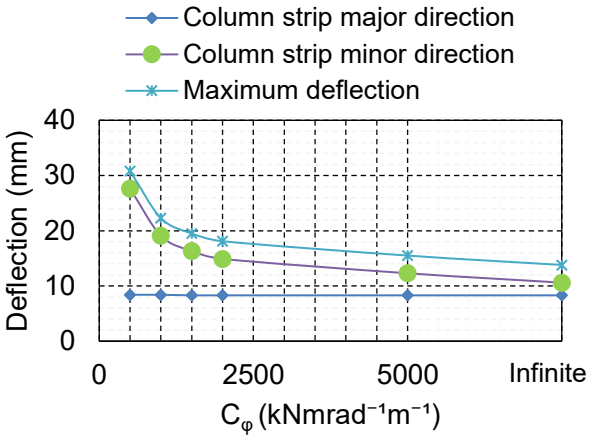

V2_7.2-7.2_LL 1.9_e 1.0

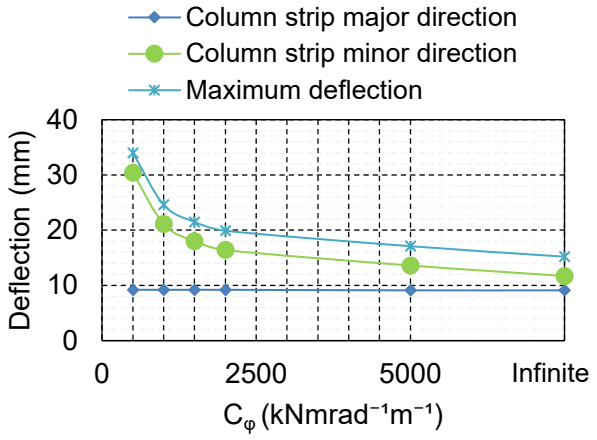

V2_7.2-7.2_LL 2.4_e 1.0

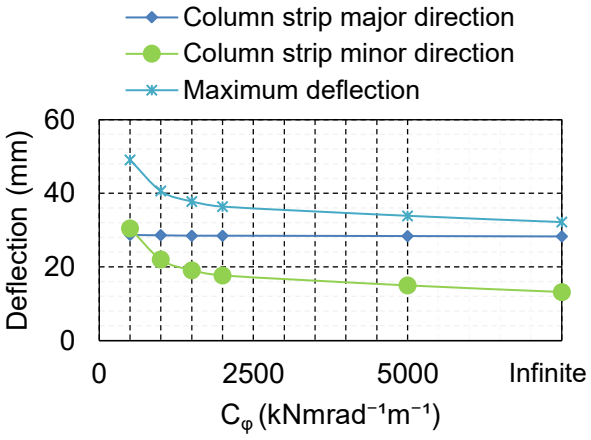

V2_9.5-7.2_LL 1.9_e 1.0

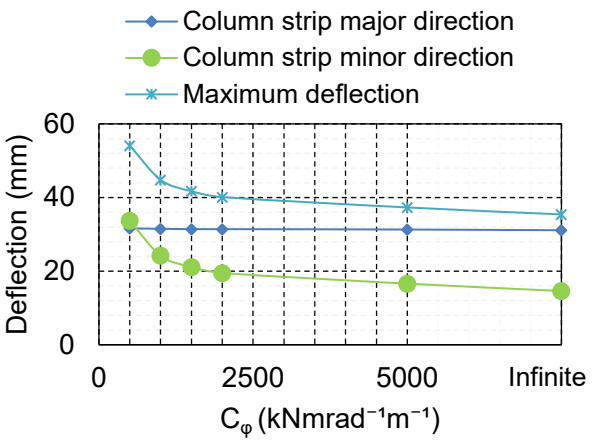

V2_9.5-7.2_LL 2.4_e 1.0

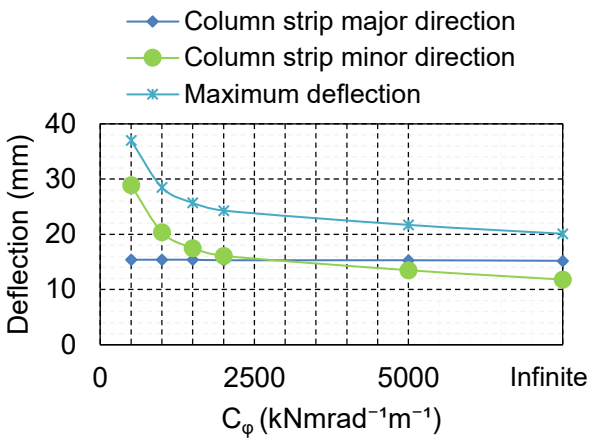

V2_9.5-7.2_LL 1.9_e 1.5

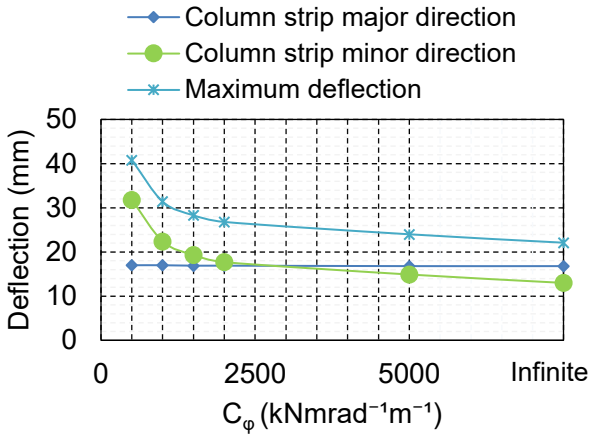

V2_9.5-7.2_LL 2.4_e 1.5

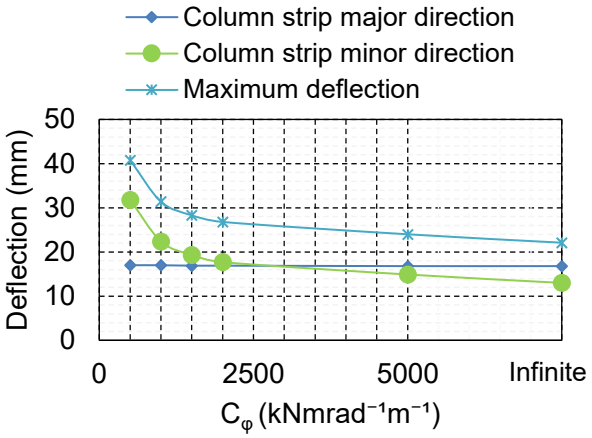

V2_9.0-9.0_LL 1.9_e 1.5

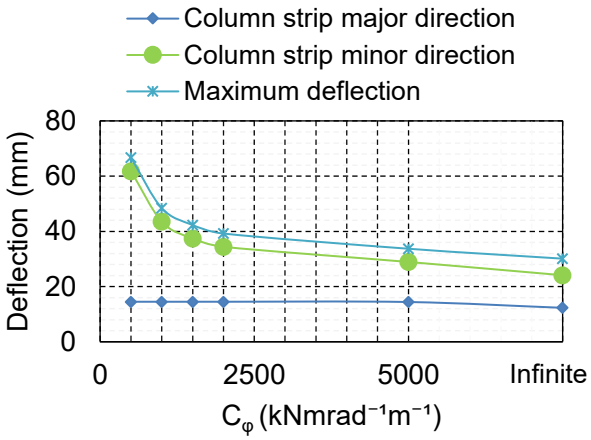

V2_9.0-9.0_LL 2.4_e 1.5

D3: Floor utilisation ratios

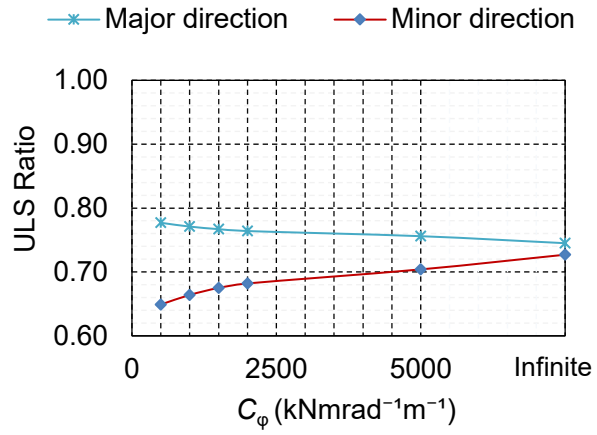

E1_7.2-7.2_LL 1.9_e 0.5

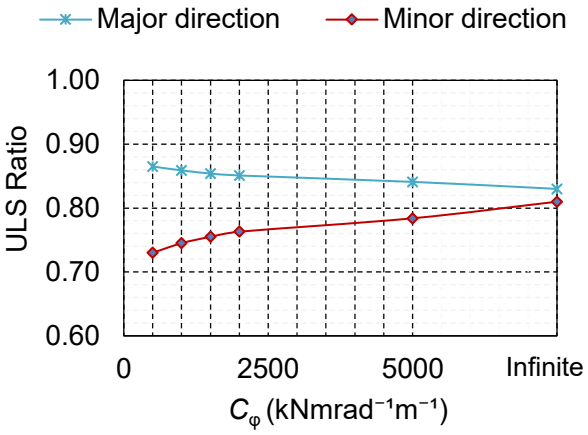

E1_7.2-7.2_LL 2.4_e 0.5

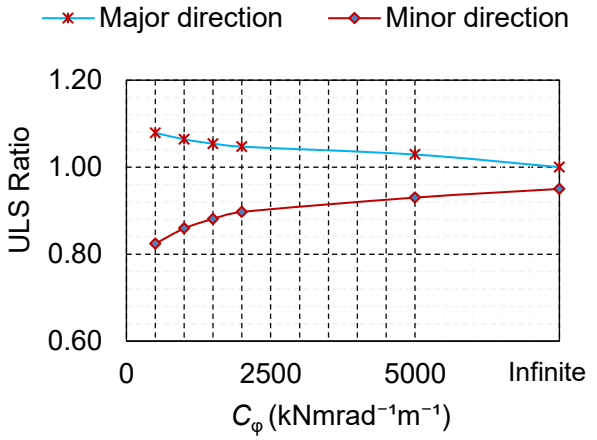

E1_9.5-7.2_LL 1.9_e 0.5

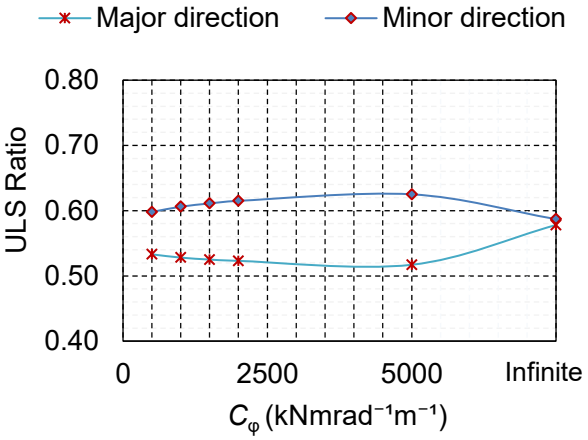

E1_7.2-7.2_LL 1.9_e 1.0

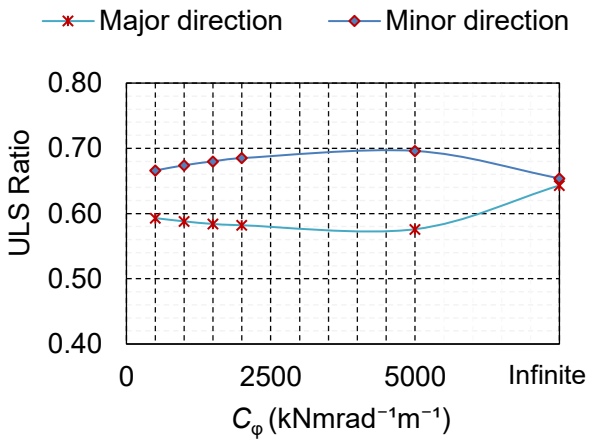

E1_7.2-7.2_LL 2.4_e 1.0

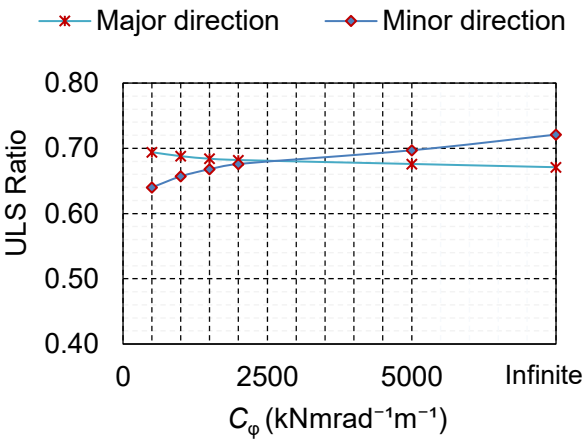

E1_9.5-7.2_LL 1.9_e 1.0

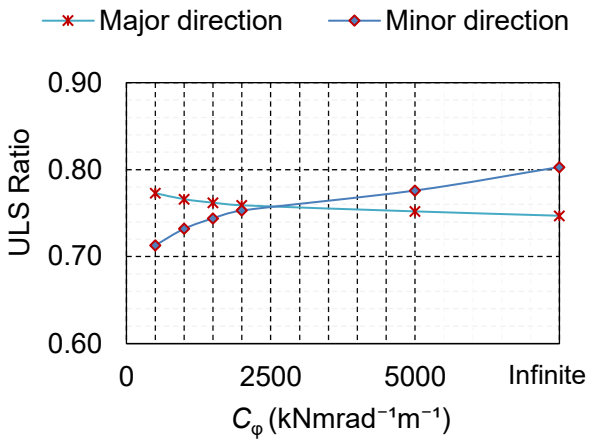

E1_9.5-7.2_LL 2.4_e 1.0

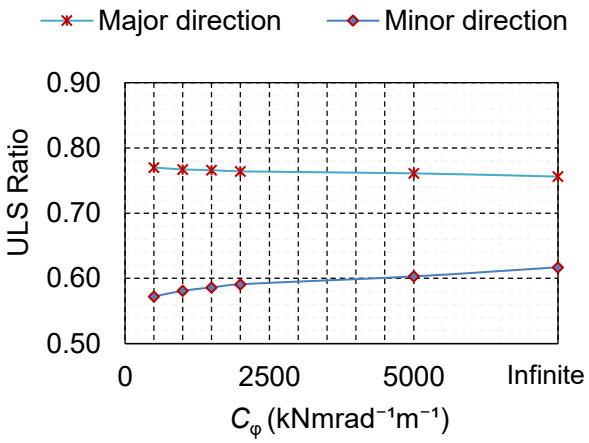

E1_9.5-7.2_LL 1.9_e 1.5

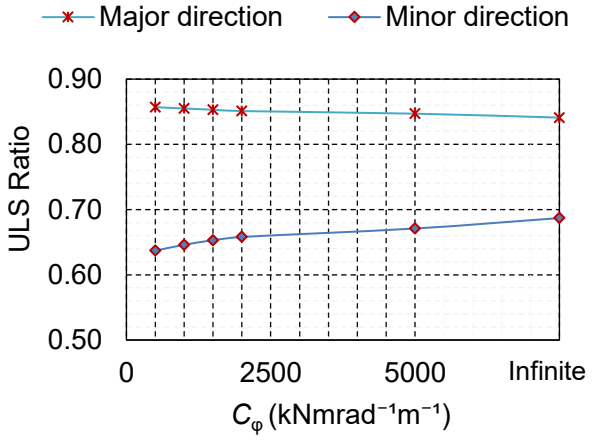

E1_9.5-7.2_LL 2.4_e 1.5

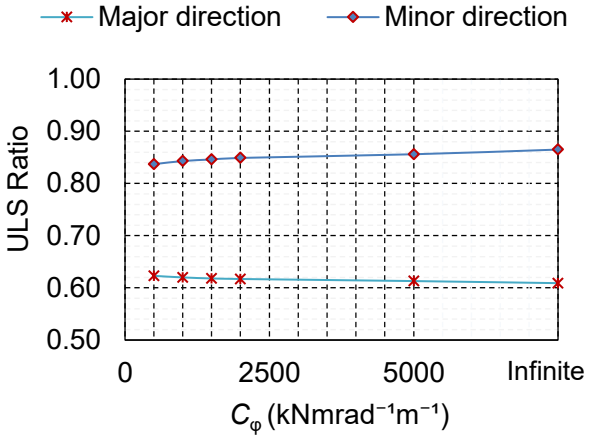

E1_9.0-9.0_LL 1.9_e 1.5

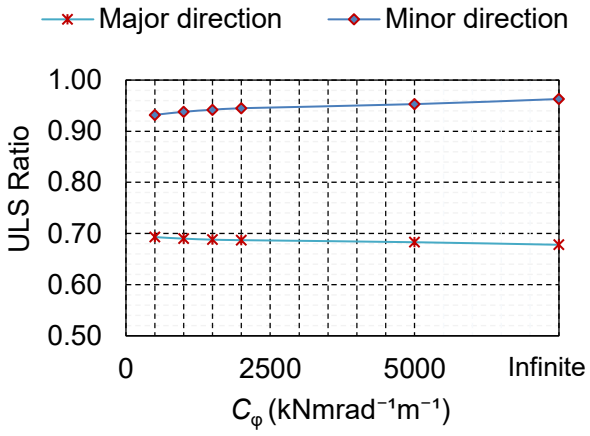

E1_9.0-9.0_LL 2.4_e 1.5

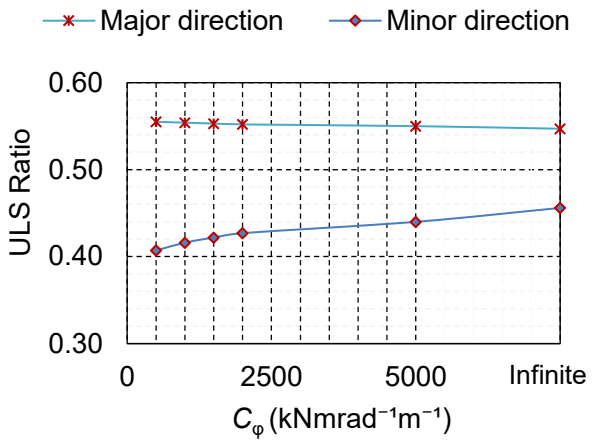

V2_7.2-7.2_LL 1.9_e 0.5

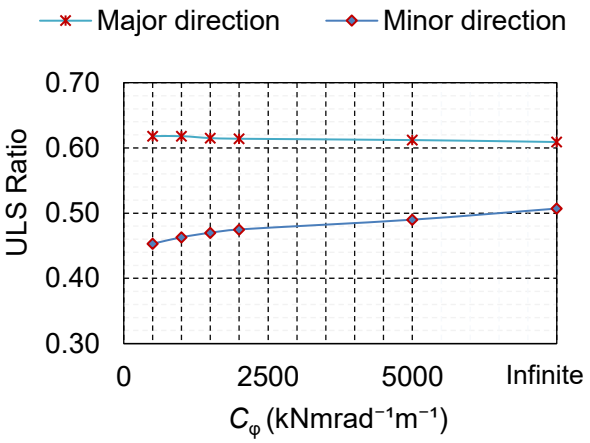

V2_7.2-7.2_LL 2.4_e 0.5

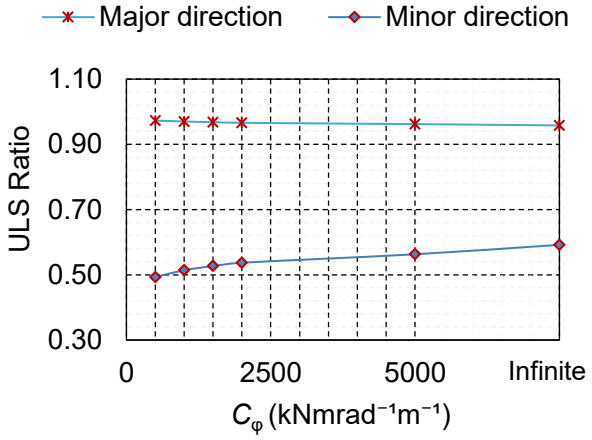

V2_9.5-7.2_LL 1.9_e 0.5

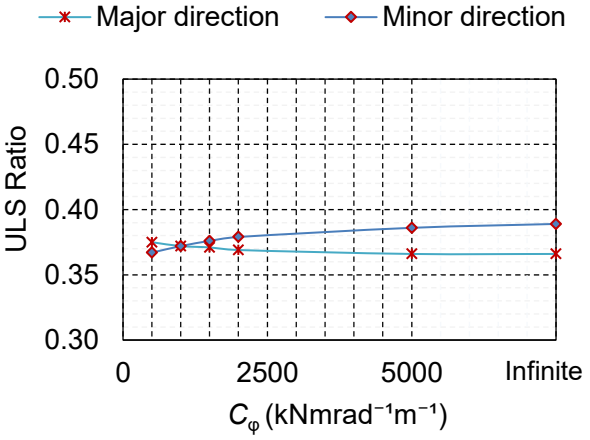

V2_7.2-7.2_LL 1.9_e 1.0

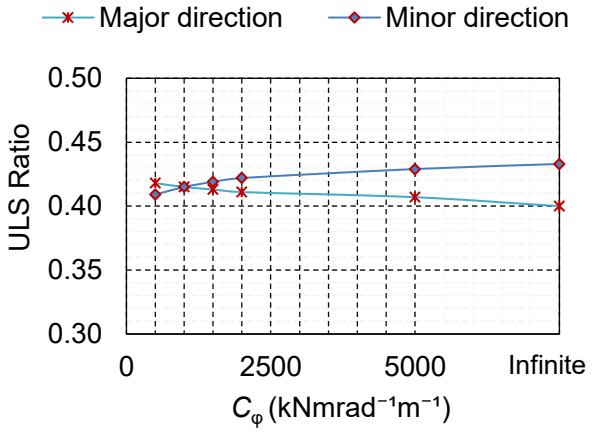

V2_7.2-7.2_LL 2.4_e 1.0

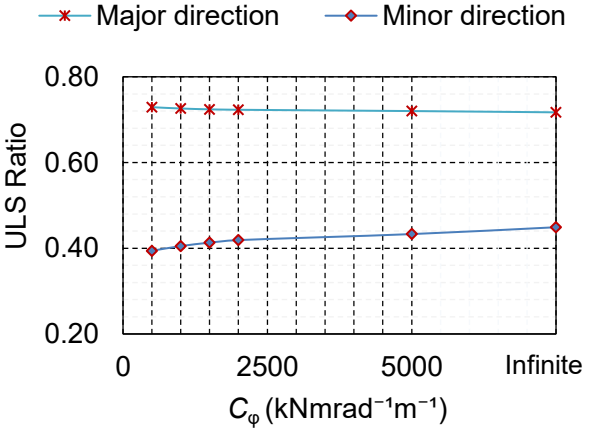

V2_9.5-7.2_LL 1.9_e 1.0

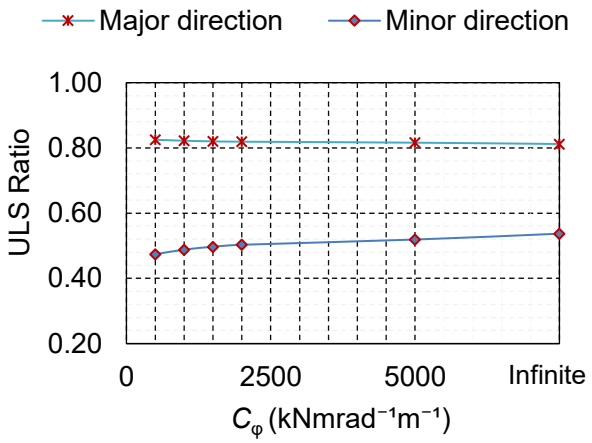

V2_9.5-7.2_LL 2.4_e 1.0

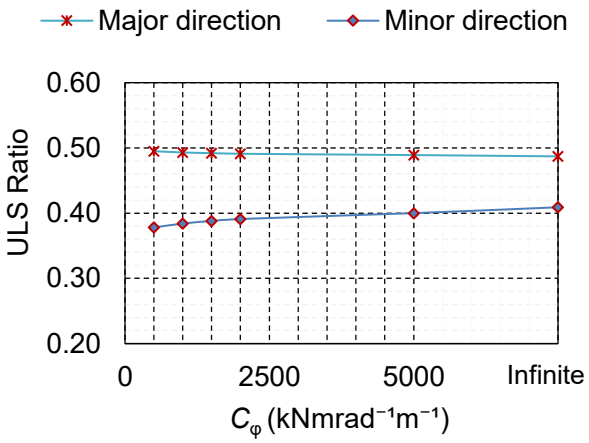

V2_9.5-7.2_LL 1.9_e 1.5

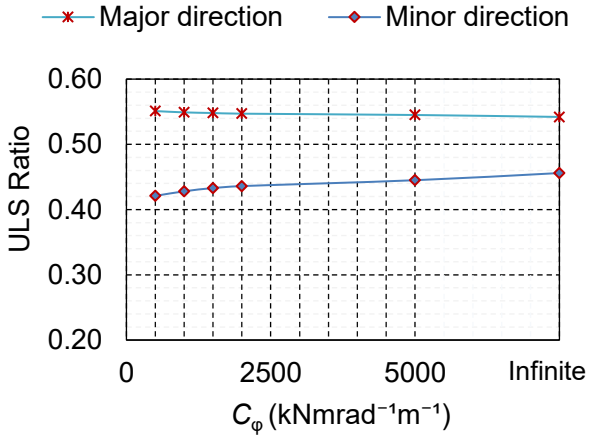

V2_9.5-7.2_LL 2.4_e 1.5

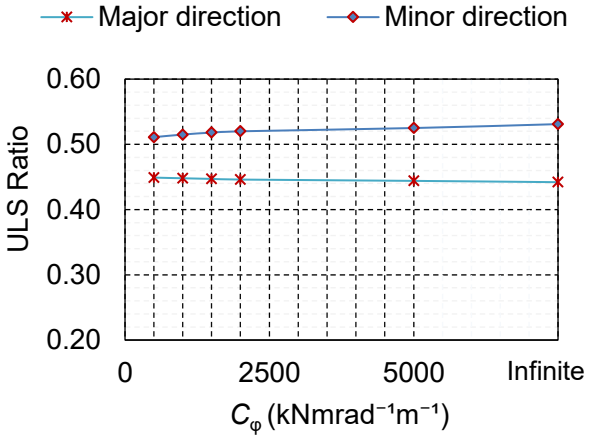

V2_9.0-9.0_LL 1.9_e 1.5

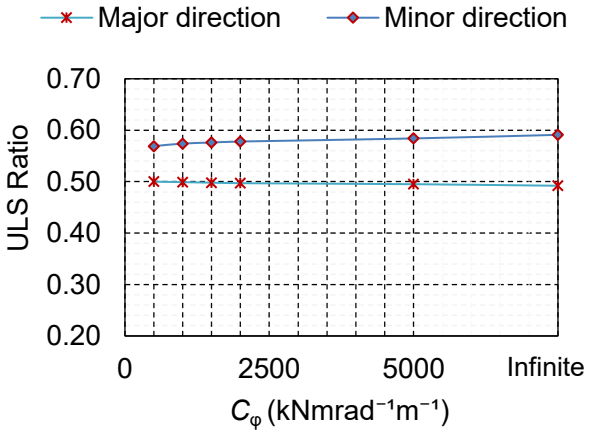

V2_9.0-9.0_LL 2.4_e 1.5

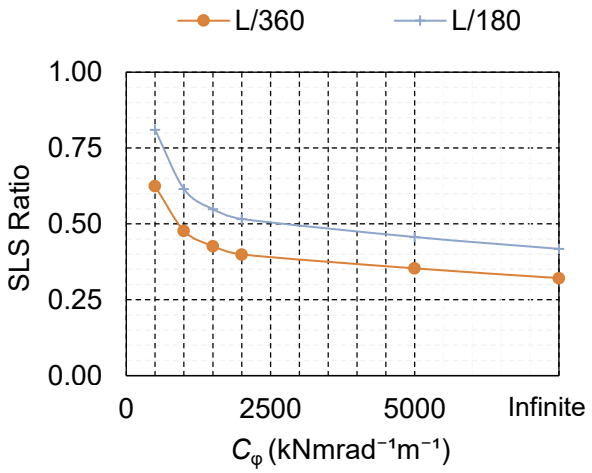

E1_7.2-7.2_LL 1.9_e 0.5

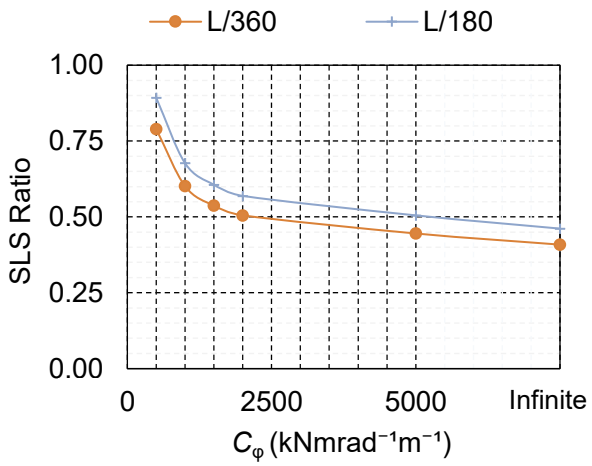

E1_7.2-7.2_LL 2.4_e 0.5

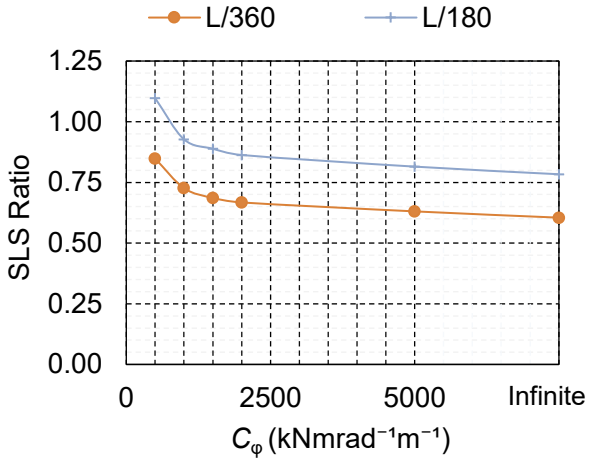

E1_9.5-7.2_LL 1.9_e 0.5

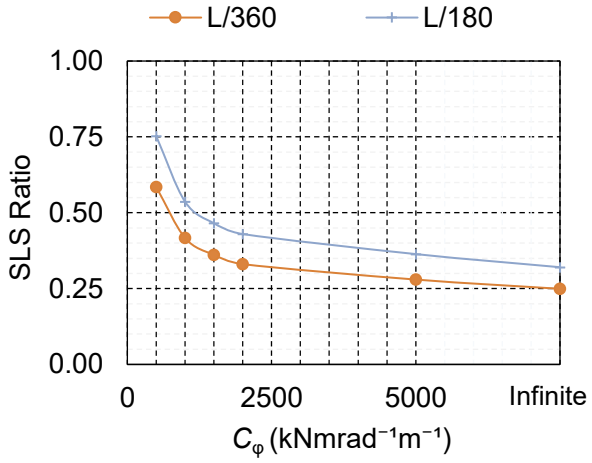

E1_7.2-7.2_LL 1.9_e 1.0

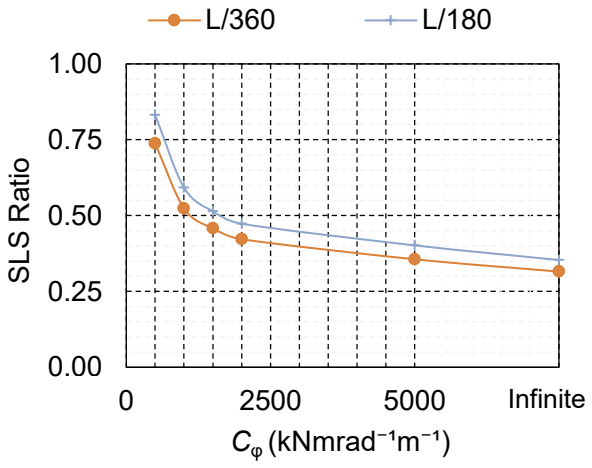

E1_7.2-7.2_LL 2.4_e 1.0

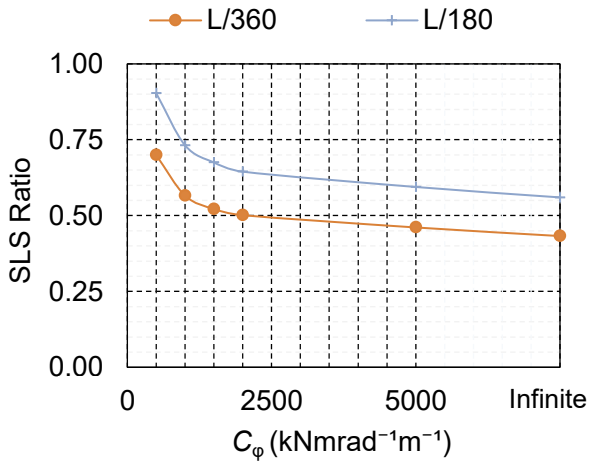

E1_9.5-7.2_LL 1.9_e 1.0

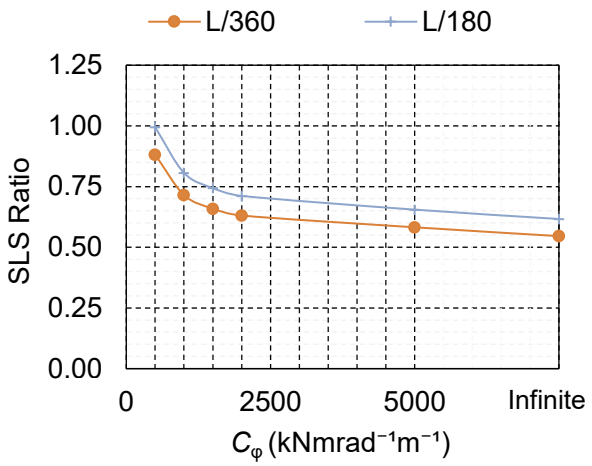

E1_9.5-7.2_LL 2.4_e 1.0

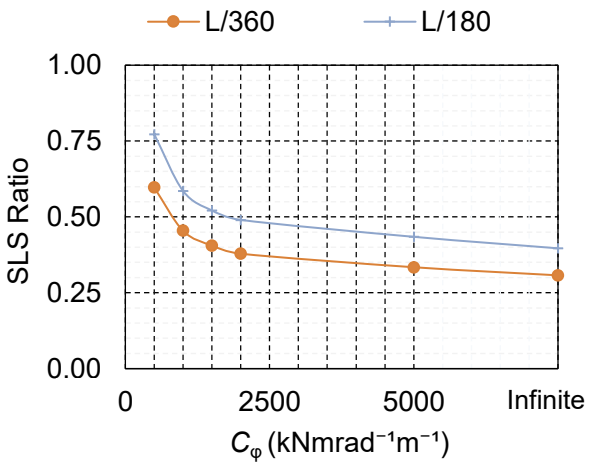

E1_9.5-7.2_LL 1.9_e 1.5

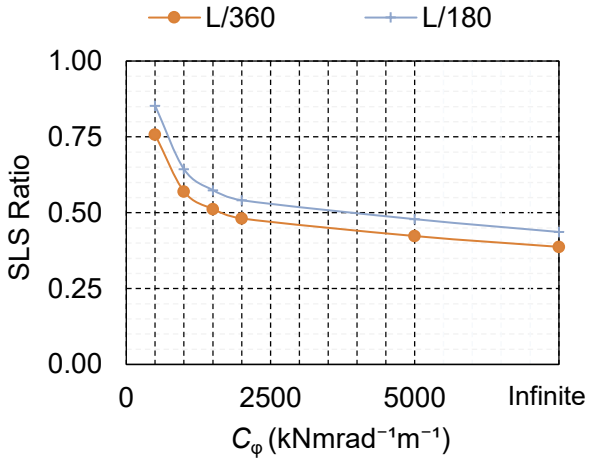

E1_9.5-7.2_LL 2.4_e 1.5

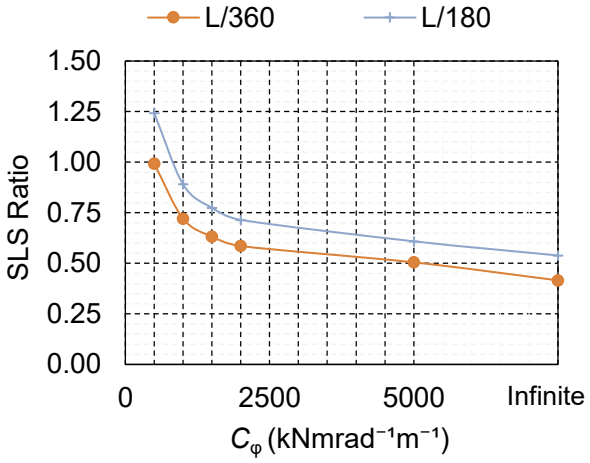

E1_9.0-9.0_LL 1.9_e 1.5

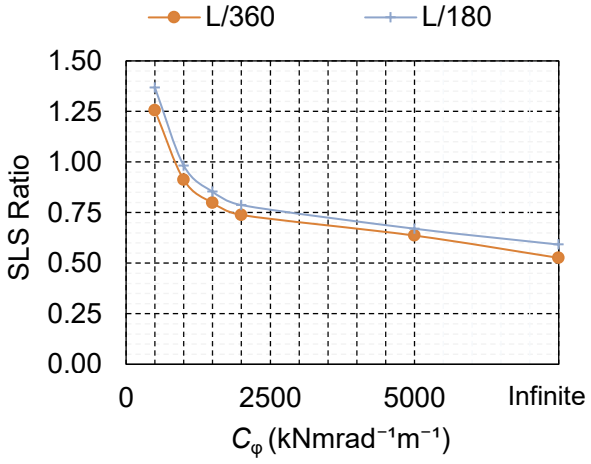

E1_9.0-9.0_LL 2.4_e 1.5

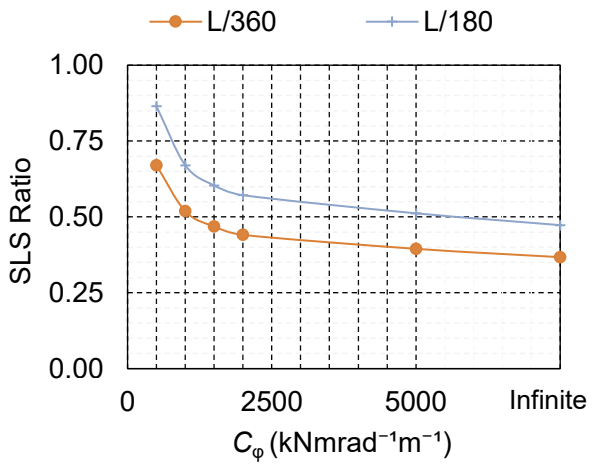

V2_7.2-7.2_LL 1.9_e 0.5

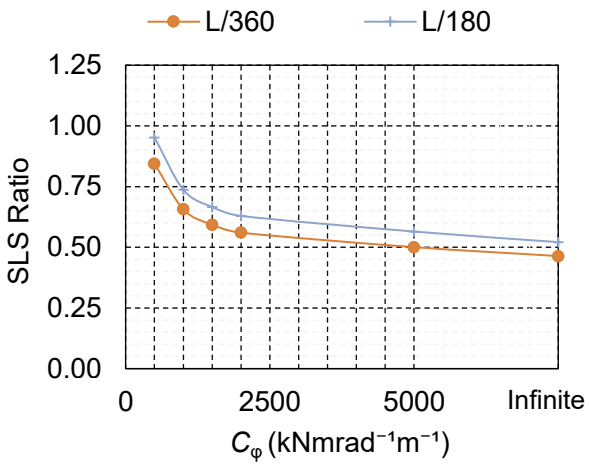

V2_7.2-7.2_LL 2.4_e 0.5

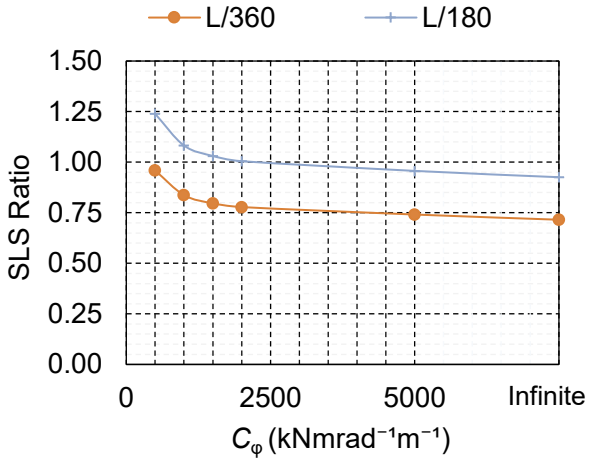

V2_9.5-7.2_LL 1.9_e 0.5

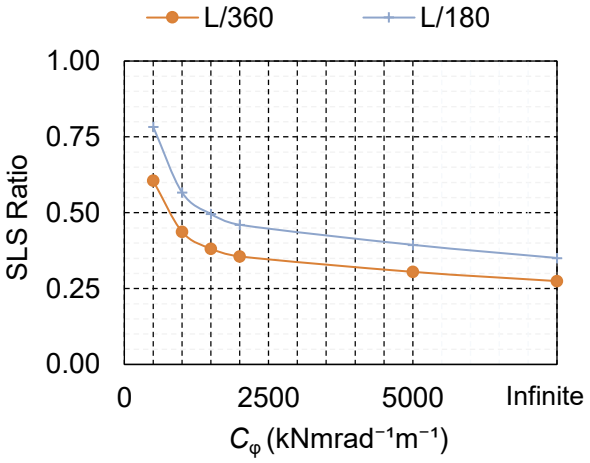

V2_7.2-7.2_LL 1.9_e 1.0

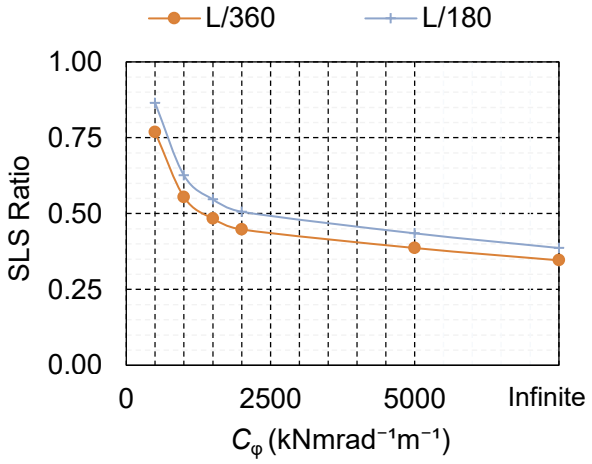

V2_7.2-7.2_LL 2.4_e 1.0

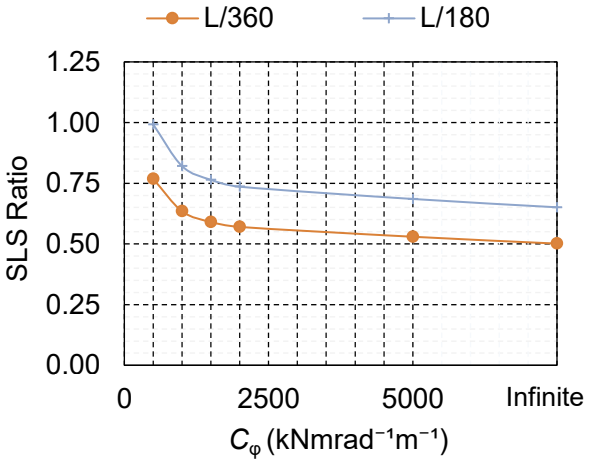

V2_9.5-7.2_LL 1.9_e 1.0

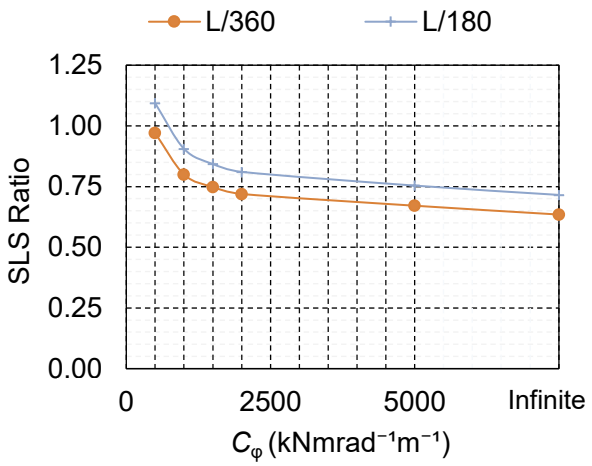

V2_9.5-7.2_LL 2.4_e 1.0

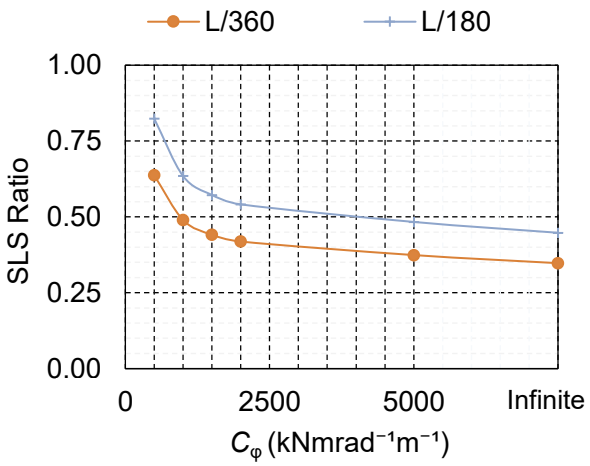

V2_9.5-7.2_LL 1.9_e 1.5

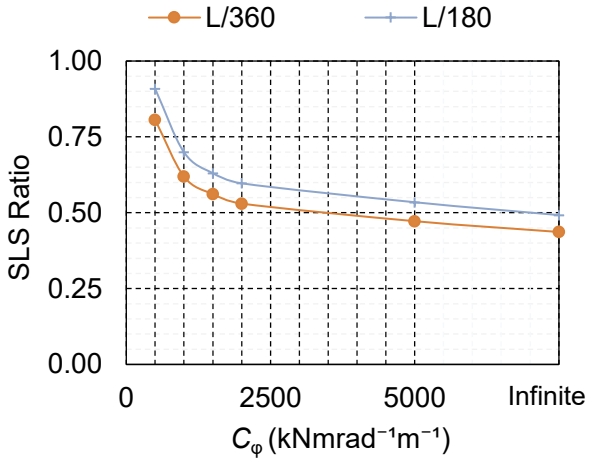

V2_9.5-7.2_LL 2.4_e 1.5

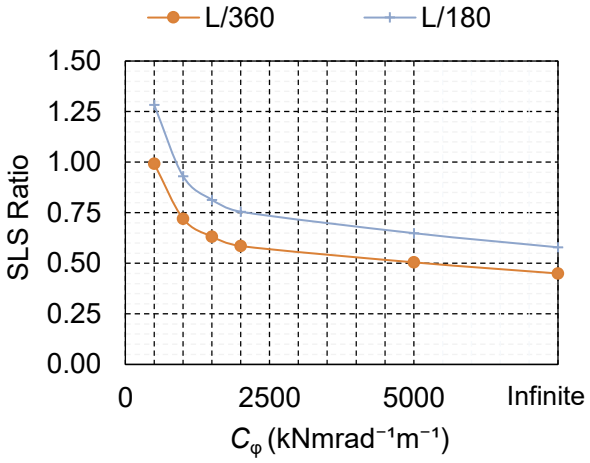

V2_9.0-9.0_LL 1.9_e 1.5

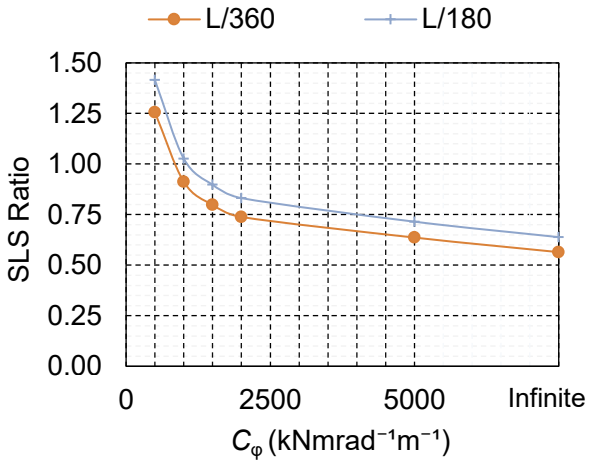

V2_9.0-9.0_LL 2.4_e 1.5